DEVELOPMENT OF BIO-BASED BONE ADHESIVE FROM LACTIC ACID OLIGOMER MODIFIED *CROTON MACROSTACHYUS* (BSANA) CRUDE LEAF EXTRACT

Rahel Tsehaye Gebregziabher

A Thesis Proposal Submitted to

The Department of Chemical Engineering

School of Mechanical, Chemical, and Materials Engineering

Presented in Partial Fulfillment of the Degree of Master's in Chemical Engineering

Office of Graduate Studies

Adama Science and Technology University

September, 2023

Adama, Ethiopia

DEVELOPMENT OF BIO-BASED BONE ADHESIVE FROM LACTIC ACID OLIGOMER MODIFIED *CROTON MACROSTACHYUS* (BSANA) CRUDE LEAF EXTRACT

Rahel Tsehaye Gebregziabher

Advisor: Melaku Tesfaye (Associate Professor)

A Thesis Submitted to

The Department of Chemical Engineering

School of Mechanical, Chemical, Material Engineering

Presented in Partial Fulfillment of the Degree of Master's in Chemical Engineering

Office of Graduate Studies

Adama Science and Technology University

September, 2023

Adama, Ethiopia

DECLARATION

I hereby declare that this master's thesis entitled "DEVELOPMENT OF BIO-BASED BONE ADHESIVE FROM LACTIC ACID OLIGOMER MODIFIED *CROTON MACROSTACHYUS* (BSANA) CRUDE" is my original work. That is, it has not been submitted for the award of any academic degree, diploma, or certificate in any other university. All sources of materials that are used for this thesis have been duly acknowledged through citation.

Student Name	Signature	Date

RECOMMENDATION

I, the advisor of this thesis, hereby certify that we have read the revised version of the thesis entitled "DEVELOPMENT OF BIO-BASED BONE ADHESIVE FROM LACTIC ACID OLIGOMER MODIFIED *CROTON MACROSTACHYUS* (BSANA) CRUDE" prepared under my guidance by Rahel Tsehaye submitted in partial fulfillment of the requirements for the degree of Masters of Science in Chemical Engineering. Therefore, I recommend the submission of the revised version of the thesis to the department following the applicable procedures.

Advisor	Signature	Date

APPROVAL PAGE

I, the advisors of the thesis entitled "DEVELOPMENT OF BIO-BASED BONE ADHESIVE FROM LACTIC ACID OLIGOMER MODIFIED *CROTON MACROSTACHYUS* (BSANA) CRUDE" and developed by Rahel Tsehaye, hereby certify that the recommendation and suggestions made by the board of examiners are appropriately incorporated into the final version of the thesis.

Advisor	Signature	Date

APPROVAL OF BOARD REVIEWERS

We, the undersigned, members of the Board of Examiners of the thesis by Rahel Tsehaye have read and evaluated the thesis entitled "DEVELOPMENT OF BIO-BASED BONE ADHESIVE FROM LACTIC ACID OLIGOMER MODIFIED *CROTON MACROSTACHYUS* (BSANA) CRUDE" and examined the candidate during the open defense. This is, therefore, to certify that the thesis is accepted for partial fulfillment of the requirement of the degree of Master of Science in Chemical Engineering.

Chair Person	Signature	Date
Internal Examiner	Signature	Date
External Examiner	Signature	Date

Finally, approval and acceptance of the thesis is contingent upon submission of its final Copy to the Office of Postgraduate Studies (OPGS) through the Department Graduate Council (DGC) and School Graduate Committee (SGC).

Department Head	Signature	Date
School Dean	Signature	Date
Postgraduate Dean	Signature	Date

ACKNOWLEDGEMENT

First and foremost, praises and thanks to God, the Almighty, for His showers of blessings throughout my research work to complete the research successfully.

My deep and sincere gratitude goes to my advisor, Melaku Tesfaye (Associate Professor); this work would not have been possible without his full support in designing experiments, analyzing results, and writing this thesis. I am forever grateful to him for being patient and believing in me to tackle this project under his supervision.

I am extremely grateful to my parents for their love, prayers, caring and sacrifices for educating and preparing me for my future. I am very much thankful to my loving and supportive father, Kesis Tsehaye G., for his understanding, prayers, and continuing support to complete this research work. I am also grateful to *Adama Science and Technology University (ASTU)* for giving me this free scholarship to this master's program.

Finally, my special thanks go to my friends at Adama Science and Technology University for their contribution to my work directly or indirectly.

TABLE OF CONTENTS

LIST OF TABLES

LIST OF FIGURES

LIST OF ACRONYMS AND ABBREVIATIONS

ASTM	American Society for Testing and Materials
CM	Croton macrostachyus
DBBM	Deproteinized bovine bone mineral
DDS	Drug Delivery System
DMSO	Dimethyl Sulfoxide
DOPA	Dihydroxyphenylalanine
DTG	First Derivative of TGA
E. coli	Escherichia coli
FTIR	Fourier-transform infrared spectrum
GC-MS	Gas chromatograph mass spectrum
LLA	L-Lactic acid
MAEP	Monoacryloxyethyl Phosphate
MBCP	Micro-porous biphasic calcium phosphate
MDI	Methylene diphenyl diisocyanate
MHA	Muller hinton agar mediu
MMA	Methyl methacrylate
MPa	Mega Pascal
MSCs	Mesenchymal stem cells
NMR	Nuclear Magnetic Resonance Spectroscopy
ORIF	Open Reduction and Internal Fixation
PEGDMA	Poly(ethylene glycol) dimethacrylate
RBF	Round bottom flask
RSM	Response Surface Methodology
S. aureus	Staphylococcus aureus
TGA	Thermo gravimetric Analysis

ABSTRACT

Complex physiological processes that call for well-coordinated biological events are involved in healing bone fractures. Through a variety of interventions, the use of bioadhesives for fracture healing has been supported in recent years. In this study, a bio-based bone adhesive made from C.macrostachyus leaf extract and Lactic acid monomer mixed at different proportions was synthesized via polycondensation reaction in order to find a more effective solution to some of the problems associated with the use of metal hardware and synthetic adhesive in fracture repair. Response surface methodology (RSM) was applied to study the optimum condition for extracting C. macrostachyus leaf with n-hexane. The experiment was conducted using the Box-Benhken method consisted of seventeen experimental points, including five replicates of center points to study the effect of three independent variables: temperature, time and mixing ratio on the crude oil yield. The result showed that the optimum conditions of C. macrostachyus leaf extraction were 60 °C, 4.25 h and 0.28 wt/wt% with an oil yield of 11.7%. Qualitative phytochemicals analysis of the crude extract was carried out using standard protocols and showed the presence of alkaloids, flavonoids, phenols, tannins and terpenes but an absence of saponins. At different mixing ratios, biobased adhesives were synthesized at a reaction temperature of 170 ^{o}C for 5 hr. The interaction between OH groups of crude extract and C=O of a lactic acid oligomer was confirmed by FTIR analysis. The OLLA-m-CM 3 had the largest inhibition zone for the synthetic bioadhesives' antibacterial properties, measuring roughly 11mm and 12mm for E. coil (gram-ve) and S. aureus (gram+ve) bacteria, respectively. According to the water contact angle investigation, OLLA-m-CM 1, 2, and 3 had contact angles of 77.8°, 65.4°, and 56.7°, respectively. Finally, a universal testing machine was used to determine the bonding strength of the three synthesized adhesives. Glass and bone substrates both experienced cohesive failure at maximum tensile strengths of 8 and 11 MPa, respectively.

Therefore, the outcome suggested the potential use of C. macrostachyus leaf extract modified with lactic acid oligomer as a substitute to synthesize bio-based bone adhesive.

Keywords: *Bone adhesive, C. macrostachyus, Lactic acid oligomer*

1. INTRODUCTION

1.1. Background of the Study

Bone fractures are frequently caused by trauma or diseases like osteoporosis and bone cancer (Augat et al., 2005). Age, gender, lifestyle, and pre-existing medical conditions all significantly impact a patient's risk of developing a fracture and their chance of experiencing complications during the healing process (Gupta et al., 2008; Nellans et al., 2012). According to a Global Burden of Disease study (Wu- A., 2021), 178 million people (53% men and 47% women) experienced bone fractures worldwide in 2019. Since 1990, this figure has increased by 34%.

Inflammation, bone production, and remodeling are the three stages overlapping when a bone fracture heals normally. After the initial bleeding into the fracture area, blood clotting and inflammation take place at the fracture site. These processes involve haematopoietic and immune cells, as well as mesenchymal stem cells (MSCs) from the bone marrow and surrounding tissue (Zhu et al., 2021). Within two to four weeks, clotted blood is replaced by fibrous tissue and cartilage (soft callus). The early stabilization provided by callus formation around the broken bone shields the healing tissue from outside forces (Kovach et al., 2015). The callus then appears on radiographic images as a result of the calcium formation that is deposited in the matrix over the course of the subsequent 4 to 12 months. The last step in the typical healing process is the successful reconstruction of the original shape and structure of bone (also known as bone remodeling).

Sometimes, the normal processes for bone repair are not followed by bone healing. Micromovement at the repair site, for instance, can hinder the healing process and result in other potential complications, such as bleeding into the joint space, which can swell the joint (haemarthrosis), and blood clot formation, which can result in blockage within a blood vessel, either locally or elsewhere in the body. Non-union fractures happen when the broken bones are unable to mend because of inadequate stability (poor immobilization), insufficient blood supply, or inadequate nutrition. The recovery process can frequently take months or even years (Bahney et al., 2019).

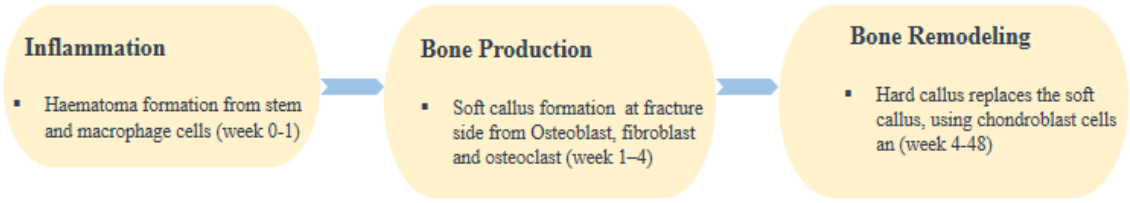

Figure 1.1: Stages of Bone Healing

Current surgical procedures for the treatment of bone fractures involve the use of invasive techniques for the reconstruction and mechanical stabilisation of the fractures using metal hardware (e.g., wires, screws, pins, rods, plates and nails). However, in cases where multiple fragments of bone have resulted from multiple breaks, there is currently no convenient way to stabilise the small fragments of the fractured bone and prevent gaps between the bone fragments (Böker et al., 2019). An alternative approach to overcome some of the challenges relating to the use of metal hardware in fracture repair is the use of adhesive materials.

In summary, treating bone fractures with bone adhesives would be an attractive alternative to metallic implants (Heiss et al., 2005), especially for small fragment fractures like basal fractures of the thumb or Rolando fractures, debris fractures, and low-stressed bone regions. Bone adhesives have the potential to shorten the treatment time and partially eliminate subsequent treatments. Taken together, there is a high clinical demand for bone adhesive bonding technology.

1.2. Statement of the Problem

Every year, millions of people suffer from complex bone fractures as a result of traumatic incidents such as sporting injuries, vehicle accidents, and falls or medical conditions such as osteogenesis imperfecta, osteoporosis, cancer-induced bone degeneration, or periodontitis. So, for the bone fractures the current surgical techniques use invasive techniques for mechanically stabilizing the fractures and reconstructing them using metal hardware (such as wires, screws, pins, rods, plates, and nails) (Augat et al., 2005). However, there is currently no practical way to stabilize the small fragments of the fractured bone and prevent gaps between the bone fragments in cases where multiple breaks have resulted in multiple fragments of bone. The use of adhesive materials is a different strategy to get around some of the issues with metal hardware in fracture repair. These substances have the ability to stabilize the broken bone and form a bond with the metal implant or between the bone and the bone. In addition to that inflammatory reactions, stress shielding, and mechanical failure that may result in early implant failure are potential drawbacks associated with the use of current adhesive materials (Ochs et al., 2012; Gardziella et al., 1990).

One of the main aspects of biomaterial development is to ensure that the biomaterial is nontoxic to cells and animals, prior to human use. Following this, many studies have included cytotoxicity and animal toxicity assays, along with testing the adhesive properties of the new bioadhesives. Cyanoacrylate (e.g., cyacrin) and polyurethane-based synthetic polymers have also been proposed as bone bioadhesives due to their high bonding strength and ability to achieve adhesion in a wet environment (Pascual et al., 2016). However, these cyanoacrylate and polyurethane-based bioadhesives have demonstrated high tensile and adhesion properties, high infection rates, non-union (e.g., fracture displacement), low biodegradation and severe local reactions have been reported. The poor outcomes from these initial materials resulted in research into alternative bioadhesives with more suitable functional properties. In addition to the cyanoacrylates derivative adhesives there are a number of adhesives that are used clinically including Bioglue (Herget et al.,2001; Menon et al., 2003) and fibrin glue (Kjaergard et al.,1992; Owen et at al., 2000; Dunn et al., 1999).

Although these adhesives have some efficacy, they suffer from poor biocompatibility or insufficient bonding strength.

Since the existing studies in the field remain rather limited; this research study was focused on the synthesized of bio based bone from traditionally known medicinal plant which is *C. macrostachyus* and lactic acid oligomer.

1.3. Research Questions

RQ1.What would be the effect of extraction temperature, extraction time and mixing ratio on the yield of crude extract?

RQ2.What would be the effect of molar ratio on the tensile strength of the synthesized adhesive?

RQ3. Can the synthesized product be used for bone adhesive testing in silica material (glass) and animal bone?

1.4. Objectives

1.4.1. General Objective

The main objective of this study is to develop bio-based bone Adhesive from lactic acid oligomer modified *Croton macrostachyus* (Bsana) crude leaf extract.

1.4.2. Specific Objectives

- To extract the leaf of *C. macrostachyus* by using a soxhlet extraction apparatus and to define the optimum condition and effects of factors on extracting phenomena
- To characterize the crude extract at optimum conditions
- To Synthesis, characterize and develop OLLA-m-*CM* crude leaf extract conjugate through oligomerization
- To examine the microbial effect of the *C. macrostachyus* extract, OLLA, and OLLA-m-*CM*
- To test the prepared OLLA-m-*CM* adhesive for selected substrates of glass and animal bone

1.5. Significance of the Study

Bio-based bone adhesives have the potential to revolutionize medical treatments by providing effective alternatives to the traditional method of bone fixation, such as screws, plates, and pins. These adhesives can be used to bond fractured or damaged bones, leading to faster healing, reduced risk of infection, and improved patient outcomes. In addition, biobased adhesives are designed to be biocompatible, compatible with living tissues and doesn't cause adverse reactions or toxicity and can promote the natural healing process of bones. That's why it is crucial in medical applications.

In this study, the main work was done to synthesize and characterize biobased adhesive from leaf extract of the traditionally known medicinal plant (*C. macrostachyus*) and lactic acid monomer. Since the selected raw materials are biocompatible and ecofriendly with different phytochemical constituents, synthesizing adhesive from those raw materials has great significance in ensuring the production of an alternative form of bio-adhesives.

1.6. Scope of the Study

The study addresses the option of developing bio-based bone adhesives to replace petrochemical bone adhesives in our nation. Bio-based adhesives avoid environmental and health problems and thus do not rely on non-renewable feedstock such as *C. macrostachyus* leaf extract and lactic acid.

2. LITERATURE REVIEW

2.1. Current Surgical Approaches for Fracture Repair

Internal fixation procedures have been using metallic plates and wires for more than 100 years to provide compression and stabilization between the fractured bone fragments. Metal hardware is frequently used, but it comes with drawbacks and frequently leads to poor healing, like mal-unions (Schmitz et al., 2008). Particularly, it is common for bone plates, screws, and pins to become loose over time after surgery; as a result, it is frequently advised to remove these devices, which results in cortical bone loss (Vainio et al., 1979). Controlling bleeding, preventing ischemic injury (i.e., bone death), and eliminating infection sources like foreign bodies and dead tissues are the goals of early fracture management. In order to maintain the fraction reduction after the fracture has been reduced, immobilization techniques are currently used in fracture management. For straightforward fractures, immobilization techniques range from the application of a cast or wrap (i.e., non-operative therapy) to the insertion of metal hardware (i.e., operative therapy) (Bauer et al., 2009).

The goal of surgical treatment methods is to provide internal or external support to stabilize the broken bones above and below the fracture site. Another goal of surgical intervention is to remove any dead bone and inadequately vascularized or scarred tissue from the fracture site in order to promote healing while also supplying the fracture site and nearby soft tissue with blood. To aid in the healing process, it is occasionally possible to remove healthy soft tissue from another area of the body and transplant it to the fracture site. Additionally, bone grafts can be used in stem cell therapy to stimulate bone healing by supplying bone-forming cells and supportive cells (Schmitz et al., 2008). Surgical intervention, such as open reduction and internal fixation (ORIF) or external fixation, is necessary for more complex fractures. Where ORIF is a surgical procedure where the fracture site is adequately exposed, and reduction of the fracture is conducted. Several devices have been used for the internal fixation of bone fractures, including plates, interlocking nail devices, intramedullary compression nail devices, bridging devices and balloons (Gellynck et al., 2011). There are a number of different types of plates, with the most common being dynamic compression plates.

Dynamic compression plates are designed to exert dynamic pressure between the bone fragments, which is achieved either by attaching a tension device to a plate or by using a special plate. For the placement of the tension device, a longer surgical incision is required, and there is a possibility of re-fracture after the plate is removed. External fixation is a procedure in which the fracture stabilisation is achieved at a distance from the site of fracture. It helps to maintain bone length and alignment without casting. Devices used for external fixation are made of metal or carbon fibre and, as with skeleton traction methods, these devices have pins placed into the bone directly through the skin (Vainio et al., 1979; Yu,Y et al., 2021). External fixation has evolved from being used primarily as a last resort fixation method to becoming a mainstream technique used to treat bone and soft tissue pathologist.

2.2. Bio-Adhesion and Bio-Based Adhesives

The process by which synthetic or organic materials adhere to body surfaces is known as bio-adhesion. Due to their sustainability, renewability, biocompatibility, biodegradability, and high molecular weight, bio-based adhesives are now used more frequently in a wide range of applications with added value (Kumar et al., 2022; Sardella et al., 2020). Numerous biomedical applications, including orthopedics, orthodontics, surgery, drug administration systems, etc., have made extensive use of bio-adhesion (Majeed et al;2020). The component used in bioadhesives can be produced synthetically or from natural resources. The bio-adhesive must have certain capabilities in its application, such as the ability to speed up surgery, strengthen seals, make materials easier to remove, be user-friendly, and improve the effectiveness of sealing air leaks, among others. In order to be effective in biological settings and meet certain requirements, bio-based adhesives used in biomedical applications must be excellently biocompatible, resorbable, simple to handle, and strong (Xiang et al., 2020). In surgery, the use of bio-based adhesives as hemostats and sealants has grown. The goal of bio-based adhesives is to keep a safe distance from the foreign body reaction at the injury site while bonding the tissues during the healing phase of injuries. Additionally, bio-based adhesives must function at a specific site and advance safely alongside the healing process, i.e., they must not harm the nearby tissues (Ramesh et al., 2020; Rathi et al., 2019). Wet surfaces present a difficult assessment of bio-adhesion, but marine organisms like mussels, fungi, and other bacteria have offered a natural solution to this issue.

Marine mussels produced bio-based adhesive proteins that allowed them to adhere to very wet surfaces. Mussels produce adhesive proteins known as mussel foot prints (MFP), which have exceptional adhesion properties. 3, 4 Dihydroxyphenylalanine (DOPA), which is derived from tyrocine, makes up the majority of the MFP. Chemical reactions cause the binding and solidifying properties of MFP, which are derived from the catechol side chain of DOPA, to be cross-linked with the substrate's surface (Rathi et al., 2019; Bolghari et al., 2022). By utilizing the benefits offered by adhesive proteins, the MFP inspired the development of novel bio-based adhesive materials to satisfy the requirements of satisfactory adhesive ability to wet surfaces.

The development of sustainable bio-based adhesives was motivated by the natural bio-adhesion properties of plants and animals to substrates and tissues. The primary element in the effective use of high-performance, bio-based adhesives in a variety of applications is similarity to characteristics found in nature. Bio-based adhesives based on proteins or polysaccharides can imitate the process of blood coagulation. Alginate, chondroitin, and chitosan are typical examples of polysaccharide-based bio-adhesives, whereas fibrin sealants, gelatin, and collagen are typical examples of protein-based bio-based adhesives (Shahryarimorag et al., 2022; Alqosaibi et al., 2022; Sanchez et al., 2019). Additionally, the bio-adhesion construct can be used for drug delivery systems (DDS) that deliver drugs to particular sites using drug carriers.

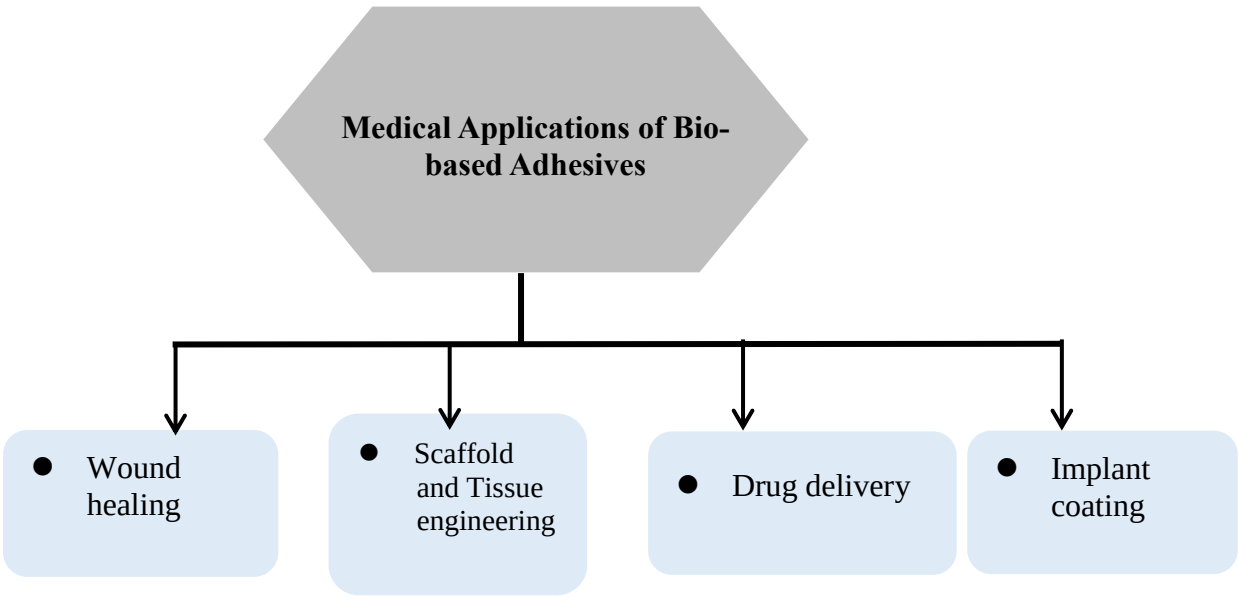

Figure 2.1: Medical Applications of Bio-based Adhesives

2.3. Sources of Bio-adhesives

2.3.1. Fibrin

A fibrous, non-globular protein known as fibrin helps to promote blood clotting. A fibrinogen source and factor XIII as a stabilizer are typically combined to create fibrin-based adhesive systems (Arbes et al., 1981). To slow down rapid fibrinolysis, thrombin, calcium, and an anti-fibrinolytic agent can also be used. Calcium ions facilitate activation and permit clot formation when thrombin and fibrinogen are combined. The formation of a covalent bond between the amino groups in the adhesive system of fibrin/fibronectin and the carboxylic acid groups in the bone collagen matrix results in adhesion. Fibrin-based adhesives for bone fixation can speed up the fixation of implants to bone, enhance bone graft filling, and facilitate fracture fixation and spinal fusion (Yang et al., 2013). Although these kinds of adhesives showed good biocompatibility, biodegradability, and clot formation, they lacked osteogenic potential and had relatively weak bonds (0.005-0.17 MPa) compared to synthetic adhesives.This can be attributed to the weak cohesive strength of the fibrin itself. Since they are unable to withstand significant tensile forces, the use of fibrin sealants is restricted to fractures where there are no mechanical forces applied to the fragments within the application site (Wanasingha et al., 2021).

There are two categories of fibrin-based adhesives: allogenic and autologous fibrin sealants. The use of autologous fibrin sealants in orthopedic surgery has significant implications (Arbes et al., 1981; Yang et al., 2013). However, due to their excellent biocompatibility, biodegradability, and cost effectiveness, fibrin-based adhesives have many advantages over synthetic-based adhesive systems like cyanoacrylates. As a result, orthopaedic surgery has made extensive use of these materials. Specific conditions must be met during clinical application for fibrin-based sealant systems to be used to their full potential. For instance, the sealant should be applied as a thin film at 37 °C and the wound surfaces should be dry. After clotting has taken place, you should avoid any additional mechanical stresses for about five minutes (Tatooles et al., 1966).

2.3.2. Gelatine Resorcinol Aldehydes

Gelatine resorcinol formaldehyde adhesives were first developed as haemostatic agents and as a tissue adhesive (Braunwald et al., 1966; Nomori et al., 1999).

Gelatine resorcinol formaldehyde adhesives have not been clinically tested as bone adhesives, in vitro testing shows that they are stronger than fibrin sealant with water resistance but less strong than many available synthetic-based adhesives. These adhesives have been reported to achieve a bond strength to bone of about 0.2 MPa in vitro (Smith D. 1973). Additionally, according to studies, these materials exhibit higher bond strength, tensile strength, and tissue compatibility when compared to methylcyanoacrylates, as well as less tissue irritation than cyanoacrylates (Kull et al., 2009). Additionally, recent research has concentrated on the improvement and modification of gelatin-based adhesives to achieve reduced swelling, enhanced degradability, and low cytotoxicity. For applications in wound healing, Liu et al. created a gelatin-based adhesive crosslinking catechol-modified gelatin (Gel-Ca) and phenol-modified gelatin (Gel-Ph). When compared to other recently reported ion-crosslinked catechol-modified gelatin adhesives, the gelatin-based adhesive showed improved mechanical and rheological properties.

2.3.3. Polysaccharides

Chitin, chitosan, chondroitin, dextran, and starch are examples of the important class of polysaccharides that are used as haemostatic and soft/hard tissue adhesives. They can produce biocompatible and biodegradable properties and are comparatively simple to prepare and apply. Chitosan-based adhesives are commercially available for bone, cartilage (Jayakumar et al., 2011), and soft tissue (Wang et al., 2007) repair and are renowned for their haemostatic properties. Chitosan and starch were combined by Hoffmann et al. (Bhatia et al., 2007) to create a bioadhesive system that could be used to close skin wounds and act as an emergency hemostasis agent. The bonding mechanism is accomplished by the creation of covalent bonds between aldehyde groups and amino groups that are either exposed in the fractured bone or present in the surrounding tissues (Hoffmann et al., 2009). This results in a powerful bonding to tissue. Additional in vitro studies showed that these adhesives, with an adhesive strength ranging from 40 MPa to 45 MPa (Bhatia et al., 2007), are biocompatible. In the first 24 hours after application, saccharide-based adhesives showed a mass loss of 10–15% (Simson et al., 2012).

For applications involving bone tissue engineering, these materials need to be further optimized to slow down the rate of degradation. Although there are a number of polysaccharide-based materials available that can be used in both wet and dry environments, their widespread use in biomedical applications is still significantly constrained by important issues with biosafety, hemostatic effect, and high cost (Li,Det al., 2020).

2.3.4. Biomimetic-Based Adhesives

Additional in vitro research revealed that these to meet specific needs to function in the natural environment (e.g., settlement, hunting, and defense), some terrestrial organisms as well as marine plants and animals combine proteins and polysaccharides to form bioadhesives (Bhagat et al., 2017). When compared to recently develop synthetic or natural polymer-based adhesives, these bioadhesives frequently exhibit higher mechanical properties, including adhesion in wet environments. These kinds of adhesives can specifically form ionic and/or covalent bonds with the surface or collagen of the bone. Research into its use as a bioadhesive for bone tissue engineering applications has been stimulated by its capacity to cure at physiological temperatures and to achieve a high bonding strength to biological materials, including bone materials. Numerous bioadhesives that resemble these plants and animals have been researched and/or developed to date, but they have not yet been put to use in bone tissue engineering applications that require clinical use. Research into the use of e materials as a bioadhesive for bone tissue engineering applications has been stimulated.

Additionally, adhesive proteins are produced by marine organisms like the blue mussel (Mytilus edulis), barnacle (Balanus hameri), and sandcastle worm (Phragmatopoma calfornica). At various salinity and humidity levels at room temperature, Mytilus edulis have the capacity to firmly attach themselves to both inorganic and organic host surfaces (Braunwald et al., 1966). Adhesion is achieved in the context of bone repair by ionic bonding between catechol hydroxyl and carboxylic acid groups of the adhesive system and Ca^{2+} that is present on the surface of bone. Technical challenges with protein extraction are caused by the complex interactions of the proteins in mussel-derived bioadhesives, which raises the cost of production and limits clinical application. The qualities of bioadhesives made from mussels have been the subject of numerous studies (Nomori et al., 1999).

The development of synthetic polymers and cell attachment proteins that resemble the elements that give mussels their strong adhesion has been the primary focus of early attempts to mimic these materials.

2.4. Bioadhesive for Bone fracture

The creation of epoxy resin-based bioadhesives, like phenol-formaldehyde resins, was a key component of early investigations into the use of bioadhesives in bone repair applications. Although these materials had a high mechanical strength, they were not biocompatible, according to reports (Kjaergard et al., 1992). Due to their high bonding strength and capacity to achieve adhesion in a wet environment, synthetic polymers based on cyanoacrylate (for example, cyacrin) and polyurethane has also been suggested as bone bioadhesives (Owen et al., 2000). Although there have been reports of high infection rates, non-union (such as fracture displacement), low biodegradation, and severe local reactions, these cyanoacrylate- and polyurethane-based bioadhesives have shown high tensile and adhesion properties. Due to the unsatisfactory clinical results of these initial materials, research has been conducted on alternative bioadhesives with better functional properties. In one of these studies, the use of a non-elastomeric crosslinked polyurethane-based bioadhesive for stabilizing and repairing bone fragments from the tibia was examined (Herget et al., 2001). Through the reaction of a polyisocyanate and polyol with a catalyst, this bioadhesive was created. Calcium and phosphate compounds were added to the bioadhesive to improve it. The stabilization and bonding of the bone fragments, as well as a de novo bone growth, were achieved in vivo, according to the results (Yang et al., 2013).

There was also some biodegradation and good biocompatibility, and there was no sign of inflammation or infection at the fracture site. Schreader et al. created a similar polyurethane-based bioadhesive for fixing bones together. This substance was a foam-like bioadhesive made of 4,4-methylene diphenyl diisocyanate (MDI) and polyol derived from caprolactone, reinforced with nanoparticles of hydroxyapatite (Yang et al., 2013; Wanasingha et al., 2021). Through the chemistry of moisture-curing polyurethane, the crosslinking took place, which may have an impact on the physical characteristics.

However, the chemistry and structure of polyol had an impact on the final physicochemical and functional properties. In comparison to traditional PMMA-based bone cement, this bioadhesive demonstrated strong bone-to-bone bonding with an adhesion strength of 4.47 MPa after 20 hours.

The development of PMMA-based bioadhesives for bone repair applications has been the subject of several studies. Due to their poor bone adhesion, particularly when used in a moist environment, these bioadhesives have primarily been used in dentistry and orthodontics. The exothermal reaction that takes place during polymerization is another problem because it can cause cellular death and necrosis of bone tissue. It has been reported that adding hydroxyapatite particles to PMMA-based bioadhesives increases their adhesive strength. The clinical use of a bioadhesive for bone repair applications has been constrained by the lack of biodegradability, despite the increase in adhesion strength (Wanasingha et al., 2021; Tatooles et al., 1966). Wistlich et al. have created a bioadhesive that exhibits improved adhesive properties, particularly in environments with high humidity, as well as improved biodegradation. They created a bioadhesive for bone repair applications by copolymerizing an isocyanate functional (six-armed) star-shaped prepolymer with ethylene oxide and propylene oxide in a ratio of 4:1 with a photocurable poly(ethylene glycol) dimethacrylate (PEGDMA) matrix. Additionally, the PEGDMA matrix was modified with biodegradable ceramic adjuvants, such as struvite ($MgNH_4PO_4 \cdot 6H_2O$), newberyite ($MgHPO_4 \cdot 3H_2O$), or gypsum ($CFaSO_4 \cdot 2H_2O$), to achieve the improved adhesive properties. These ceramic-based adjuvants increased the bioadhesive's porosity while also enhancing its adhesive properties, which encouraged the ingrowth of new bone through ion release. Additionally, this bioadhesive has demonstrated appropriate bone-to-bone adhesion in a wet environment, is simple to apply, and supports bone formation during fracture healing. It is also cytocompatible and easy to apply.

Natural polymers based on fibrin have also been used in medicine as bone adhesives because they are biocompatible, affordable, and biodegradable. In bone tissue engineering applications, these bioadhesives have been widely used, primarily for the acceleration, union, and revascularization of osteochondral fragments (Smith D. 1973). An in vivo experiment showed that tricalcium phosphate particles form a dense network of osteoid tissue. By combining ceramic granules made of macro- and micro-porous biphasic calcium phosphate (MBCP) with a fibrin-based sealant, Kul.S et al. created a bioadhesive [42]. In

particular, the osteoinductive properties of a fibrin-based sealant with 60% hydroxyapatite and 40% beta-tricalcium phosphate (-TCP) were assessed.
In between the MBCP particles, a well-mineralized ectopic bone formed, demonstrating the ability of the MBCP-fibrin-based sealant to encourage osteogenesis.
A bioadhesive was created by Cassaro et al. that contained biphasic calcium phosphate (BCP) particles, mesenchymal stem cells (MSCs), and a fibrin-based biopolymer that demonstrated haemostatic, sealant, adhesive, scaffolding, and drug-delivery properties (Liu et al., 2019). According to Cassaro et al., the bioadhesive has good biocompatibility, is cost-effective to produce, and effectively repairs fractured bone while also stimulating the growth of new bone. Bioadhesives based on polysaccharides have also been created for applications such as bone repair. For instance, Kumbar et al.'s investigation of bioadhesives derived from linear polysaccharides of D-glucose called celluloseacetate. According to this study, the polysaccharide-based bioadhesive can create adhesive bonds between cellulose and bone using carboxylic acid groups and exhibit compressive strength (27–33 MPa) that is comparable to that of human trabecular bone. Biocompatible chitosan or dextran and degradable starch were combined to create two component bioadhesives made from polysaccharides (Jayakumar et al., 2011). L-3,4-dihydroxy-l-phenylalanine (DOPA), a periodic acid, was first used to oxidize the polysaccharides in order to produce aldehyde groups, which are primarily used by mussels to adhere to the surface of rocks. A covalent bond that was created in this bioadhesive allowed for both high cohesion strength within the bioadhesive as well as a strong adhesion bond at the bone-bone interface.

Compared to fibrin glues, this bioadhesive showed superior biocompatibility and stronger mechanical properties. For bone tissue engineering applications, L-DOPA, an hydroxylated form of tyrosine, has also been combined with the functional binder (mussel-derived adhesive protein, or MAP)) to successfully retain deproteinized bovine bone mineral (DBBM) inside the bone defect (Tabatabaei et al., 2021). The formation of an aggregate by the binding of the DBBM particles was demonstrated by an evaluation of the biomechanical properties. Bone remodeling and regeneration were sped up as a result of an increase in osteoconductivity and the development of osteoinductivity, with the density of the new bone being comparable to that of the old bone. Due to their capacity to quickly achieve high adhesion in a wet environment, sandcastle worm-based adhesives have demonstrated particular promise in bone repair applications.

One such instance is a water-borne adhesive that was created by incorporating phosphate, primary amine, and catechol sidechains and was based on the proteins from the sandcastle worm-based adhesive (Hou et al., 2021).
In order to bind and stabilize bone fragments, mixtures of polymerized monoacryl oxyethyl phosphate (MAEP), dopamine methacryl-amide (DMA), acrylamide and fluoroscein isothiocyanate were used.

The resulting bioadhesive showed an adhesive strength that was 40% greater than bioadhesives based on cyanoacrylates. The sandcastle worm-based bioadhesive showed good biocompatibility and osteoconductivity in in vitro studies, and it could reassemble broken bones in a moist environment. A biodegradable bioadhesive with nearly instantaneous adhesion (10 s) was created using a sandcastle worm-derived bioadhesive made of O-phospho-L-serine, a protein found in many natural secretions (Bhatia et al., 2007). When combined with calcium phosphates, the phosphor-related amino acid O-phospho-L-serine, which is a part of osteopontin (OPN) and has a sequence resembling that of adhesion protein peptides, quickly develops into a bioadhesive with high biodegradability and mechanical strength (i.e., adhesive and cohesive strength) (Tao et al., 2021).

Another bioadhesive with a setting time of less than 10 min. and the capacity to achieve high bone-to-bone adhesive strength was created by Kirillova et al. using an alternative strategy that included O-phosphoserine and tetracalcium phosphate (Simson et al., 2021). This bioadhesive outperformed PMMA bone cements and calcium phosphate cements in terms of shear strength by a factor of ten. Both sandcastle worm-derived bioadhesives demonstrated osteointegration, bone ingrowth, and biodegradability in addition to the high adhesive strength attained.

A new class of bioadhesives with the potential to combine hard and soft tissue as well as connect hard and soft tissue to metallic and polymeric prosthetic implants was described. These bioadhesives with marine origin combined phosphoserine-modified alpha tricalcium phosphate powder.

Phosphoserine is mainly found in phosphoproteins that are involved in a variety of biological processes, such as adhesion, which is accomplished by marine-based bioadhesives, tissue adhesion, cohesion, and load dissipation in animals, and biomineralization, which is accomplished by matrix proteins and matrix vesicles (Li D et al., 2020).
The adhesive strength of these bioadhesives was reported to be 2.5–4 MPa in a subsequent study, which is 40–fold greater than that of commercial cyanoacrylates (0.1 MPa) and 100–fold greater than that of surgical fibrin glue (0.04 MPa) (Kumbar et al., 2022).
It has been demonstrated that these bioadhesives are effective at bonding soft tissue (such as skin) ex vivo. Within 30 minutes, the bioadhesive provided bond strengths of 200 kPa, and after 90 minutes, the bond strengths were close to 332 kPa.

The phosphoserine based bioadhesive had a bond strength that was 44 times greater than that of fibrin-based bioadhesives and three times greater than those made from mussels. Ex vivo evaluation of the biodegradation behavior of phosphoserine-based bioadhesives showed that the rate of degradation decreased as the adhesive's density (lower porosity) and surface area increased (Tabatabaei et al., 2021). An efficient bioadhesive for bone tissue engineering applications must have high mechanical strength, minimal biodegradation, and retention of bond strength during the first few days and weeks after fracture stabilization. In addition to exhibiting amorphous calcium phosphate and metastable alpha-tricalcium phosphate on its surface, the phosphoserine-based bioadhesive displayed a relatively high bond strength (39–50 MPa) and slow biodegradation (8–14% mass loss after 14 days) until the formation of new hard tissue. The first in vivo biological safety evaluation of a different phosphoserine-based bioadhesive for bone tissue engineering applications was shown also (Hou et al., 2021).

The study showed that there was no evidence of redness, swelling, inflammation, fibrotic tissue, disruption, or bleeding in any of the phosphoserine-based bioadhesives that were investigated. Instead, all of them supported a rate of cell proliferation of 45–64%. The absence of ectopic bone formation and the absence of an augmented immune response, as shown in this study, support the highly desirable properties of sandcastle worm adhesives for gluing bone fragments together successfully while successfully directing osteogenesis to promote bone repair and regeneration.

2.5. Preparation of Bio-based Adhesive

The conclusion that there are two main processes used to produce a bio-adhesive, namely polymerization and cross-linking; can be drawn from the numerous studies that have been conducted to examine the bioadhesive synthesis and preparation (Guo et al., 2020; Bu Y et al., 2022; Zussma et al., 2022). The cross-linking procedure typically makes use of one or more types of bonds that may form during the reaction.
Some of examples are; hydrogen bonds, ionic bonds, host-guest interactions, hydrophobic bonds, imine bonds, disulfide bonds, Acylhydrazone bonds, Diels-Alder reactions, boronate bonds, and oxime bonds (Hyldbakk et al., 2022) Poly (methyl methacrylate)s (PMMA) have been used extensively in orthopedic surgery and orthodontics.

PMMA is made by polymerizing methyl methacrylate (MMA) using a free radical process with an azo compound or peroxide as the initiator. Commercially, polymerization can be carried out in the following forms: granular, liquid, suspension, or emulsion. After combining these components, which solidify through monomer radicals or anionic polymerization (Gellynck et al., 2011; Yu Y et al., 2021; Kumar et al., 2022), a viscous paste will be created. Alkyl 2-cyanoacrylates are currently the most extensively studied and utilized class of bone adhesives. The alkyl chain's length can be changed to create a wide variety of different 2-cyanoacrylate esters. Due to these materials' extreme reactivity, the polymerization process can be carried out at room temperature without the use of a heating step, a catalyst, or the application of pressure. The anionic polymerization of the monomers, which is triggered by water, is the first step in the reaction that must occur in order to produce these materials. Weak bases like water or amines can attack the acrylate bond nucleophilically to break it.
An electron-withdrawing nitrile group polarizes the acrylate bond to achieve bio-adhesion to bone. Because of this, weak bases like the amines present in the collagenous matrix of bone tissues can attack the acrylate bond nucleophilically. Alkyl chains with longer lengths tend to polymerize more quickly, have stronger bonds with bone tissues, and form chains that are more flexible (Bu. Y et al.,2022).

The most popular technique for making fibrin-based adhesive systems involves mixing a solution with a fibrinogen source or with another separate solution made up of thrombin source (from bovine, human, or recombinant), anti-fibrinolytic agent, and calcium to slow down rapid fibrinolysis. When combined, these elements result in the development of a clot devoid of cells. Thrombin breaks down fibrinogen during this process, releasing soluble fibrin monomers (Zussma et al., 2022). Following the formation of loosely aggregated fibrils by hydrogen bonding, these monomers self-assemble into a more durable cross-linked fibrin polymer by covalent bonding. Additionally, factor XIII is activated by thrombin, and when calcium is present, this allows for the covalent bonding of fibrin polymer chains.

Before using this biomaterials-based adhesive, though, there must be a lot of preparation (Pei et al., 2021).

Chitosan served as the amino-group carrier during the oxidation of starch with periodic acid to produce aldehyde side groups (Chopra et al., 2020). Amino groups from the surrounding tissues will react with aldehyde groups in the bio-based adhesive system in a way similar to how chitosan does. The two components form a Schiff's base when combined in water, resulting in a covalent cross-linking that enables a powerful adhesion to tissue. Covalent bonds are produced in order to achieve this. Any other exposed amino groups, such as those found in broken bone, for instance, or those present in the bio-based glue, had the potential to form bonds with it. Additionally, starch or dextran compounds can be conjugated with 3,4-dihydroxyphenylalanine (DOPA) to increase the bio-adhesion strength to bone (Fernandez., 2021; Km et al., 2020).

According to a study, the production of bio-mimetic adhesive complexes uses the free radical copolymerization of monoacryloxyethyl phosphate (MAEP), dopamine methacrylate (DMA), and acrylamide (Aam). This bio-based adhesive demonstrated suitability for use in the reconstruction of craniofacial fractures and has the ability to bind wet bones together both in vitro and in vivo.

Table 2.1: Summary of Bio-adhesive Materials, Preparation, Medical Properties, and Applications

No.	Materials	Preparation	Medical Properties	Reference
1	-Chitosan graft polypeptide -N-carboxyanhydrides (NCAs)—3,4-dihydroxyphenylalanine-Ncarboxyanhydride (DOPA-NCA)	Ring Opening Polymerization	*Lap-shear adhesion strength 195.97 ± 21.1 kPa and 3080 ± 320 kPa *Tensile adhesion strength 642.70 ± 61.1 kPa	(Chopra et al., 2020)
2.	-Soybean,Xanthan Gum, Calcium Chloride and Ethyl ether	Polymerization	*Adhesion strength 361 kPa	(Fernandez., 2021)
3.	-Polysaccharide-based hydrogels,Carboxymethyl chitosan , Modified sodium alginate and Tannic acid	Cross linking	*Adhesion strength 162.6 kPa	(Kim et al., 2020)
4.	-Multifunctional gelatin based adhesive double-network hydrogel (DNGel)	Cross-linking	*Adhesive strength 3.75 MPa	(Tao et al., 2021)

5.	-Dopamine-conjugatedialdehyde−HA (DAHA) hydrogels	Cross-linking	*Adhesive strength of 90.0 ± 6.7 kPa	(Negrescu et al., 2022)
6.	-Silk fibroin (SF), Poly(ethylene glycol) (PEG)	Cross-linking	* Tensile strength of 16.54 kPa	(Scalzone et al., 2020)
9.	-Chitosan-based Adhesive	Cross-linking	*Tensile strength 0.024 ± 0.0036 MPa, *Shear strength 0.031 ± 0.0069 MPa *Fracture toughness 2.38 ± 0.54 J/m2	(Zou et al., 2022)
10	-3,4-dihydroxyphenyl propionic acid (DPA) , Chitosan (CS)	Cross-linking	*Adhesive strength150 kPa	(Moon et al., 2021)
11.	-Dopamine (DA) , Sodium carboxymethyl cellulose (CMC) and Catechol- modified CMC–DA	-Carbodiimide chemistry method - Crosslinking	* Adhesion strength 11.37 ± 2.62 kPa	(Pei et al., 2021)
12.	-Chitosan Protocatechuic acid (PCA)	Michael-type addition	* Adhesion strength of 4.56 ± 0.54 MPa	(Tabatabeai et al., 2021)
13	-Lactic acid, C.macrostachyus leaf extract (The current study)	Polycondensation reaction	---	---

2.6. *Croton macrostachyus* (Bsana)

2.6.1. Botanical and Ecological Information of *C. macrostachyus*

Croton macrostachyus is commonly known as rush foil or broad-leaved Croton in English and Bisana in Amharic (Breitenbach., 1993). It belongs to the Euphorbiaceae, a very large family with 300 genera and 8,000 to 10,000 species, and is the most numerous in the tropics (Heywood., 1993). The name of the genus Croton comes from a Greek word Kroton, which means ticks, because of the seeds' resemblance to ticks. The genus contains over 1,200 species, which are distributed throughout the world (Mairura et al., 2007). Eight of these species (C. dichogamus, C. zambesicus, C. menyhartii, C. somalense, C.schimperianus, C. sylvaticus, C. lobatus, and C. macrostachyus) are found in Ethiopia, but the most common species is Croton macrostachyus. The name of the species is from the Greek macro – (large) and – stachyus (relating to spike), hence, macrostachyus means "with a large spike" (Amare et al., 2010).

Croton macrostachyus is native to Eritrea, Ethiopia, Kenya, Tanzania, Uganda and Nigeria. It is a medium sized deciduous tree of East Africa particularly wide spread between 200-2500 m in mountainous forests and savannah of the tropical regions and ever green bush land areas that receive between 700-2000 mm rainfalls annually (Kapingu et al., 2000).

Figure 2.2: Picture of Leaf of *C. macrostachyus*

2.6.2. The Role *C. macrostachyus* in Traditional Medicine

In areas where it is native, the plant parts are used for treatment of cough (boiled leaf decoction), venereal diseases and tapeworm (root decoction, crushed seeds and leaves in water), to hasten clotting of wounds (fresh leaves juice), remedy for skin rash (Bark from the stems and roots is boiled in water), and as abortifacient and uterotonic (Bark maceration and seed) (Matu et al., 2003; Berry., 2000; Kapingu et al., 2000). *C. marcostachyus*, which is widely distributed throughout tropical Africa, is endowed with a number of ethnomedicinal uses in Ethiopia. Traditionally, the leaves are used to treat Diabetes mellitus (Mazzanti et al., 1987), scabies, hepatitis, jaundice, Tinea versicolor, and as an anti-dote for snake and scorpion venom (Tefera., 2006).
In addition to this, it is used to treat fever, edema (leaves or young shoots), hemorrhoids (mashed leaves), ear problems (seedpreparations) diarrhea (leaves powder mixed with water) (Megersa, 2010; Salatino et al., 2007).

Ethnopharmacological studies revealed that hydroalcoholic extracts of C.macrostachyus leaves has shown promising activity against Neisseria gonorrhoeae (Taniguchi, 1993), Plasmodium berghei and Mycobacterium tuberculosis (Kelecha, 1977). Apart from this, it has analgesic and antiinflammatory (aqueous and methylene chloride/methanol stem bark extracts) (Matu & Van, 2003), anti-convulsant and sedative (bark decoction) (Abebe, 1986)and anti-leishmanial activities (crotepoxide, isolated compound from berries) (Tariku et al., 2010).

2.6.3. Phytochemical Information of *C. macrostachyus*

Phytochemical studies on the genus Croton showed the presence of secondary metabolites such as alkaloids, terpenoids, and flavonoids. Amongst them, diterpenoids are the predominant phytochemical constituents in the genus (Mazzanti et al., 1987); fourteen secondary metabolites have been isolated from C. macrostachyus and five of them were isolated from the genus for the first time. The compounds include phenolic and triterpenes of the lupane and hopane groups (Zelalem, 2007).
Much research has not been done concerning the chemical composition of Croton macrostachyus (Mairura, 2007) but phytochemical study on the genus Croton has lead to the isolation and characterization of different classes of secondary metabolites.

Terpenes, flavonoids and alkaloids have been isolated from the different croton species. Terpenoids are the predominant secondary metabolite constituents in the genus, chiefly diterpenoids, which may belong to the clerodane, neoclerodane, kaurane, labdane, phorbol and trachylobane skeletal types. Triterpenoids, either pentacyclic or steroidal, have frequently been reported for croton species. Apparently, clerodane is the widest spread class of diterpenoids in croton, which has been found in species from America (e.g. C. cajucara), Africa (e.g. C. macrostachyus) and Asia (e.g. C. tiglium) (Amare, 2010).

Several species of the genus are aromatic, indicating the presence of volatile oil constituents. As most Euphorbiaceae, croton species may contain latex, which is red-coloured in some species, a characteristic usually with medicinal properties (Tala et al., 20).

2.7. Lactic Acid

Lactic acid (IUPAC systematic name: 2-hydroxy-propanoic acid), an organic acid obtained by fermenting glucose or maltose or taken from milk), is a viable alternative to petroleum raw materials (Komesu et al., 2017). Optimally preferably pure lactic acid is now created by the batch fermentation process of maize and other carbohydrates (Martinez et al., 2013). $C_3H_6O_3$ is the chemical formula for this carboxylic acid. It's an alpha hydroxy acid since it has a hydroxyl group next to the carboxyl group (AHA). It can lose a proton from the acidic group in the solution, resulting in the lactate ion (CH_3CH (OH) COO-). Two optical isomers of lactic acid exist L-(+)-lactic acid, also known as (S)-lactic acid, is one, while D-(-)-lactic acid, also known as (R)-lactic acid, is the other. The biologically relevant isomer is L- (+)-lactic acid. The chiral carbon atom has a hydroxyl group connected to it, whereas one of the terminal carbon atoms belongs to the carboxylic group and the other to the methyl group. As a result, lactic acid exists in two optically active isomeric forms (Martinez et al., 2013).

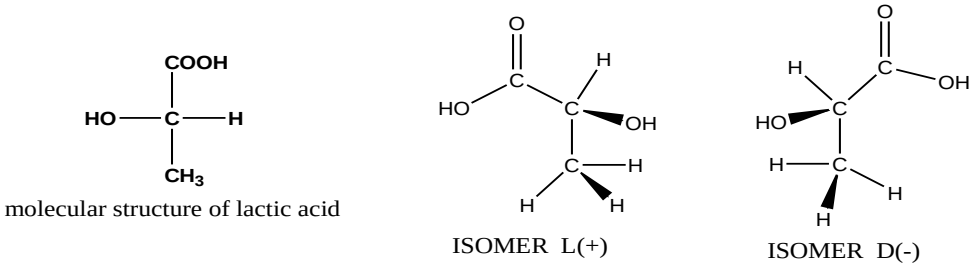

Figure 2.3: Molecular Structure and the Stereoisomers of Lactic Acid

Lactic acid is colorless to yellow liquid after melting, sour in taste, odorless and soluble in all proportions in water, alcohol and ether but not in chloroform (Marayanan, 2004). It is a weak acid with low instability. The two functional groups (hydroxyl and carboxyl) present in lactic acid permits a wide variety of chemical reactions for it. The main classes of these reactions include oxidation, reduction, condensation and substitutions (Rashid, 2008).In solutions with roughly 20% or more lactic acid, self-esterification occurs because of the hydroxyl and carboxyl functional groups and it may form a cyclic dimmer (lactide) or more linear polymers (Holten et al.,1971; Champomier et al., 2002).

Unlike in adhesive industries, lactic acid is currently the most extensively used organic acid in the food, pharmaceutical, cosmetics, and chemical industries (Marayanan, 2004) that can be used as neutralizers, solvents, cleaning agents , and employed to make biodegradable polymers with medicinal applications (Komesuet al., 2017). But there are few papers which are published on the synthesis of lactic acid-based adhesives as shown in Table 2.2.

Table 2.2: Related Works on Lactic Acid-based Adhesives

Author	**Types of Adhesives**	**Ingredients**	**Method**	**Title**
(Tripathi, and V. Katiyar, 2018)	Structural (Glass, Ceramic)	LA, Gum Arabic	Graft co-polymerization	L-LA (88% aqueous solution) and Gum Acacia (gum Arabic)
(Moini, N., et al.,2019)	Structural (Steel)	LA, amidosulfunic acid and methyl methacrylate	Insitu Polycondensation Reaction	Engineered Green Adhesives Based on Demands: Star-Shaped Glycerol – LA Oligomers
(Sweah, Z.J. and A.J. Mohammed, 2021)	Structural (wood)	PVA , aloe Vera gel, lactic acid	Mixing	Study of mechanical properties behavior of biodegradable blends based on wood adhesive, LA, PVA alcohol, and aloe Vera

3. MATERIALS AND METHODS

3.1. Materials and Consumables

L-lactic acid (88% aqueous solution) and n-hexane were purchased from the local market. Leaf of *C. macrostachyus* (CM) was collected from the forest around Adama city, and the animal bone, as well as the glass substrate used in this study, was sourced from a butcher and mirror shop respectively in Adama City, which were utilized in the tensile test. All the chemicals used in this study were analytical grade and purified. Those chemicals and materials are listed below the table in a well-organized way.

Table 3.1: Summary of Materials and Consumables for the Experimental Work

Final Products	**Chemicals**	**Equipment/Materials**
Extraction of Croton Macrostachyus (Bsana)	Tap water, Distilled water, Hexane, dried leaf powder of *C. macrostachyus*	Flask, Soxhlet apparatus, Erlimiyer flask, round bottom flask, filter paper, rotavapour, chiller and Condenser
Oligomerization of Lactic Acid	Lactic Acid (88% aqueous solution)	Oven, Horizontal Condenser, RBF, cylinder, chiller.
phytochemical screening of CM and OLLA -m-CM	Mayer's reagent, NaOH, H_2SO_4, $FeCl_3$, $CuSO_4$	Balance, test tubes, crude extract
Anti-bacterial study	DMSO, distilled water	Petri dishes, OLLA-m-CM, CM,OLLA
Synthesis of OLLA -m-CM bio-conjugate	Lactic acid (88% aqueous solution)	CM leaf extract, RBF, measuring cylinder, horizontal condenser, oven, spatula

3.2. Methods

3.2.1. Natural Product Preparation

The *C. macrostachyus* leaf used in this investigation was collected randomly at varying stages of maturation (oldest, medium, and youngest trees) from the forest around Adama. Afterward, they were packed in polythene bags and transported to the chemical engineering laboratory at Adama Science and Technology University. The collected *C. macrostachyus* leaf was cleaned and air-dried for 4 days. The air-dried Croton macrostachyus leaf was ground into powdered form using a grinder to increase the surface area for oil recovery and screened to pass through a 60-mm mesh sieve to achieve uniform particles. The powdered particles were then sealed in glass bottles for further analysis and recovery of oil (Matu & Van, 2003).

3.2.2. Extraction and Optimization

In this study, the crude oil extract was optimized using response-surface methodology. Moreover, three variables, extraction temperature, extraction time, and mixing ratio, were selected and analyzed using the Box-Benhken method.

Although several studies have been carried out on extracting crude oil from *C. macrostachyus*, there is a shortage of information on the optimum conditions for oil extraction. The present study was therefore undertaken to model the yield of oil from *C. macrostachyus* via Soxhlet extraction, considering the interaction of extraction temperature, the mass of *C. macrostachyus* to the volume of extraction solvent (mixing ratio) and extraction time as process parameters, using RSM in order to determine the optimal extraction conditions.

The factor level used for the optimization was derived from the previous undergraduate final year project work in the chemical engineering department at Adama Science and Technology University in 2020.

This study employed the Design-Expert software for experimental design and data analysis yield. Table 3.2 presents the coded levels of independent variables. Moreover, the design included 17 runs, as shown in Table 3.3.

Table 3.2: Level of Each Factor

S.no	Factor	Unit	Level	
			Low	High
1	Temperature	ºC	45.0	75.0
2	Time	hr	3:00	5:50
3	Mixing ratio	Wt/Wt%	0.20	0.36

Table 3.3: Box Behnken Arrangement and Response for Yield Extraction

	Factor 1	Factor 2	Factor 3	Response
Run	A: Time (Hr.)	B: Temperature (ºC)	C: Mixing Ratio(Wt/Wt%)	Yield (%)
1	4.25	60	0.28	
2	4.25	45	0.2	
3	4.25	60	0.28	
4	3	45	0.28	
5	5.5	75	0.28	
6	4.25	75	0.2	
7	4.25	60	0.28	
8	5.5	60	0.2	
9	5.5	60	0.36	
10	3	60	0.2	
11	4.25	45	0.36	
12	4.25	60	0.28	
13	4.25	60	0.28	
14	3	75	0.28	
15	4.25	75	0.36	
16	3	60	0.36	
17	5.5	45	0.28	

3.2.3. Investigation of Preliminary Phytochemical Screening of CM extract

Detections of common secondary metabolites were performed on crude extract of leaves of *C. macrostachyus* using the preceding analytical procedures (Salem et al., 2013).

Test for Terpenes (Salkowski test): 2 mL of crude extract was mixed with 2 mL of chloroform and 3 mL of concentrated H_2SO_4 was added carefully to form a layer. Reddish-brown coloration of the interface indicates the presence of terpenes.

Test for Flavonoids (Shinoda Test): Four pieces of Magnesium fillings (ribbon) were added to the extract in the test tubes, followed by a few drops of concentrated hydrochloric acid. A pink or reddish color indicates the presence of flavonoids.

Test for saponins (Froth Test): To 2 mL of crude extract, 5 mL of distilled water was added to a test tube. Then, the solution was shaken vigorously and observed for a stable persistent froth. The formation of froth indicates the presence of Saponins.

Test for Tannins: 5 mL of crude extract was mixed and filtered in 10 mL distilled water. 1% aqueous Iron chloride ($FeCl_3$) solution was added to the filtrate. Dark-green solution indicates the presence of tannins.

Test for alkaloids (Wagner's Test): The extract was stirred separately with 1% HCl (6 ml) in a water bath for 5 min and filtered into test tubes. Few drops of Wagner's reagent (Iodine in potassium iodide) were added; a brown/reddish colored precipitate indicates the presence of alkaloids.

Test for Phenols: To 1 mL of crude extract of sample, 2 mL of distilled water followed by a few drops of 10 % aqueous ferric chloride solution were added. The formation of blue, green, or blue-black color indicated the presence of phenols.

3.2.4. Characterization of CM extract

GC-MS Analysis and Conditions

The crude oil that was obtained from the optimized conditions was analyzed using gas chromatography coupled mass spectrometer. The gas chromatography was equipped with a 30-m DB-5 (5% biphenyl+95% methyl polysiloxane) fusedsilica capillary column, 0.53mm I.D., and 1.5μm film thicknesses. Besides, Helium (99.999% purity) was used as carrier gas with a flow rate of 1.2 mL/min. The temperatures of the injector and detector were set at 250° C and 300° C, respectively. Oven temperature program was 100° C for 1 min, increased to 200° C at a rate of 4° C/min held for 2 min, and raised at a rate of 1° C/min to 250° C and held for 2 min, and finally raised at a rate of 4° C/min to 300° C and held for 3 min. Moreover, the structures were determined using a mass spectrometer (HP5970, USA) operating in EI mode at 70eV. The interface temperature was 250° C. Mass range was 30-600 amu (Majidi et al., 2019; Ghasemi et al., 2010). The sample (1 μL) was injected with a split ratio of 1/10. The library searches and spectral matching of the components were conducted on the NIST MS 2.0 database.

Functional Group Analysis

The functional groups available in the crude extract of *C. macrostachyus* were determined using Fourier transform spectroscopy (FTIR). Fourier transform spectrophotometer measured on Spectrum 65 FT-IR (PerkinElmer) in the range 4000-400 cm^{-1} (resolution 4 cm^{-1}, number of scans 4) using KBr pellets.

Thermal Property Analysis

The TGA was performed in order to determine the thermal degradation temperature of the crude extract of *C. macrostachyus*. Samples were heated from 30°C to 700 °C at 5, 10, 15 and 20 °C/min heating rates under a nitrogen (N_2) atmosphere.

3.2.5. Synthesis of Lactic Acid Oligomer

As a control system, lactic acid oligomer was synthesized by polycondensation reaction. The reaction temperature was set at 170 ^{o}C because experimental reports for lactic acid polymerization in the temperature range of 130 ^{o}C -180 ^{o}C are available (Narayanan, 2004; C. Miller et al., 2019; S.Figalla et al., 2018). The lactic acid (88%) undergoes step-growth polycondensation reaction, forming ester bonds and releasing water as a byproduct, as shown in Figure 3.1. The reaction setup for oligomerization of L-Lactic acid was also shown in Figure 3.2.

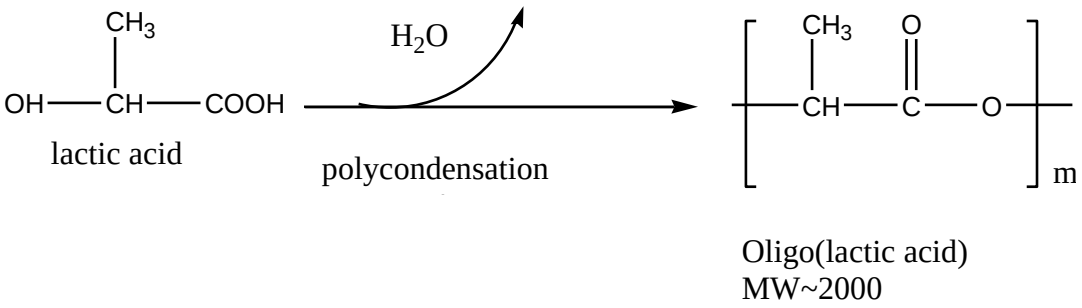

Figure 3.1: Production Scheme of OLLA

Figure 3.2: Reaction Setup for Oligomerization of L-Lactic Acid

3.2.6. Synthesis of OLLA-m-CM Bio-adhesive

The desired amount of lactic acid and *C. macrostachyus* leaf extract (as tabulated in Table 3.4) was initially taken into the reactor vessel and mixed using a spoon. After the reactor setup was installed polycondensation reaction was conducted by adjusting time and temperature on a fixed value. The experiment was repeated by varying the mixing ratio until to do the desired number of experiments. As a result, OLLA-m-CM was synthesized after the completion of the reaction. Finally, the synthesized material, i.e., OLLA- m-CM was converted into a high viscous liquid form upon cooling, which will be kept in a sealed container for further analysis (Tripathi &V. Katiyar, 2018).

The reaction setup for oligomerization of L-Lactic acid-modified C.macrostachyus leaf extract is shown in Figure 3.3.

Table 3.4: Reaction Condition for the Synthesis of OLLA -m-CM Bio-adhesive

Reaction time (hr)	Reaction temperature (°C)	Mixing ratio (mg/ml)	Product
For 5 hrs	At 170 °C	500:10	OLLA -m-CM 0
		500:30	OLLA -m-CM 1
		500:50	OLLA -m-CM 2
		500:70	OLLA -m-CM 3
		500:90	OLLA -m-CM 4

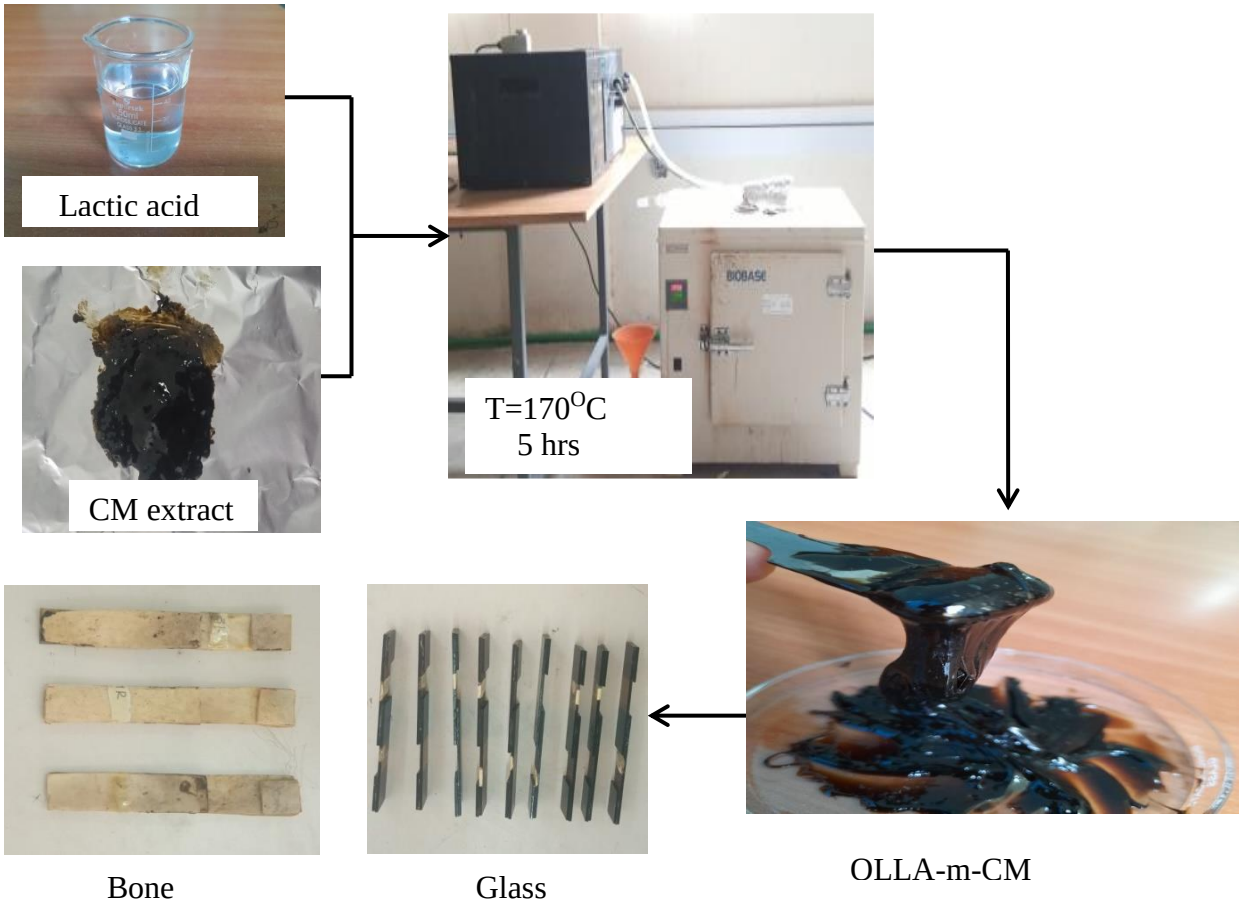

Figure 3.3: Synthesis of OLLA-m-CM with Dfferent Mixing Ratio

Since the bond strength of the synthesized adhesive of OLLA-m-CM 0 and OLLA-m-CM 4 have a lubricant property rather than adhesive property, further analysis weren't performed.

3.3. Characterization of OLLA-m-CM Bio-adhesive

3.3.1. Functional Group Analysis

The functional groups available in the OLLA, OLLA-m-CM 1, OLLA-m-CM 2, and OLLA-m-CM 3 were determined using Fourier transform spectroscopy (FTIR). Fourier transform spectrophotometer measured on Spectrum 65 FT-IR (PerkinElmer) in the range 4000-400 cm^{-1} (resolution 4 cm^{-1}, number of scans 4) using KBr pellets.

3.3.2. Water Contact Angle

The water contact angle measurement was performed in this study work by dropping distilled water on the three synthesized OLLA-m-CM bio-adhesive poured on a substrate, which is typically used to explain the surface wettability behavior of the adhesive (Le, P & K.T. Nguyen, 2020). A high-resolution camera was used, and the photograph was managed to be captured and analyzed accordingly using ImageJ software.

3.3.3. Antibacterial Test

The in vitro antibacterial activity of leaf extract of *C.macrostachyus*, OLLA and synthesized OLLA-m-CM bio-adhesives were determined by disk diffusion method (J.A. Kiehlbauch et al., 2000). The medium was prepared by dissolving 38 hm of Muller Hinton Agar medium (MHA) in 1000 mL of distilled water and autoclaved at 121 °C for 15 minutes. The autoclaved media was poured into sterile plates (20-25 mL/plate) and the plates were allowed to solidify. After solidification, the plate was seeded with an overnight grown culture of approximately $1.5*10^8$ CFU/mL by swabbing evenly onto the surface of the medium with a sterile swab. The samples under investigation, which are a leaf extract of *C. macrostachyus*, OLLA, and synthesized OLLA-m-CM bio-adhesives at a concentration of 1 mg/mL, were prepared by dissolving in DMSO. Whatman filter paper number 1 was used to prepare discs approximately 6 mm in diameter. The sterile discs were infused with the samples under and positioned on the surface of the medium with sterile forceps and gently pressed down to ensure contact with MHA. Ampicillin was used as a positive control and the plates were inverted and incubated at 37 for 24 hours. After the incubation, the inhibition zone produced by the six samples, including the positive control, was evaluated by measuring the diameter in (mm) of the clear visible zone around the disc against each test sample using a ruler without opening the lid.

3.3.4. Tensile Strength Test

Preparation of specimens: A Test specimen was constructed under the procedure of the ASTM standard method. The specimens were prepared from glass and bone substrates using ASTM standards (ASTM D1002), as shown in Figure 3.4.

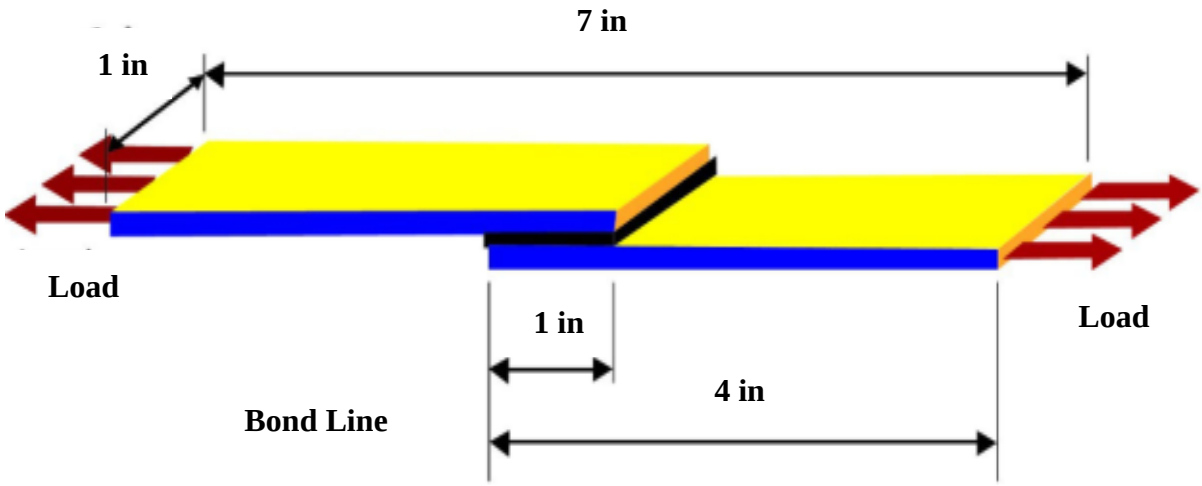

Figure 3.4**:** Geometry of Specimen Preparation

4. RESULTS AND DISCUSSION

4.1. Optimization of Crude Oil Extraction from *C. macrostachyus*

The oil content of *C. macrostachyus* leaf varied from 8.1 to 11.7% (Table 4.2), which was lower than *C. macrostachyus* extracted using the ultrasound-assisted extraction method because the ultrasonic power's intensity caused additional vibration in the sample particles, allowing the solvent to penetrate deeper into the tissue and aiding the recovery of the target component from the solid material to the liquid solvent phase, which leads to high extraction efficiency (Ermias et al., 2021), which is 3.09 to 38.46%.

4.1.1. Statistical Analysis

Table 4.1: Design Experiment Response

Response	Name	Unit	Observations	Analysis	Mini	Max.	Mean	Std. Dev.	Ratio	Model
R1	Yield	%	17	Polynomial	8.1	11.7	9.88	1.32	1.44	Quadratic

Table 4.2: Box Behnken Arrangement and Response for Extraction Yield

	Factor 1	Factor 2	Factor 3	Response 1
Run	A: Time	B: Temperature	C: Mixing Ratio	Yield
	Hrs.	^{o}C	Wt/Wt%	%
1	4.25	60	0.28	11.7
2	4.25	45	0.2	9.5
3	4.25	60	0.28	11.5
4	3	45	0.28	9
5	5.5	75	0.28	9.7
6	4.25	75	0.2	9.7
7	4.25	60	0.28	11.6
8	5.5	60	0.2	9.5
9	5.5	60	0.36	8.5
10	3	60	0.2	9.3
11	4.25	45	0.36	8.3
12	4.25	60	0.28	11.3
13	4.25	60	0.28	11.4
14	3	75	0.28	9.6
15	4.25	75	0.36	8.4
16	3	60	0.36	8.1
17	5.5	45	0.28	9.8

4.1.2. ANOVA for Quadratic Model

Analysis of Variance

The experimental results of the influence of three factors, time, temperature and mixing ratio, were designed using the box Behnken of ANOVA. As shown in Table 4.3 below, As can be seen from the **p-values** of the model coefficients, the values of time, temperature, and mixing ratio are much less than 0.0001. This indicated that all factors have a significant effect in determining the model.

The **Model F-value** of 7999.54 implies the model is significant. There is only a 0.01% chance that an F-value this large could occur due to noise.

P-**Values** less than 0.0500 indicate model terms are significant. In this case, A, B, C, AB, AC, BC, A^2, B^2, and C^2 are significant model terms. The values greater than 0.1000 indicate the model terms are not significant.

Another useful statistic here was the one labeled "Adeq Precision". This is a kind of signal-to-noise ratio that measures the ratio of the range of variation in the predicted response to an estimate of the standard error of the predictions and is obtained by subtracting the minimum predicted value from the maximum predicted value and then dividing by the average standard deviation of a prediction.

As shown in the table below, With respect to the above model, the Predicted R^2 of 0.9984 is in reasonable agreement with the Adjusted R^2 of 0.9998; i.e., the difference is less than 0.2. Adeq Precision measures the signal-to-noise ratio. A ratio greater than 4 is desirable. The ratio of 228.538 indicates an adequate signal. This model can be used to navigate the design space.

Table 4.3: Fit Statistics

Std. Dev.	0.0189	**R^2**	0.9999
Mean	9.87	**Adjusted R^2**	0.9998
C.V. %	0.1915	**Predicted R^2**	0.9984
		Adeq Precision	228.5385

Table 4.4: Analysis of Variance (ANOVA)

Source	Sum of Squares	Df	Mean Square	F-value	p-value	
Model	25.71	9	2.86	7999.54	< 0.0001	**Significant**
A-Time	0.0313	1	0.0313	87.50	< 0.0001	
B-Temperature	0.5000	1	0.5000	1400.00	< 0.0001	
C-Mixing Ratio	0.7813	1	0.7813	2187.50	< 0.0001	
AB	0.0400	1	0.0400	112.00	< 0.0001	
AC	0.0025	1	0.0025	7.00	0.0331	
BC	0.0400	1	0.0400	112.00	< 0.0001	
A^2	4.53	1	4.53	12690.26	< 0.0001	
B^2	6.71	1	6.71	18791.32	< 0.0001	
C^2	10.61	1	10.61	29711.32	< 0.0001	
Residual	0.0025	7	0.0004			
Lack of Fit	0.0025	3	0.0008			
Pure Error	0.0000	4	0.0000			

The coefficient estimate in Table 4.5 represents the expected change in response per unit change in factor value when all remaining factors are held constant. The intercept in an orthogonal design is the overall average response of all the runs. The coefficients are adjustments around that average based on the factor settings. When the factors are orthogonal, the VIFs are 1; VIFs greater than 1 indicate multi-collinearity. The higher the VIF, the more severe the correlation of factors. As a rough rule, VIFs less than 10 are tolerable.

Final Equation in Terms of Coded Factors

Yield = **+11.7 + 0.0625A + -0.25B+ -0.3125C+ -0.1AB+ -0.025AC+ 0.1BC+ -1.0375A^2+ -1.2625B^2+ - 1.5875C^2**

The equation in terms of coded factors can be used to make predictions about the response for given levels of each factor. By default, the high levels of the factors are coded as +1, and the low levels are coded as -1. The coded equation is useful for identifying the relative impact of the factors by comparing the factor coefficients.

Table 4.5: Coefficients in Terms of Coded Factors

Factor	Coefficient Estimate	Df	Standard Error	95% CI Low	95% CI High	VIF
Intercept	11.70	1	0.0085	11.68	11.72	
A-Time	0.0625	1	0.0067	0.0467	0.0783	1.0000
B-Temperature	-0.2500	1	0.0067	-0.2658	-0.2342	1.0000
C-Mixing Ratio	-0.3125	1	0.0067	-0.3283	-0.2967	1.0000
AB	-0.1000	1	0.0094	-0.1223	-0.0777	1.0000
AC	-0.0250	1	0.0094	-0.0473	-0.0027	1.0000
BC	0.1000	1	0.0094	0.0777	0.1223	1.0000
A^2	-1.04	1	0.0092	-1.06	-1.02	1.01
B^2	-1.26	1	0.0092	-1.28	-1.24	1.01
C^2	-1.59	1	0.0092	-1.61	-1.57	1.01

Final Equation in Terms of Actual Factors

Yield = -38.3166 + 6.084 * Time + 0.656 * Temperature + 131.062 * Mixing Ratio + -0.00533333 * Time * Temperature + -0.25 * Time * Mixing Ratio + 0.0833333 * Temperature * Mixing Ratio + -0.664 * $Time^2$ + -0.00561111 * $Temperature^2$ + -248.047 * $Mixing\ Ratio^2$

The equation in terms of actual factors can be used to make predictions about the response for given levels of each factor. Here, the levels should be specified in the original units for each factor.

This equation should not be used to determine the relative impact of each factor because the coefficients are scaled to accommodate the units of each factor and the intercept is not at the center of the design space.

4.1.3. Diagnostics and Contour Plots

The residual plots are the main notes that offer the usual range of residual plots for checking assumptions such as Normality and constant variance. The Box-Cox plot for power transformations helps us decide whether we could improve the model's fit by measuring the response on a different scale, e.g., by using the log of the response values. Plots of leverage and influence statistics show the influence of individual data points on the fitted model.

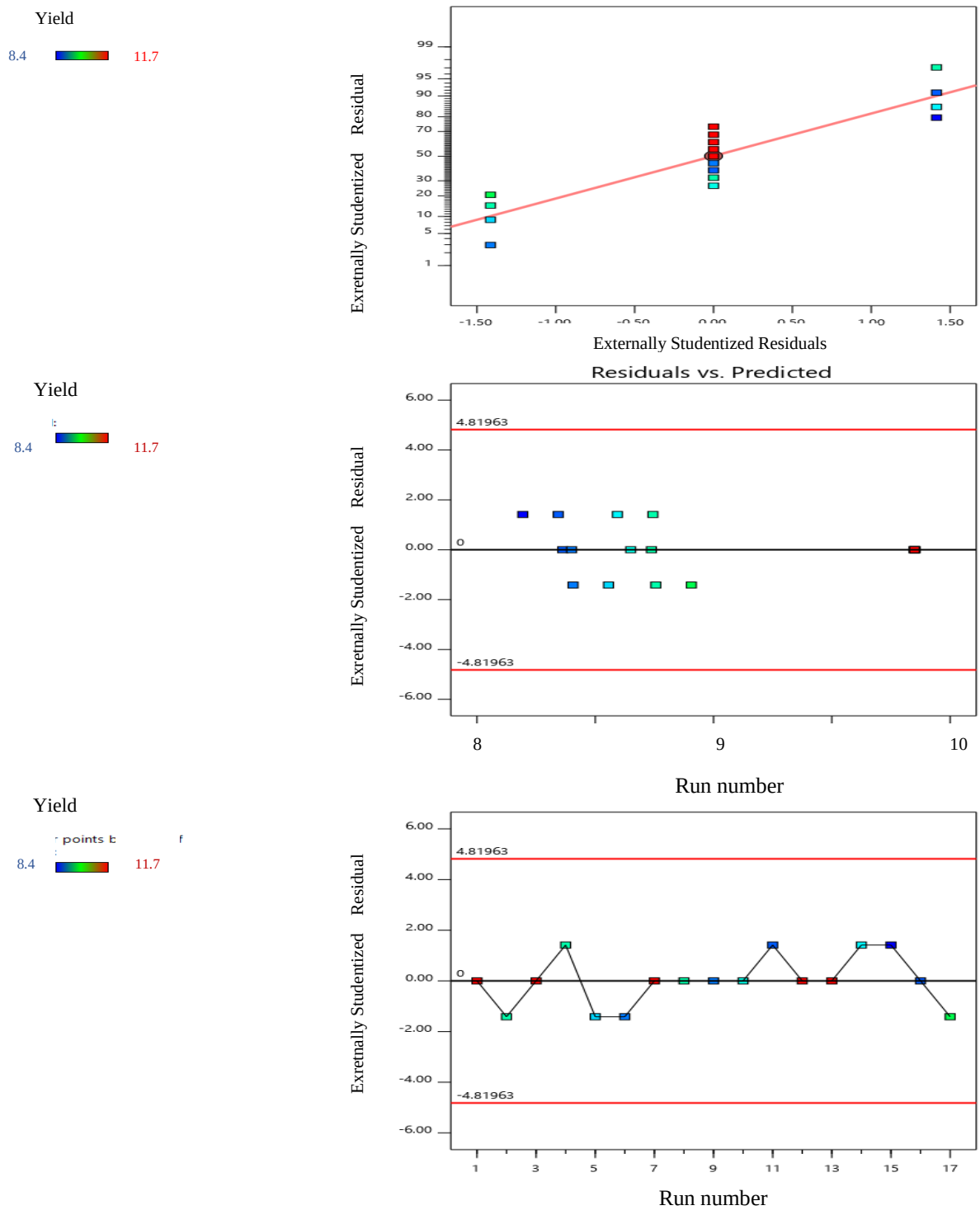

Figure 4.1: Diagnostics Graphs in Terms of Coded Factors

The graph of the predicted values obtained using the developed correlation versus actual values is shown in Figure 4.2. This plot, therefore, clarifies the performance of the correlation in an evident way.

Hence, the regression model equation granted a very accurate description of the experimental data, in which all the points are very close to the line of perfect fit. This outcome indicates that it was successful in creating the correlation between the three process variables to the yield extraction.

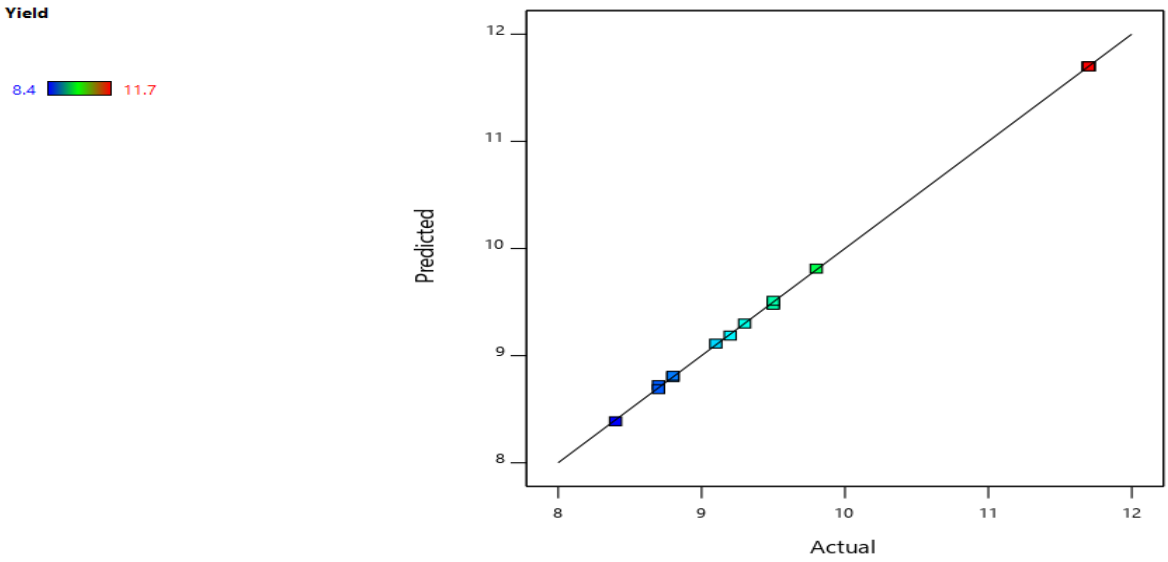

Figure 4.2: Actual versus Predicted Value

Table 4.6: Diagnostics Case Statistics

Run	Actual Value	Predicted Value	Residual	Leverage	Internally Studentized Residuals	Externally Studentized Residuals	Cook's Distance	Influence on Fitted Value DFFITS
1	11.70	11.70	0.0000	0.200	0.000	0.000	0.000	0.000
2	9.50	9.51	-0.0125	0.750	-1.323	-1.414	0.525	-2.449(1)
3	11.50	11.70	0.0000	0.200	0.000	0.000	0.000	0.000
4	9.50	9.49	0.0125	0.750	1.323	1.414	0.525	2.449(1)
5	9.10	9.11	-0.0125	0.750	-1.323	-1.414	0.525	-2.449(1)
6	8.80	8.81	-0.0125	0.750	-1.323	-1.414	0.525	-2.449(1)
7	11.60	11.70	0.0000	0.200	0.000	0.000	0.000	0.000
8	9.50	9.47	0.0250	0.750	2.646	0.000	2.100(1)	0.000
9	8.80	8.80	0.0000	0.750	0.000	0.000	0.000	0.000
10	9.30	9.30	0.0000	0.750	0.000	0.000	0.000	0.000
11	8.70	8.69	0.0125	0.750	1.323	1.414	0.525	2.449(1)
12	11.30	11.70	0.0000	0.200	0.000	0.000	0.000	0.000
13	11.40	11.70	0.0000	0.200	0.000	0.000	0.000	0.000
14	9.20	9.19	0.0125	0.750	1.323	1.414	0.525	2.449(1)
15	8.40	8.39	0.0125	0.750	1.323	1.414	0.525	2.449(1)
16	8.70	8.72	-0.0250	0.750	-2.646	0.000	2.100(1)	0.000
17	9.80	9.81	-0.0125	0.750	-1.323	-1.414	0.525	-2.449(1)

(1) Exceeds limits.

4.1.4. Effects of Individual Parameters on Oil Yield

Figures 4.3a, b, and c show how an independent variable affects oil recovery. As extraction time, temperature, and the proportion of solid-to-solvent ratio all directly correlated with the percentage of oil yield recovered, it follows that increasing any one of these independent variables will improve oil extraction until the optimal values are reached. However, further raising those process variables will result in a significant decrease in oil extraction because excessively high values cause oil decomposition and a decrease in solvent volume.

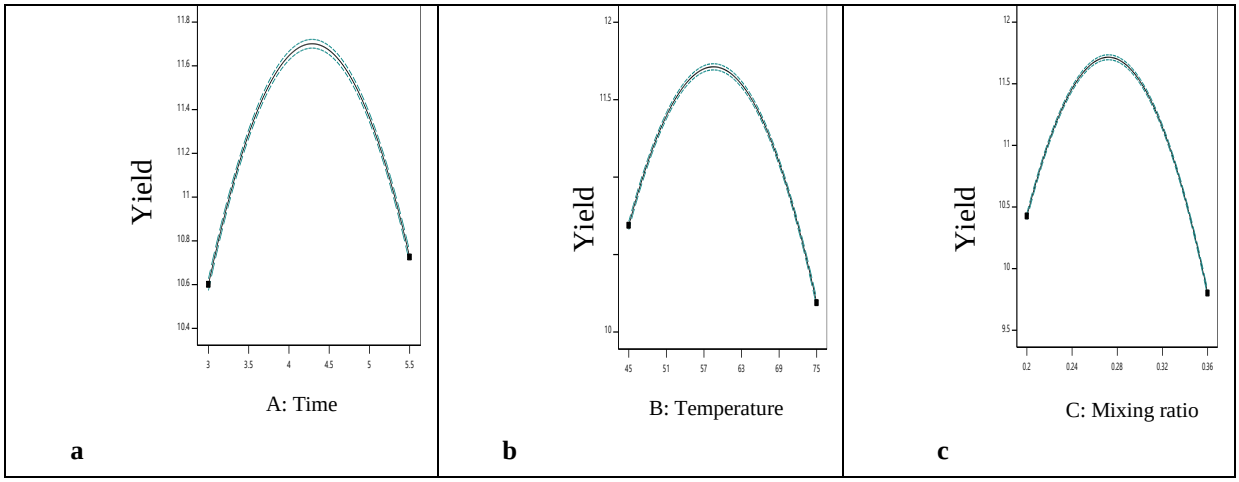

Figure 4.3: Effect of Independent Variables: a time, b temperature, c percentage of solid-to-solvent ratio on the oil yield.

Extraction Time:

Fig. 4.3a illustrates the effect of extraction time on oil extraction, demonstrating that oil extraction increased as extraction time increased while keeping all other variables constant. The relationship between extraction time and oil yield suggests that as extraction time was increased, oil extraction became more advantageous until the maximum value, or 4.25 hours, was reached. Longer extraction times increase the diffisive phenomenon, the solvent's contact time with leaf powder causes severe cell wall crushing, and the solvent's contact surface with oil cells grows, all of which increase oil recovery. The oil yield, however, gradually starts to decline as the extraction time lengthens as a result of the oil's decomposition once it reaches the optimal level. Another instance of this phenomenon was noted in the UAE C.macrostachyus leaf oil optimization (Ermias et al., 2021).

Extraction Temperature:

The influence of extraction temperature on the oil extraction was shown in Fig. 4.3b, which displays that oil extraction increases with extraction temperature increasing while holding all other factors constant. The results revealed that extraction temperature substantially influences oil recovery, followed by extraction time and percentage solid-to-solvent ratio.

It has been demonstrated that raising the extraction temperature value would increase oil extraction up to 60 ºC. The extraction temperature was directly proportional to the recovery of oil. This phenomenon fit in nicely with Li et al.'s, report on peony seed oil optimization. According to various studies like Jalili et al., 2018, raising the temperature during the soxhlet extraction may increase the amount of air bubbles produced and increase the contact surface between the solvent and the cell membranes, thereby improving the efficiency of oil extraction. However, the oil yield decreases when the extraction temperature is higher than 60 °C because the solvent evaporates quickly at high temperatures and loses viscosity. This phenomenon was well supported by Tan et al.'s report that, virgin avocado oil yield increased as temperature rose from 20 to 40 °C and by Jalili et al.'s report that, canola seed oil recovery increased from 18 to 20% when applied temperature rose from 40 to 50 °C.

The justification for this could be that Saxena et al.'s similar experimental observations show that oil's solubility in a given solvent increases with temperature elevation. As a result, the value of percentage oil recovery rises.

Mixing Ratio:

The influence of the percent of solid-to-solvent ratio on oil yield varied in ranges from 8.1% to 11.7% and was examined by keeping other variables unchanged. While examining the effects of the percent solid-to-solvent ratio on oil yield, other variables were left unaffected and ranged from 8.1% to 11.7%. Figure 4.3c shows how oil recovery increased while keeping all other factors constant as the solid-to-solvent ratio increased. Oil yield and the percentage of solid-to-solvent ratio are directly correlated, and it has been demonstrated that increasing the percentage of solid-to-solvent ratio increases oil yield because a higher oil concentration gradient between the solid and solvent encourages effective mass transfer and more efficient extraction. However, when the ratios went above 28%, the oil yield fell. Decomposition, saturating solvent recovery, and oil volatilization could be to blame for this.This might be due to the decomposition, saturating solvent recovery, and oil volatilization. A similar phenomenon has been presented in annatto seeds (Samaram et al., 2015), peony seed oil (Li et al., 2021), and papaya seed oil (Yolmeh et al., 2014).

4.1.5 The Effects of Interaction of Process Variables on the Oil Yield

The influence of interaction between independent process variables on oil recovery was investigated using response surface plots, as shown below. The result revealed that the interaction of extraction time and temperature, as well as the extraction temperature and percentage of solid-to-solvent ratio, has the most substantial ($p<0.0001$) influence on the oil yield, followed by extraction time with a percentage of solid-to-solvent ratio.

Effect of Temperature with Time on Yield

The interaction plot was used to show the effect of changing one control variable with changes in a second control. The interaction effect of all factors could also determine from ANOVA in Table 4.5. From Figure 4.4 below, the interaction effect of temperature and time on the oil yield shows that when both the temperature and time increase, the oil yield also increased and reached optimal value. After the optimal point, the oil yield decreased.

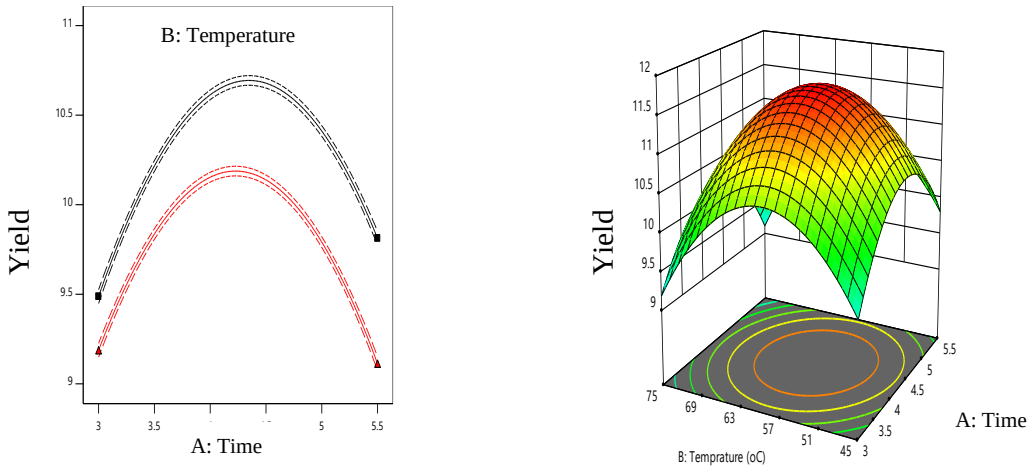

Figure 4.4: Interaction Effect of Temperature and Time

Effect of Mixing Ratio with Time on Yield

From Figure 4.5 below, the interaction effect of mixing ratio and time on the oil yield shows that, when both the mixing ratio and time increased, the oil yield also increased and reached optimal. After the optimal point, the oil yield decreased.

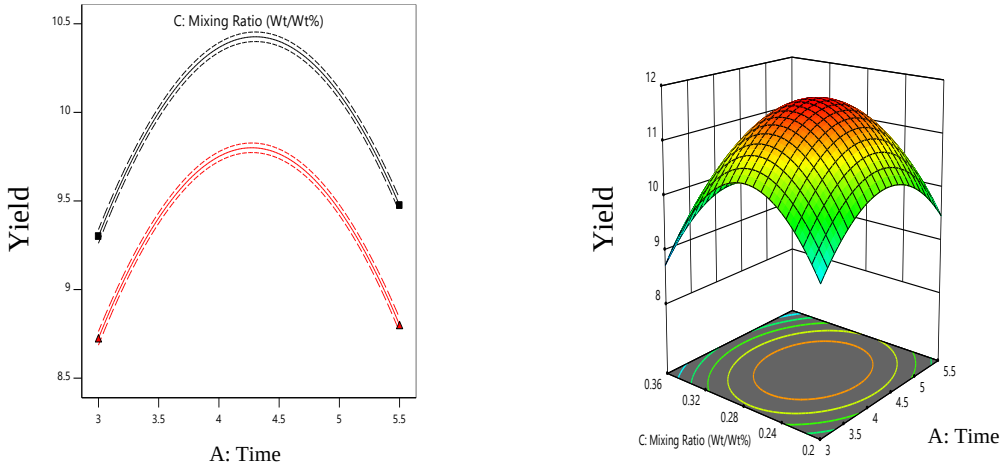

Figure 4.5: Interaction Effect of Mixing Ratio and Time

Effect of Temperature with Mixing Ratio on Yield

Figure 4.6 elucidates the impact of the interaction between extraction temperature and the % of solid-to-solvent ratio on oil extraction at constant extraction time. When compared with extraction temperature and the solid-to-solvent ratio at constant extraction time, the impact of extraction temperature was more prominent on oil yield because the system had already attained equilibrium at high temperature. Increasing the interaction between temperatures and the % ratio of solid to solvent increased oil extraction. However, a further increment of both variables exhibited a decreasing tendency in oil yield. A similar phenomenon was observed during oil extraction from Diospyros lotus seed (Sodeifan et al., 2019).

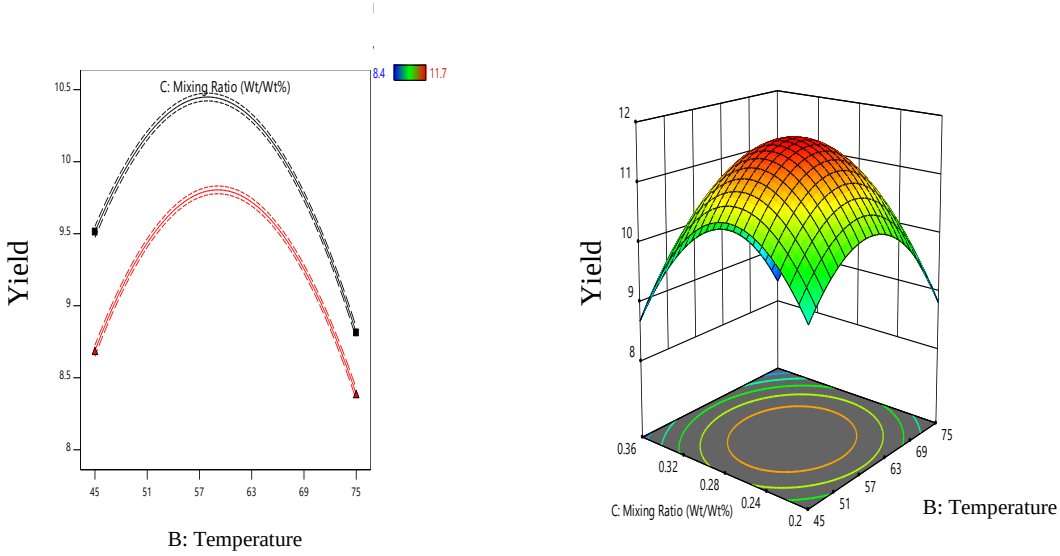

Figure 4.6: Interaction Effect of Temperature and Mixing ratio

Numerical Optimization

Table 4.7: Optimization Constraints

Name	Goal	Lower Limit	Upper Limit	Lower Weight	Upper Weight
A:Time	In range	3	5.5	1	1
B:Temprature	In range	45	75	1	1
C:Mixing Ratio	Minimize	0.2	0.36	1	1
Yield	Maximize	8.4	11.7	1	1

Solutions

The cost of mixing ratio of the raw materials (solvent extraction and leaf of the sample) are relatively high cost than other factors, so mixing ratio were minimizing by considering to maximize yield of extract was found.

Table 4.8: Numerical Optimization Solution

Number	Time	Temperature	Mixing Ratio	Yield	Desirability	
1	**4.305**	**58.110**	**0.228**	**11.257**	**0.845**	**Selected**

Ermias et al., studied the optimization of ultrasonic-supported extraction of the leaf of *C. macrostachyus* by RSM. In this study, the extraction was carried out according to an orthogonal array design and independent selected variables were sonication temperature (35–45 °C), sonication time (25–35 min), ultrasound power (250–550 W), and percentage of solid-to-solvent ratio (10–20%) on the oil yield was investigated. The optimal conditions of C. macrostachyus leaf oil were found to be 42 °C of temperature, 30.61 min of sonication time, 425.79 W of ultrasound power, and 18% (w/v) of solid to solvent. Under these circumstances, the optimum extraction efficiency of oil was found to be 38.63% with a desirability value of 1.00.

4.2. Phytochemical Analysis of CM Extract

In this study, preliminary phytochemical investigation of the hexane extract of *C. macrostachyus* leaf showed the presence of phytochemical constituents, namely terpenoids, flavonoids, phenols, tannins, and alkaloids but the absence of saponins, as described in Table 4.9.

Table 4.9: Preliminary Phytochemical Investigation

Phytochemical Screening	Test Method	Crude Extract
Terpenoids	Salkowski's Test	++
Flavonoids	Shinoda Test	++
Phenols	Ferric chloride Test	++
Tannins	Ferric chloride Test	++
Alkaloids	Wagner's Test	++
Saponins	Froth forming	--

Notice: + indicates presence, - indicates absence of the secondary metabolite

The presence of these phytochemicals in the hexane fraction of *C. macrostachyus* leaves possibly indicates its numerous medicinal properties, such as anti-inflammatory, anti-bacterial, and anti-oxidative properties, among others. The report also showed the presence of alkaloids, phenolic compounds, tannins, and flavonoids in hydroalcoholic crude extracts of the seed and root of *C. macrostachyus* (Mekonnen, 2015).

4.3. Characterization of Crude Extract of *C. macrostachyus*

4.3.1. GC-MS Analysis

The GC–MS chromatogram of hexane leaf extracts of C.macrostachyus recorded a total of tweny-nine peaks corresponding to the bioactive compounds that were recognized by relating their peak retention time, peak area (%), height (%) and mass spectral fragmentation patterns to that of the known compounds described by the National Institute of Standards and Technology (NIST) library as shown in the below Figure 4.7. Table 4.10 lists twenty major componrnts out of those tweny-nine components of the oil compounds, along with their retention time (RT), molecular formula, peak area%, and score. The hexane extract of *C. macrostachyus* represents the presence of secondary phytochemical compounds like phenols, alkaloids, and fatty acids and their esters.

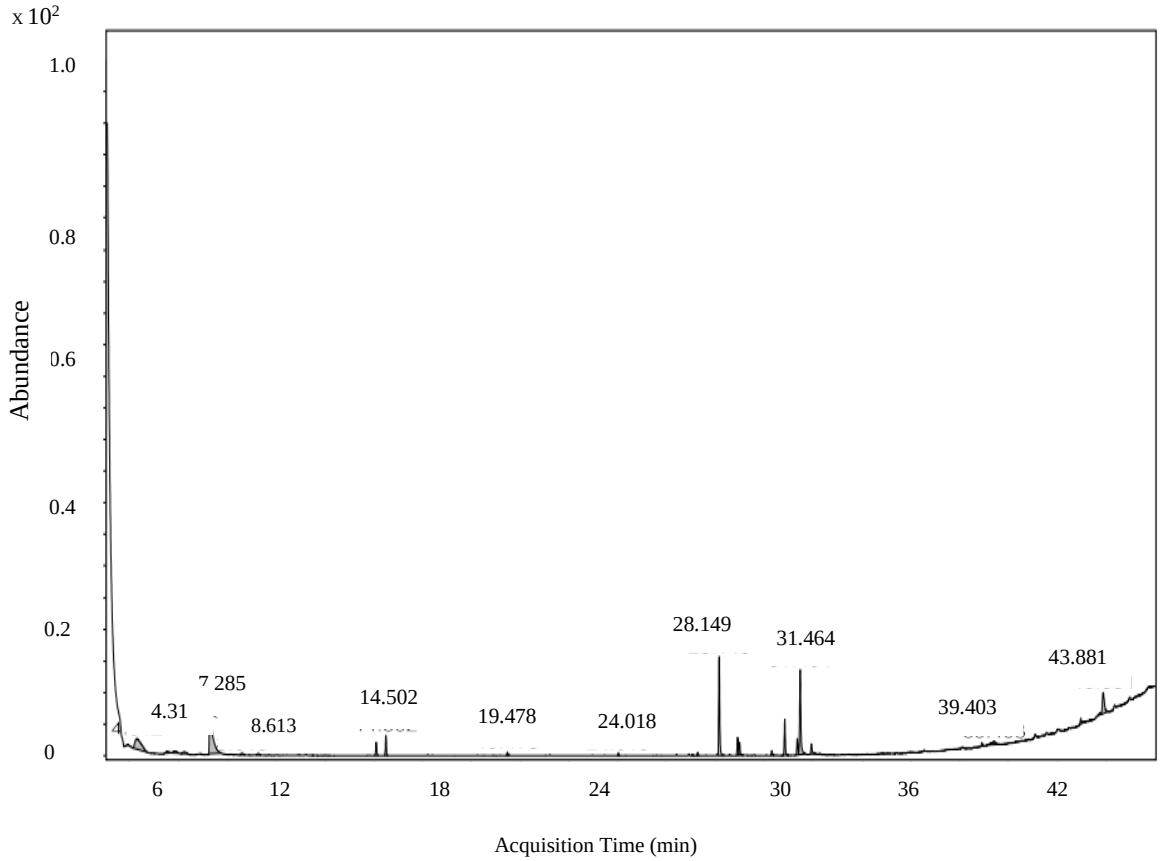

Figure 4.7: GC-MS Chromatograms of CM Extract

The presence of fatty acid esters such as hexadecanoic acid methyl ester and 9,12 - octadecanoic acid methyl ester has various bioactivities, including anti-fungal, antioxidant, anti-androgenic, and anti-microbial activity (Parimalakrishnan et al., 2015). The 9, 12-octadecanoic acid methyl ester also had potential cancer-preventive, anti-inflammatory, and anti-arthritic activities (Parthipan et al., 2015). A similar result was observed in the study carried out in Croton tiglium seed by Mangunwidjaja et al. Therefore, the C.macrostachyus leaf extract may serve as a potent source of medicinal compounds responsible for its pharmacological activities.

Table 4.10**:** Chemical Constituents Identified from the CM Extract

S/N	Name	Formula	RT	Area	Area %	Score
1	2-Hexenal	$C_6H_{10}O$	4.31	210543	9.45	74.88
2	(3S,5R,5aR)-(+-)-3-Trifluoroacetylamino-5-hydroxy-5-phenyl-1-azabicyclo[4.2.0]octan-2-one	$C_{16}H_{19}F_3N_2O_2$	5.52	118462	4.65	75.26
3	Butanoic acid, 3-hydroxy-, 3-(1,1-dimethylethoxy)-1-methyl-3-oxopropyl ester, [R-(R*,R*)]	$C_{12}H_{22}O_5$	5.84	57683	2.23	63.47
4	5-Methyl-6-oxa-1-aza-bicyclo[3.1.0]hexane	C_5H_9NO	7.28	94684	3.61	78.46
5	(S)-(-)-4-Benzoyloxy-5-oxopentyl pivalate	$C_{17}H_{22}O_5$	8.61	62843	2.81	71.28
6	Butyl 2,4-dimethyl-2-nitro-4-pentenoate	$C_{11}H_{19}NO_4$	11.23	57057	2.12	74.74
7	2-Ethylhexyl methacrylate	$C_{12}H_{22}O_2$	14.10	59374	2.31	83.23
8	Capric acid methyl ester	$C_{11}H_{22}O_2$	14.50	75422	3.32	88.61
9	Diethyl 3-cyclopentenyl -phosphonate	$C_9H_{17}O_3P$	21.21	67983	2.92	86.22
10	Eicosanoic acid, methyl ester	$C_{21}H_{42}O_2$	24.01	60847	2.24	79.98
11	10,13-Dimethyl-9(Z)-tetradecen-1-ol	$C_{16}H_{32}O$	27.27	84946	3.51	78.68
12	Hexadecanoic acid, methyl ester	$C_{17}H_{34}O_2$	28.14	314083	12.66	90.56
13	[(1R,2R,4S)-3-methyl-3-azabicyclo[2.2.1]heptan-2-yl]methanol	$C_8H_{15}NO$	28.57	157860	7.15	75.55
14	Dibutyl phthalate	$C_{16}H_{22}O_4$	28.90	74543	3.30	95.00
15	Phthalic acid, isohexyl tridec-2-yn-1-yl ester	$C_{27}H_{40}O_4$	28.98	65172	2.64	72.97
16	1-Ethynylcyclopentanol	$C_7H_{10}O$	30.30	215543	9.85	73.52
17	Phytyl, 2-methylbutanoate	$C_{25}H_{48}O_2$	30.83	139543	6.14	82.93
18	9,12-Octadecadienoic acid (Z,Z)	$C_{19}H_{34}O_2$	31.35	69771	3.03	84.53
19	Linolenic acid methyl ester	$C_{19}H_{32}O_2$	31.46	101471	4.09	84.41
20	Stearic acid methyl ester	$C_{19}H_{38}O_2$	31.92	61128	2.37	72.09

4.3.2. FTIR Analysis

Following the step-by-step analysis procedure, the graph has more than five peaks, confirming that the hexane leaf extract of C.macrostachyus is a multifunctional compound. The result profile showed the presence of functional groups like hydroxyl group (3404 cm^{-1}), alkane with CH_2 asymmetry stretching(2922 cm^{-1}), aldehyde (2853 cm^{-1}), acids (1735 cm^{-1}), alkane with C-H deformation vibration (1460cm^{-1}), C–O stretch (1378 cm^{-1},1165 cm^{-1}), C-C skeletal vibration (1245 cm^{-1}), C-O-H stretching vibrations (1063 cm^{-1}) which is phenol (Q. Wang et al., 2020) or tertiary alcohol (M.Zafer et al., 2012), and C-H rock (717 cm^{-1}).

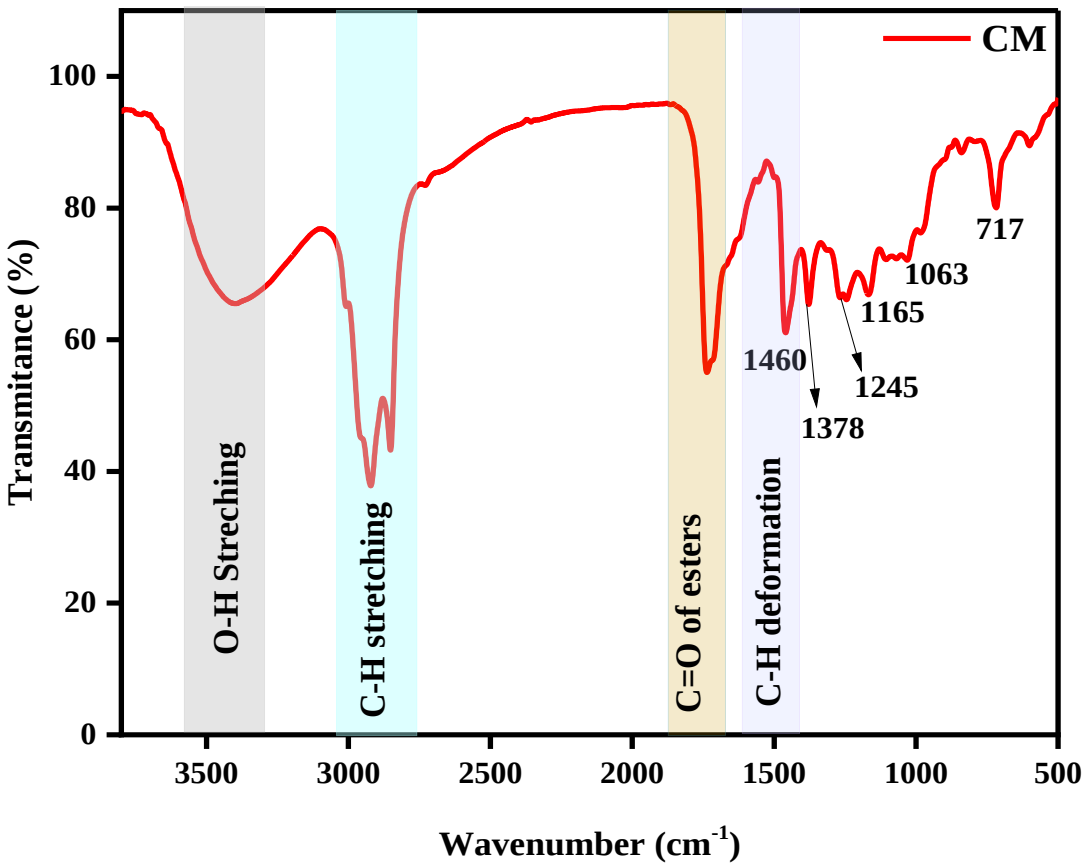

Figure 4.8: FT IR Spectra for CM Extract

4.3.3. Thermal Property Analysis

Only 5% of the weight is lost at 265 ^{o}C, as can be seen from the TGA graph below. It is, therefore, promising to synthesize the bio-adhesive at a temperature of 170 ^{o}C.

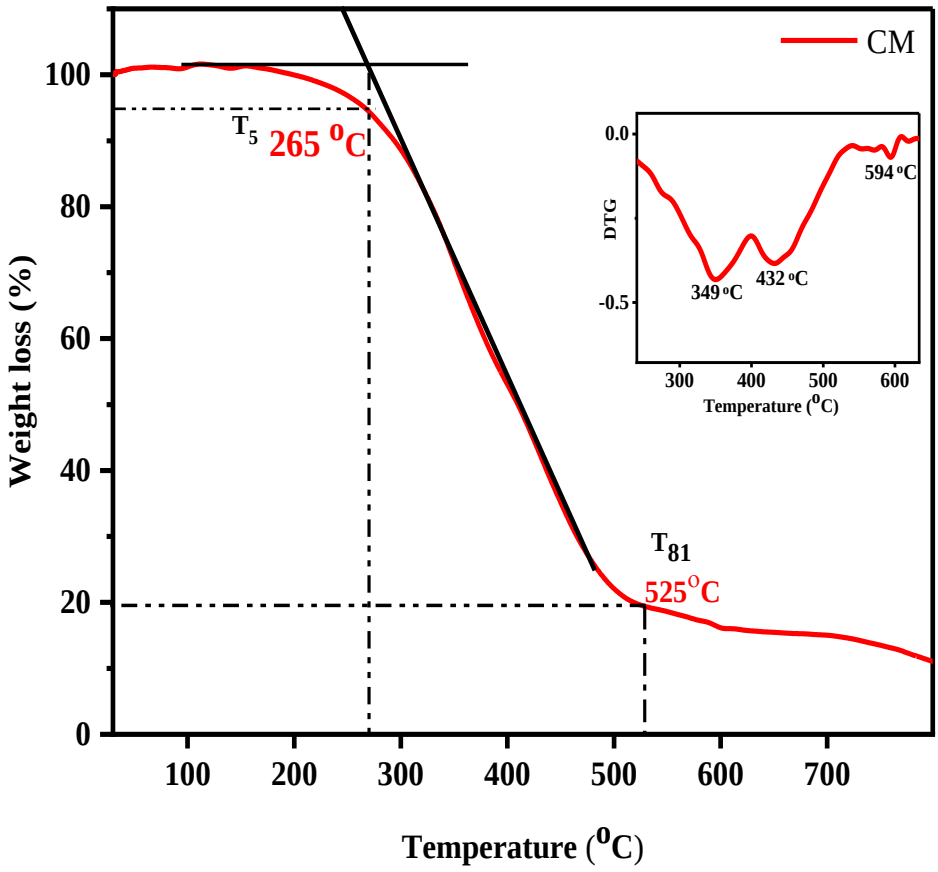

Figure 4.9**:** TGA and DTG Curve for the CM Extract

4.4. Characterization for the Synthesized OLLA-m-CM Bio adhesive

4.4.1. Functional Group Analysis of the Bio-adhesive

The functional group of the three synthesized bioadhesives was analyzed by Fourier transform spectroscopy with comparison to the leaf extract of the *C. macrostachyus* and lactic acid oligomer. The broad absorption peak observed at 3515 cm^{-1} shows the OH group attributed to the OH phenols and alcohol of the leaf extract of the C.macrostachyus unreacted or the OH terminal of the lactic acid (S. Jarmelo et al., 2012). When compared to the starting materials that are leaf extract of the *C.macrostachyus* and OLLA this peak shows the availability of the hydroxyl group has become narrowed and decreased in intensity. This shows the decrease of the OH groups in the system as the water is being removed. The characteristic peak observed at the product, i.e., 2990 cm^{-1} and 2945 $cm^{-1,}$ attributed to CH_2 and CH_3 asymmetric stretching respectively, results in shifts from lactic acid oligomer of 2920cm^{-1} and 2859cm^{-1} respectively, and followed by the formation of a new peak at 2355 cm^{-1}. The C-H stretch at 2728 cm^{-1} of the leaf extract of *C. macrostachyus* also shifted to 2627 cm^{-1}.

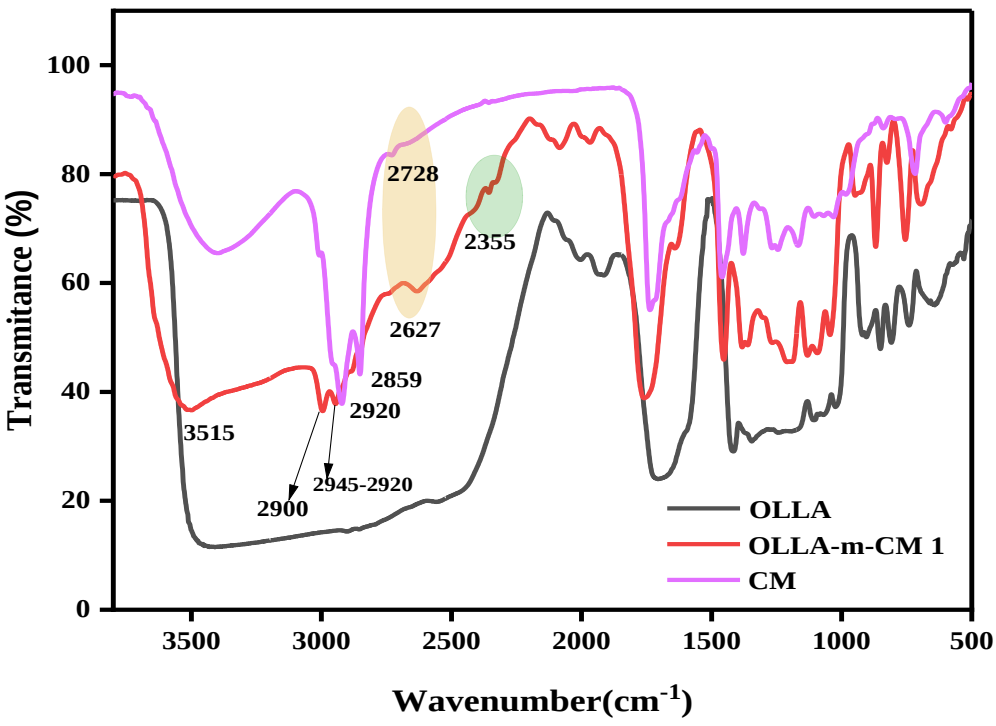

Figure 4.10: The IR Spectrum of CM, OLLA and OLLA-m-CM 1

As indicated in Figure 4.11, the aforementioned interaction is supported by the observed OLLA major peak shift from 1735 cm^{-1} to 1760 cm^{-1} with the loading of *C. macrostachyus* crude extract, and this was observed due to the increased availability of O-H groups of the extract towards the carboxyl groups (-C=O) of lactic acid. Furthermore, an extended broader shoulder-like peak is shown up to 1550cm-1 with the loading of *C.macrostahyus* crude extract. This molecular interaction occurred due to hydrogen bonding and Van der Waals interaction (Meseret et al., 2022). The sholder-like peak observed at 1595 cm^{-1} for the lactic acid oligomer was also shifted to the higher wavenumbers of 1637 cm^{-1}, 1640 cm^{-1}, and 1643 cm^{-1}, respectively, for OLLA-m-CM 1, OLLA-m-CM 2 and OLLA-m-CM 3 samples. This can be correlated with the formation of hydrogen bonding due to the availability of OH groups that are responsible for improved molecular interaction. The IR spectrum can also be used to compare the change that occurred to the change in the mixing ratio of the starting materials. Figure 4.11 shows the FT IR spectrum for the OLLA, OLLA-m-CM 1, OLLA-m-CM 2 and OLLA-m-CM 3 bio-adhesives.

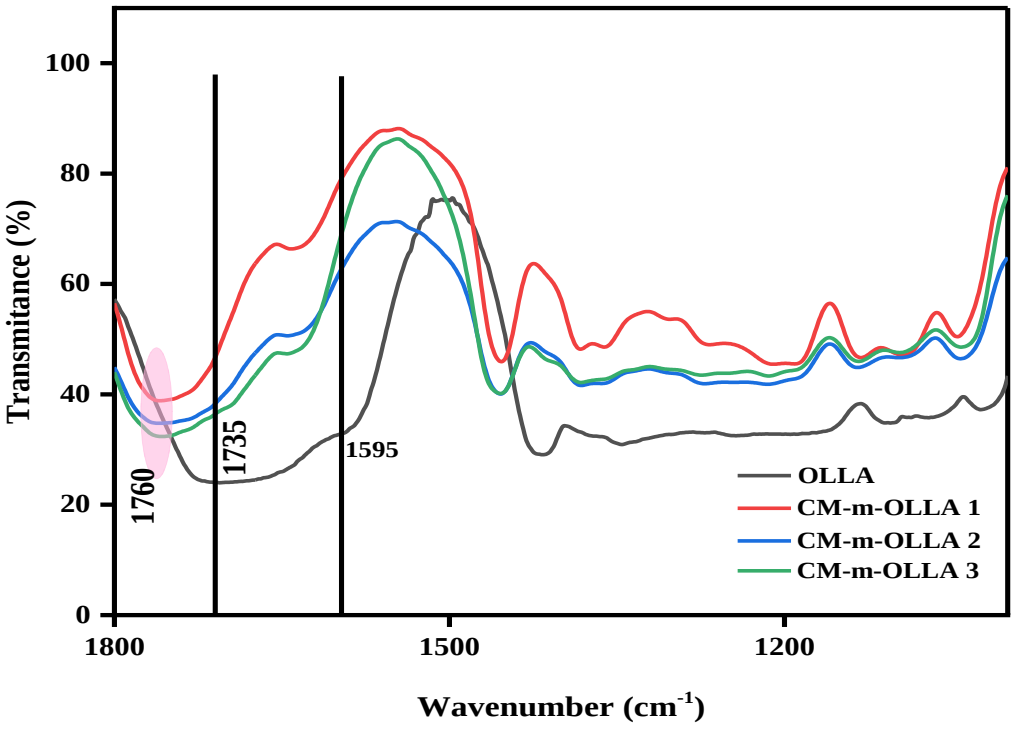

Figure 4.11: C=O Stretching of OLLA, OLLA-m-CM 1, OLLA-m-CM 2 and OLLA-m-CM 3

4.4.2. Reaction Mechanism

This study used leaf extract of *C. macrostachyus* and lactic acid as green starting materials to synthesize the bio-adhesive. The hydroxyl groups in the crude extract are active for reaction, and the carboxylic group from the lactic acid attaches to it via a polycondensation reaction. L-Lactic acid is esterified, forming an oligomer that attaches to the OH at the hydroxyl groups of the crude extract. The reaction mechanism for the synthesis of OLLA-m-CM bio-adhesive is thought to consist of both lactic acid oligomerizations and the OLLA attachment to the crude extract's hydroxyl groups. The reaction mechanism is postulated in the Figure 4.12.

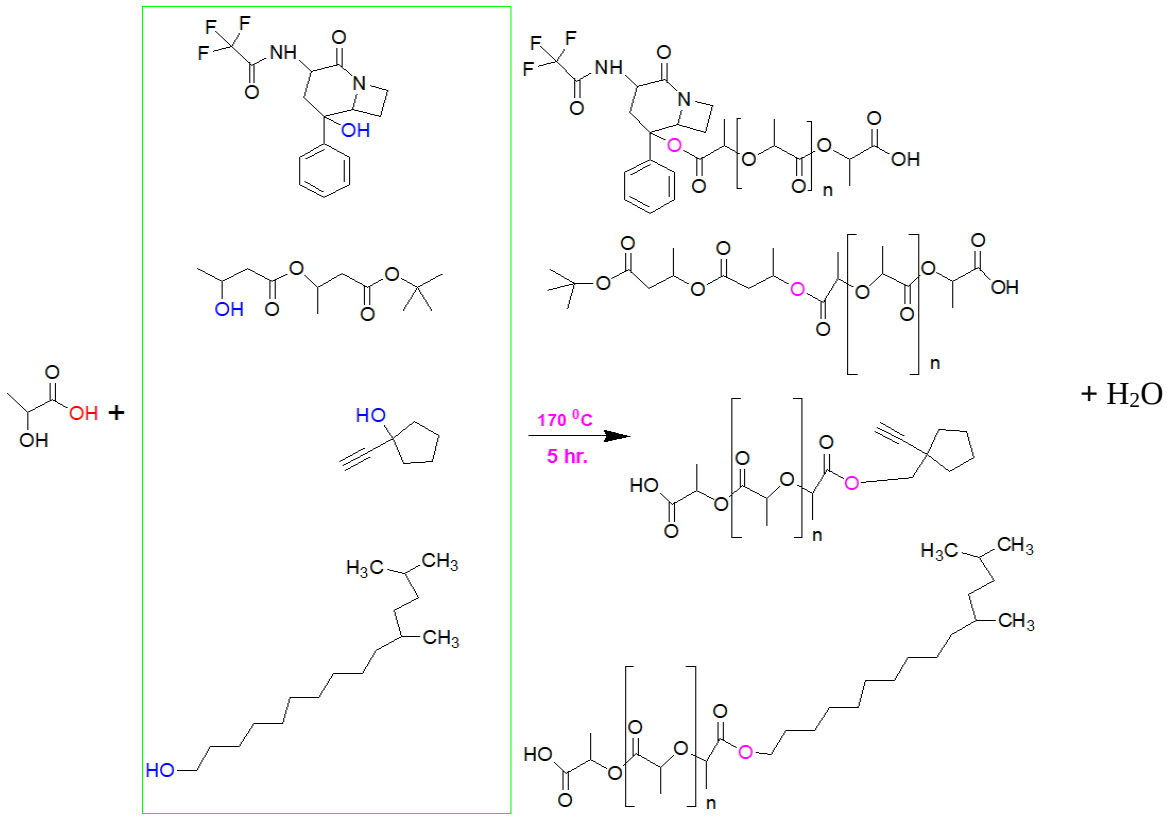

Figure 4.12: Postulate Reaction Mechanism of OH Groups of CM Extract with COOH Group of LA Oligomer

Finally, it can be concluded that the product is made of hexane leaf extract of *C. macrostachyus* compounds and lactic acid chain unit, where the carboxyl group (COOH) of the lactic acid oligomer is attached with present reactive hydroxyl groups of the crude extract.

4.4.3. Water Contact Angle Analysis

The three OLLA-m-CM bioadhesive matrix samples, OLLA-m-CM 1, 2, and 3, had measured water contact angles of 77.8°, 65.4°, and 56.7°, respectively. The contact angle decreases as the ratio of *C. macrostachyus* crude extract to L-Lactic acid increases, indicating that many OH groups, including water molecules, are formed on the surface of the synthesized bioadhesive in addition to the potential replacement of the existing polar hydrophilic groups by the newly formed ester groups of the OLLA. When adding a drop of distilled water, it was spread on the OLLA-m-CM 3 surface and gave the lowest contact angle value when compared with OLLA-m-CM 1 and OLLA-m-CM 2.

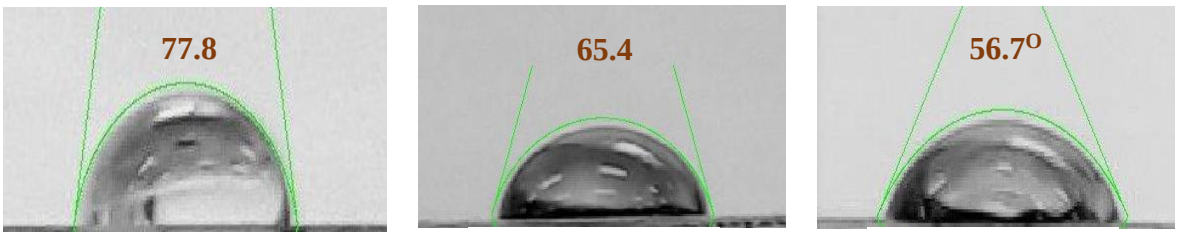

Figure 4.13: Contact Angle at Different Concentration of Synthesized Bioadhesive

4.4.4. Tensile Strength Test

As shown in Figure4.14, a universal testing machine was used to load the specimens in accordance with their corresponding standard system (ASTM D-1002 specimens) after the sample had been melted and applied to the surface of the various substrates at 40 °C. Each specimen's maximum load at the point of failure was noted. The preparation environment was kept at 25 °C. The adhesive strength was demonstrated for glass and animal bone substrates. Accordingly, it can be assumed that the adhesive has the ability to bind not only bone to bone but also silica-based substrates like glasses. As shown fro the Figure 4.15, the maximum tensile strength was found at 11±0.5 MPa and 8±0.3 MPa for glass and bone substrates, respectively. For both substrates, cohesive failure was observed. The graph below demonstrates that the glass substrates have a higher tensile strength than the bone substrates, which may be caused by the presence of fat on the surface of the bone.

Figure 4. 14: Tensile Strength Test Setup (a) Glass, (b) Bone

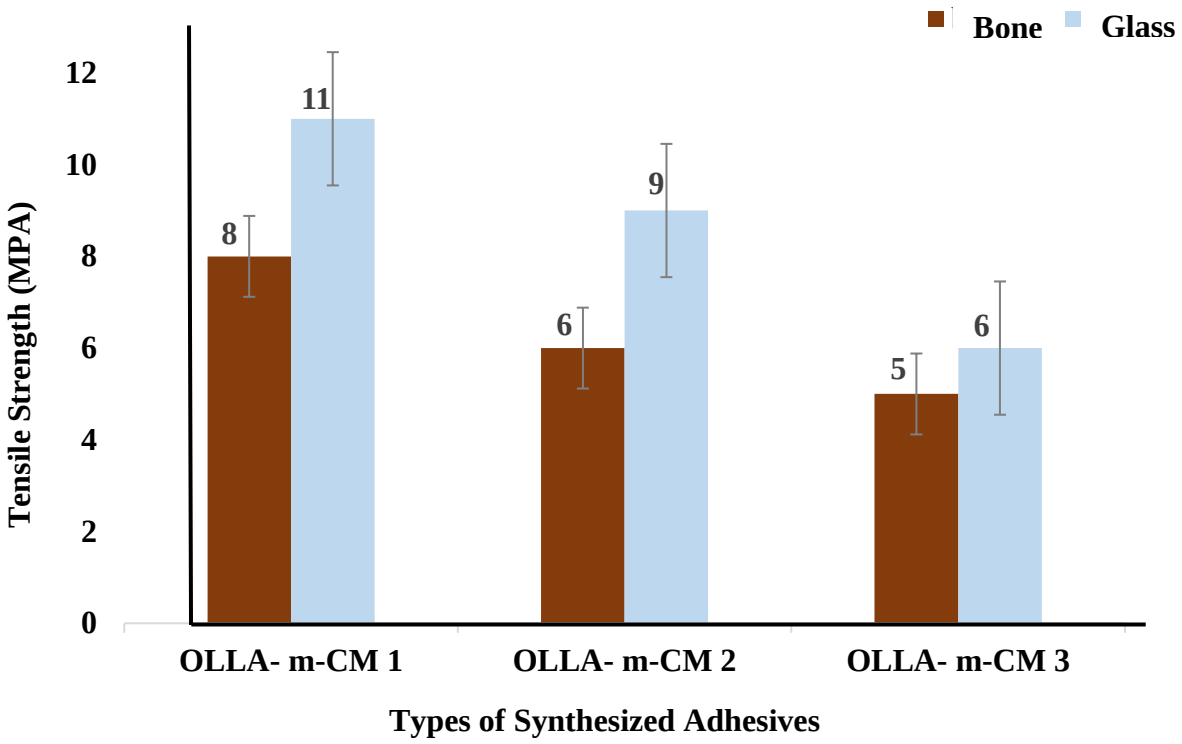

Figure 4.15: Comparison of Tensile Strength for Glass and Bone Substrates

4.4.5. Antibacterial Test

The in vitro antibacterial activity of the synthesized bioadhesives was investigated against one Gram-negative bacteria and one Gram-positive bacteria with agar disk diffusion assay at a concentration of 1 mg/ml. In parallel to this investigation, the lactic acid oligomer and the leaf extract of *C.macrostachyus* were also tested for their anti-bacterial effect and the result was used to confirm the effect of the synthesized adhesive.

C.macrostachyus leaf extract: The leaf extract of *C. macrostachyus* was tested for its antimicrobial properties against the test pathogens. As seen in Table 4.11, the diameter of the inhibition zones is 8 mm and 8.5 mm for E.coil and S.aures, respectively. A comparative result is also observed with the ethanol extract of the leaf of *C.macrostchyus* tested for E.coil (Workitu et al., 2018). The results proved that extracts possessed potential antibacterial effects, which might be because of the presence of high content of compounds such as flavonoids, tannins, phenols and alkaloids (Zelalem, 2007; Tala et al., 2013; Alemu et al., 2017).

L-Lactic acid oligomer: With a similar test procedure to that of the *C.macrostachyus* leaf extract, the lactic acid oligomer was tested for its anti-bacterial effect against the two bacteria. From the zone of inhibition measurement, it was observed that the oligomer has an anti-bacterial effect with a zone of inhibition of 6.5 mm and 7.0 mm for E.coli and S. aureus, respectively, with a concentration of 1 mg/mL.

OLLA-m-CM: The bacteria activity of the three synthesized bio-adhesives were conducted for both two bacteria E.coli and S.aureus, with a similar test method to that of the C.macrostachyus leaf extract and L-Lactic acid oligomer. As shown in Table 4.11 below, the zone of inhibition shows 8mm, 9mm, and 11mm for E. coli and 9mm, 10mm, and 12mm for S. aureus for the synthesized bio-adhesive with a concentration of 1 mg/mL for OLLA-m-CM 1, OLLA-m-CM 2, and OLLA-m-CM 3, respectively. This inhibition effect for the three synthesized OLLA-m-CM bio-adhesive is higher than the crude extract and lactic acid oligomer. This might be due to the synergistic effects of the two starting materials and the zone of inhibition for OLLA-m-CM 1 is higher than the other two synthesized bioadhesives, this can be taken as that the antibacterial activity of the OLLA-m-CM bio-adhesive get its anti-bacteria activity more of from the leaf extract of *C.macrostachyus* than that of the lactic acid oligomer. As seen from the attachments below in Figure 4.15 and Table 4.11, OLLA-m-CM 1 is the result most similar to the positive control used in this study, which is 14 mm and 15 mm for E. coli and S. aureus, respectively.

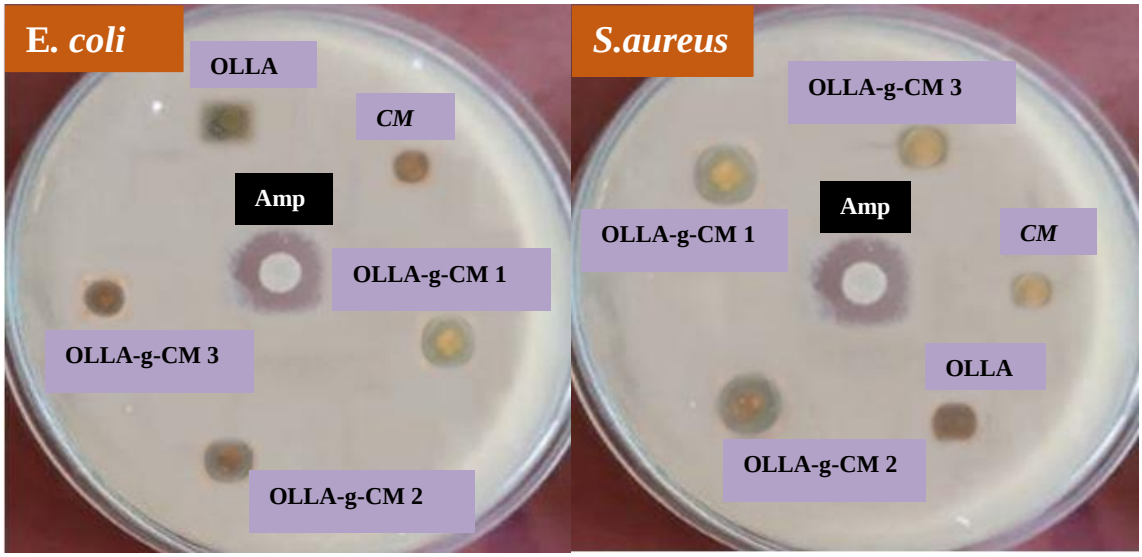

Figure 4.16: Result for Anti-bacteria Analysis of CM, OLLA, and OLLA-m-CM

Table 4.11: Anti-bacterial Activity of CM, OLLA, OLLA-m-CM 1, OLLA-m-CM 2, and OLLA-m-CM 3 Bio-adhesives in Zone of Inhibition (mm)

Compound Conc. (1mg/ml)	**zone of Inhibition (mm)**	
	***E. coli* ATCC25922**	***S. aureus* ATCC25923**
CM	8.0	8.5
OLLA	6.5	7.0
OLLA-m-CM 1	11.0	12.0
OLLA-m-CM 2	9.0	10.0
OLLA-m-CM 3	8.0	9.0
Ampicillin (+ve control)	14.0	15.0

\

5. CONCLUSION AND RECOMMENDATION

5.1. CONCLUSION

This research work discussed the investigation of bio-based bone adhesive from the traditionally known medicinal plant *C. macrostachyus* leaf extract and lactic acid monomer via polycondensation reaction at a controlled temperature of 170 ºC for 5hr by varying the mixing ratios of both starting materials. The oil extracted from the leaf of C. macrostachys using the soxhlet apparatus was optimized using Response surface methodology (RSM). To examine the impact of three independent variables temperature, time, and mixing ratio on the crude oil yield, the experiment used the Box-Benhken method and a central composite design with seventeen experimental points, including five replicates of the center points. The optimum yield was found to be 11.7% at 60 ºC, 4:25 hr and 0.28 wt/wt% of temperature, time and mixing ratio, respectively. Phytochemicals qualitative analysis of the crude extract was carried out using standard protocols and showed the presence of alkaloids, flavonoids, phenols, tannins and terpenes but an absence of saponins. Twenty-nine compounds have been identified using GC-MS by comparing their spectra data to those available in the chemical libraries. These compounds are mainly fatty acid esters, phenols, alkanes and alkenes. The fatty acids and phenols are the more represented. Most of the identified compounds are cited in the literature for their antimicrobial, antifungal, antioxidant, anti-cancer, and anti-inflammatory properties. The FTIR analysis is also supported as the crude extract is a multi-functional compound.

From preliminary investigation, *C. macrostachyus* leaf extract was modified by L-Lactic acid with different mixing ratios at a reaction temperature of 170 ºC for 5 hrs via polycondensation reaction. The aforementioned interaction is supported by the observed OLLA major peak shift from 1735 cm^{-1} to 1760 cm^{-1} with the loading of *C. macrostachyus* crude extract, and this was observed due to the increased availability of O-H groups of the extract towards the carboxyl groups (-C=O) of lactic acid. Furthermore, an extended broader shoulder-like peak is shown up to 1550cm-1 with the loading of *C. macrostahyus* crude extract.

The sholder-like peak observed at 1595 cm^{-1} for the lactic acid oligomer was also shifted to the higher wavenumbers of 1637 cm^{-1}, 1640 cm^{-1}, and 1643 cm^{-1} respectively for OLLA-m-CM 1, OLLA-m-CM 2 and OLLA-m-CM 3 samples.

This can be correlated with hydrogen bonding due to the availability of OH groups responsible for improved molecular interaction. The IR spectrum can also be used to compare the change that occurred by the change in the mixing ratio of the starting materials. The in vitro anti-bacterial activity of the synthesized bio-adhesives were investigated against one Gram-negative bacteria and one Gram-positive bacteria with agar disk diffusion assay at a concentration of 1 mg/ml. For the antibacterial properties of the synthesized bioadhesives, the OLLA-m-CM 3 had the largest inhibition zone, which was approximately 11mm and 12mm for E.coil (gram-ve) and S.aureus (gram+ve) bacteria respectively. The water contact angle investigation of OLLA-m-CM gave a contact angle of 77.8°, 65.4°, and 56.7° for OLLA-m-CM 1, 2, and 3, respectively. This indicated that the hydrophobic nature of the OLLA-m-CM decreased with increasing the amount of starting material of Lactic acid.

Finally, a universal testing machine was used to determine the bonding strength of the three synthesized adhesives. Glass and bone substrates both experienced cohesive failure at maximum tensile strengths of 8 and 11 MPa, respectively.

5.2. RECOMMENDATION

This research work was intended to synthesize and characterize *C. macrostachyus* based bioadhesive via polycondensation reaction of L-Lactic acid. The characterization of OLLA-m-CM included functional group analysis, contact angle determination, anti-bacterial activity test, and tensile strength. As this research work is new, additional works for the future can be considered for further investigations:

- Investigation of the temperature response to the tensile strength using DMA is needed,
- Further NMR analysis is needed to define the exact reaction mechanism on the synthesize of Oligomer of Lactic acid modified C. macrostachyus,
- Since the presence of free lactic acid monomers in the conjugate affects the tensile strength, purification of the conjugate from the unreacted lactic acid is crucial. Further study can be explored in this area,
- With the obtained mechanical and antimicrobial properties of the adhesive, it can be a good candidate for other medical applications,
- The tensile strength test of the developed adhesive should be tested at wet environment
- As the mixing ratio is increased, the synthesized adhesive nature of OLLA-m-CM is changed to lubricant. It can be a good research area on the formulation of herbal ointment.

Research Fund Acknowledgement

This research project is funded by Adama Science and Technology University under the grant number of ASTU/SM-R/942/23 Adama, Ethiopia.

REFERENCE

Abebe W. (1986). *Survey of prescriptions used in traditional medicine in Gondar region, Northwestern Ethiopia: general pharmaceutical practice.* Journal of Ethnopharmacology. 18:147-165.

Alemu A, Mathewos A, and Desta E, Ashenafi. (2017). *In-vitro and In-vivo antibacterial activities of Croton macrostachyus methanol extract against Escherichia coli and Staphylococcus aureus*. Adv Anim Vet Sci;5:107-14.

Alqosaibi, A.I. (2022). *Nanocarriers for Anticancer Drugs: Challenges and Perspectives*. Saudi J. Biol. Sci, 29, 103298.

Amare A. (2010). *Determination of Essential, Non-Essential and Toxic Metals in Croton macrostachyus Leaves and its infusions*. MSc. Thesis, Addis Ababa University, pp 5-10

Augat, P.; Simon, U.; Liedert, A.; Claes, L. (2005). *Mechanics and mechano-biology of fracture healing in normal and osteoporotic bone. Osteoporos*. Int, 16 (Suppl. 2), 36–43.

Arbes, H.; Bösch, P.; Lintner, F.; Salzer, M. (1981). *First clinical experience with heterologous cancellous bone grafting combined with the Fibrin Adhesive System (F.A.S.).* Arch. Orthop. Trauma. Surg. 98, 183–188.

Bahney, C.S.; Zondervan, R.L.; Allison, P.; Theologis, A.; Ashley, J.W.; Ahn, J.; Miclau, T.; Marcucio, R.S.; Hankenson, K.D. (2019). *Cellular biology of fracture healing*. J. Orthop. Res., 37, 35–50.

Bauer, N.B.; Brinke, N.; Heiss, C.; Skorupa, A.B.; Peters, F.; Kraus, R.; Schnettler, R.; Moritz, A. (2009). *Biodegradable beta-Tri-Calciumphosphate/hydroxyethyl methacrylate enhanced three component bone adhesive demonstrates biocompatibility without evidence of systemic toxicity in a rabbit model*. J. Biomed. Mater. Res. Part B Appl. Biomater, 90, 767–777.

Berry PE. (2000). *Floristic and molecular phylogeny of a giant genus Croton Euphorbiaceae*). http://www.botany.wisc.edu/berry/bio.htm. 2000.

Bhagat, V.; Becker, M.L. (2017). *Degradable Adhesives for Surgery and Tissue Engineering. Biomacromolecules*, 18, 3009–3039.

Bhatia, S.K.; Arthur, S.D.; Chenault, H.K.; Figuly, G.D.; Kodokian, G.K. (2007). *Polysaccharide-based tissue adhesives for sealing corneal incisions*. Curr. Eye Res, 32, 1045–1050.

Böker, K.O.; Richter, K.; Jäckle, K.; Taheri, S.; Grunwald, I.; Borcherding, K.; von Byern, J.; Hartwig, A.; Wildemann, B.; Schilling, A.F.; et al. (2019). *Current state of bone adhesives-Necessities and hurdles.* Materials, 12, 3975.

Bolghari, N.; Shahsavarani, H.; Anvari, M.; Habibollahi, H. (2022). *A Novel Recombinant Chimeric Bio-Adhesive Protein Consisting of Mussel Foot Protein 3, 5, Gas Vesicle Protein A, and CsgA Curli Protein Expressed in Pichia Pastoris.* AMB Express, 12, 1–19.

Braunwald, N.S.; Gay, W.; Tatooles, C.J. *(*1966*). Evaluation of crosslinked gelatin as a tissue adhesive and hemostatic agent: An experimental study*. Surgery, 59, 1024–1030.

Breitenbach F. (1963). *The Indigenous Trees of Ethiopia*, Second Revised and Enlarged Edition, Ethiopian Forestry Association, Addis Ababa, pp. 306.

Bu, Y.; Pandit, A. (2022). *Cohesion Mechanisms for Bioadhesives*. Bioact. Mater, 13, 105–118.

Champomier-Vergès, M.-C., et al., (2002). *Lactic acid bacteria and proteomics: current knowledge and perspectives*. Journal of Chromatography B, 771(1-2): p. 329-342.

Chopra, H.; Kumar, S.; Singh, I. (2020). *Bioadhesive Hydrogels and Their Applications. In Bioadhesives in Drug Delivery*; John Wiley & Sons: Inc Hoboken, NJ, USA,; pp. 147–170. ISBN 9781119640240.

C. Miller, A. Fosmer, B. Rush, T. McMullin, D. Beacom, and P. Suominen,. (2019). *Industrial production of lactic acid*, *Compr. Biotechnol.*, no. January, pp. 208–217, doi: 10.1016/B978-0-12-809633-8.09142-1.

Dunn, C. J. & Goa, K. L. (1999). Fibrin sealant: *A review of its use in surgery and endoscopy.* Drugs 58, 863–886.

Ermias G. ,Ramachandran K.,Edo B.,Samuel G.,Venkata R. (2005). *Ultrasonic supported oil extraction, process modeling, and optimization by response surface methodology tool from Croton Macrostachyus leaf".* Biomass conversion and Biomass refinery. https://doi.org/10.1007/s13399-022-02357-9

Feng, C.; Wang, F.; Xu, Z.; Sui, H.; Fang, Y.; Tang, X.; Shen, X. (2018). *Characterization of Soybean Protein Adhesives Modified by Xanthan Gum*. Coatings, 8, 342.

Fernandez, M.J.S. (2021). *Development of Poly (2-Oxazoline) -Based Bone-Adhesive Biomaterials.* J. Biomed. Mater. Res. Part B Appl. Biomater..

Gardziella, A.; Mueller, R. (1990) .*Phenolic Resins. Kunstst*. Ger. Plast, 80, 66–68.

Gellynck, K.; Neel, E.A.A.; Li, H.; Mardas, N.; Donos, N.; Buxton, P.; Young, A.M. (2011). *Cell attachment and response to photocured, degradable bone adhesives containing tricalcium phosphate and purmorphamine*. Acta Biomater, 7, 2672–2677

Ghasemi E, Raofie F, Najafi NM. (2011). *Application of response surface methodology and central composite design for the optimisation of supercritical fluid extraction of essential oils from Myrtus communis L. leaves. Food* Chem; 126(3):1449-53. [DOI:10.1016/j.foodchem.2010.11.135]

Guo, Q.; Chen, J.; Wang, J.; Zeng, H.; Yu, J. (2011*). Recent Progress in Synthesis and Application of Mussel-Inspired Adhesives.* Nanoscale, 12, 1307–1324.

Gupta, H.S.; Zioupos, P. (2008). *Fracture of bone tissue: The 'hows' and the 'whys'*. Med. Eng. Phys., 30, 1209–1226.

Habenicht, G. Kleben. Grundlagen, Technologien, Anwendungen; 5., erw. und aktualisierte Aufl.; Ed. (2006). Springer: Berlin, Germany, ISBN 3-540-26273-3.

Heiss, C.; Schnettler, R. Bioresorbierbare Knochenklebstoffe. *Historischer Rückblick und heutiger Stand. (2005). Unfallchirurg*, 108, 348–355.

Herget, G. W. et al. (2001). *Experimental use of an albumin-glutaraldehyde tissue adhesive for sealing pulmonary parenchyma and bronchial anastomoses*. Eur. J. Cardiothorac. Surg. 19, 4–9.

Heywood V .(1993).*Flowering Plants of the World. Andromeda Oxford Ltd*., Oxford, pp. 335.

Hoffmann, B.; Seitz, D.; Mencke, A.; Kokott, A.; Ziegler. (2009). *G. Glutaraldehyde and oxidised dextran as crosslinker reagents for chitosan-based scaffolds for cartilage tissue engineering*. J. Mater. Sci. Mater. Med, 20, 1495–1503.

Holten, C. H., Muller, A. and Rehbinder, D. (1971). *Lactic acid*. International Research Association, VerlagChemie, Copenhagen, Denmark.

Hou, M.; Wang, X.; Yue, O.; Zheng, M.; Zhang, H.; Liu, X. (2021). *Development of a Multifunctional Injectable Temperature-Sensitive Gelatin-Based Adhesive Double-Network Hydrogel*. Mater. Sci. Eng, 134, 112556.

Hyldbakk, A.; Mørch, Y.; Snipstad, S.; Åslund, A.K.O.; Klinkenberg, G.; Nakstad, V.T.; Wågbø, A.M.; Schmid, R.; Molesworth, P.P. (*2005*). *Identification of Novel Cyanoacrylate Monomers for Use in Nanoparticle Drug Delivery Systems Prepared by Miniemulsion Polymerisation—A Multistep Screening Approach*. Int. J. Pharm, 4, 100124

Jalili F, Jafari SM, Emam-Djomeh Z, Malekjani N, Farzaneh V.(2018). *Optimization of ultrasound-assisted extraction of oil from canola seeds with the use of response surface methodology. Food* Anal. Methods.11(2): 598-612. https://doi.org/10.1007/s12161-017-1030-z

J. A. Kiehlbauch, G. E. Hannett, M. Salfinger, W. Archinal, C. Monserrat, and C. Carlyn. (2000) "*Use of the National Committee for Clinical Laboratory Standards guidelines for disk diffusion susceptibility testing in New York State Laboratories*," J. Clin. Microbiol., vol. 38, no. 9, pp. 3341–3348, doi: 10.1128/jcm.38.9.3341-3348.2000.

Jayakumar, R.; Prabaharan, M.; Kumar, P.T.S.; Nair, S.V.; Tamura, H. (2011). *Biomaterials based on chitin and chitosan in wound dressing applications*. Biotechnol. Adv, 29, 322–337.

Kapingu MC, Dominique G, Mbwambo ZH, Moshi MJ, Uiso FC, Mahunnah RLA. (2000). *Diterpenoids from roots of Croton macrostachys. Phytochemistry*; 54:767-770

Karunamoorthi K, Ilango K. (2010). *Larvicidal activity of Cymbopogon citratus (DC) Stapf and Croton macrostachyus against Anopheles arabiensis Patton, a potent malaria vector*. Eur Rev Med Pharmacol Sci; 14:57-62.

Kelecha WM. (1977). *A Glossary of Ethiopian plant names*. Second Edition. Addis Ababa, Ethiopia, 63-168.

Kim, M.H.; Lee, J.N.; Lee, J.; Lee, H.; Park, W.H. (2020). *Enzymatically Cross-Linked Poly(γ-Glutamic Acid) Hydrogel with Enhanced Tissue Adhesive Property. ACS Biomater*. Sci. Eng, 6, 3103–3113.

Kjaergard, H. K., Weis-Fogh, U. S., Sorensen, H., Thiis, J. & Rygg, I. (1992).*utologous fibrin glue–preparation and clinical use in thoracic surgery.* Eur. J. Cardiothorac. Surg. 6, 52–54.

Komesu, A., et al., (2017). *Study of lactic acid thermal behavior using thermoanalytical techniques*. Journal of Chemistry,. 2017. 101.

Kovach, T.K.; Dighe, A.S.; Lobo, P.I.; Cui, Q. (2015). *Interactions between MSCs and immune cells*: Implications for bone healing. J. Immunol. Res, 248.

Kull, S.; Martinelli, I.; Briganti, E.; Losi, P.; Spiller, D.; Tonlorenzi, S.; Soldani, G. Glubran2. (2009). *Surgical Glue: In Vitro Evaluation of Adhesive and Mechanical Properties.* J. Surg. Res, 157, e15–e21.

Kumar, M.; Tomar, M.; Punia, S.; Dhakane-Lad, J.; Dhumal, S.; Changan, S.; Senapathy, M.; Berwal, M.K.; Sampathrajan, V.; Sayed, A.A.S.; et al. (2022). *Plant-Based Proteins and Their Multifaceted Industrial Applications.* Lwt, 154, 112620.

Le, P.T. and K.T. Nguyen. (2020). *Hydrophobizing cellulose surfaces via catalyzed transesterification reaction using soybean oil and starch*. Heliyon, 6(11): p. e05559.

Li, D.; Chen, J.; Wang, X.; Zhang, M.; Li, C.; Zhou, J. (2020). *Recent Advances on Synthetic and Polysaccharide Adhesives for Biological Hemostatic Applications*. Front. Bioeng. Biotechnol, 8, 926.

Li M, Zhao G, Liu J, Liang X, Zhang M, Zhou G, Wang Y .(2021). *Optimization of ultrasound-assisted extraction of peony seed oil with response surface methodology and analysis of fatty acid.* Agric. Res. 10(4): 543-555. https://doi.org/10.1007/s40003-021-00554-y

Li T, Qu XY, Zhang QA, Wang ZZ .(2012). *Ultrasound-assisted extraction and profle characteristics of seed oil from Isatis indigotica Fort*. Ind Crops Prod 35:98–104. https://doi.org/10.1016/j. indcrop.2011.06.013

Liu, Y.; Ng, S.C.; Yu, J.; Tsai, W.-B. (2019). *Modification and crosslinking of gelatin-based biomaterials as tissue adhesives.* Colloids Surf. B Biointerfaces, 174, 316–323.

Mairura F (2007). *Croton macrostachyus Hochst. ex Delile*. In: Schmelzer G & Gurib (Editors). Prota 11(1): *Medicinal plants/Plantes médicinales* 1. [CD-Rom]. PROTA, Wageningen, Netherlands.

Majidi A, Ziaei Hezarjaribi H, Arab H, Momeni Z, Davoodi A, Azadbakht M. (2019). *In vitro antitrichomonal activity of some species of Allium.* Jundishapur J Nat Pharm Prod; 15(1):e89649. [DOI:10.5812/jjnpp.89649]

Mangunwidjaja, D. S., Kardono, S. R., & Iswantini, L. B. (2006). *Gas chromatography and gas chromatography-mass spectrometry analysis of Indonesian Croton tiglium seeds*. Journal Applied Sciences, 6, 1576–1580.

Marayanan, N. (2004). L (+) *lactic acid fermentation and its product polymerization*. Electron. J. Biotechnol. 7:167-169.

Martinez, F.A.C., et al., (2013). *Lactic acid properties, applications and production: a review*. Trends in food science & technology, 30(1): p. 70-83. 102.

Matu E and van Staden J .(2003). *Antibacterial and anti-inflammatory activities of some plants used for medicinal purposes in Kenya*. Journal of Ethnopharmacology, 87: 35–41.

Mazzanti G, Bolle P, Martinoli L, Piccinelli D, Grgurina I, Animati F et al. (1987). *Croton macrostachyus, a plant used in traditional medicine: purgative and inflammatory activity*. Journal of Ethnopharmacology; 19:213-219.

Megersa M. (2010). *Ethnobotanical Study of Medicinal Plants in Wayu Tuka Wereda, East Wollega Zone of Oromia Region, Ethiopia In*: Graduate thesis for M.sc Addis Ababa University.

Mekonnen L. B. (2015). *In vivo antimalarial activity of the crude root and fruit extracts of Croton macrostachyus (Euphorbiaceae) against Plasmodium berghei in mice*. Journal of traditional and complementary medicine, 5(3), 168–173.

Menon, N. G., Downing, S., Goldberg, N. H. & Silverman, R. P. (2013). *Seroma prevention using an albumin-glutaraldehyde-based tissue adhesive in the rat mastectomy model.* Ann. Plast. Surg. 50, 639–643.

Meseret E, Tatek T, & Melaku T.(2022). *In-situ oligomerization of lactic acid within broiler skin extracted elastin/collagen matrix for the efficacy of ointment base.* Heliyon,28;8(8). doi: 10.1016/j.heliyon.2022.e10346

Moini, N., et al., (2013). *Engineered Green Adhesives Based on Demands: Star-Shaped Glycerol–Lactic Acid Oligomers in Anaerobic Adhesives*. ACS Sustainable Chemistry & Engineering, 7(19): p. 16247-16256. 106.

Moon, Y.J.; Yoon, S.J.; Koo, J.H.; Yoon, Y.; Byun, H.J.; Kim, H.S.; Khang, G.; Chun, H.J.; Yang, D.H. (2021). *β-Cyclodextrin/Triclosan Complex-Grafted Methacrylated Glycol Chitosan Hydorgel by Photocrosslinking via Visible Light Irradiation for a Tissue Bio-Adhesive.* Int. J. Mol. Sci, 22, 700.

M. Zafar et al., (2020). *Preventive effect of Euphorbia royleana Boiss on diabetes induced by streptozotocin via modulating oxidative stress and deoxyribonucleic acid damage*. Toxin Rev., vol. 0, no. 0, pp. 1–14, doi: 10.1080/15569543.2020.1780262.

Negrescu, A.M.; Mitran, V.; Draghicescu, W.; Popescu, S.; Pirvu, C.; Ionascu, I.; Soare, T.; Uzun, S.; Croitoru, S.M.; Cimpean, A. (2022). *TiO2 Nanotubes Functionalized with Icariin for an Attenuated In Vitro Immune Response and Improved In Vivo Osseointegration*. J. Funct. Biomate, 13, 43.

Nellans, K.W.; Kowalski, E.; Chung, K.C. (2012). *The Epidemiology of Distal Radius Fractures*. Hand Clin. , 28, 113–125.

N. Narayanan. (2004). *L (+) lactic acid fermentation and its product polymerization*, vol. 7, no.

Nomori, H.; Horio, H.; Morinaga, S.; Suemasu, K. (1999). *Gelatin resorcinol formaldehyde glutaraldehyde glue for sealing pulmonary air leaks during thoracoscopic operation.* Ann. Thorac. Surg, 67, 212–216.

Ochs, B.G.; Gonser, C.E.; Baron, H.C.; Stöckle, U.; Badke, A.; *Stuby, F.M. Refrakturen nach Entfernung von Osteosynthesematerialien. Eine vermeidbare Komplikation?* Unfallchirurg 2012, 115, 323–329.

Owen, R. J. et al. (2000). *Percutaneous ablation of an internal iliac aneurysm using tissue adhesive.* Cardiovasc. Intervent. Radiol. 23, 389–391.

Parimalakrishnan, S., Akalanka, D., Rajeswari, J., & Ravikumar, K. (2015). *Extraction and Characterization of Phytoconstituents Cleome chelidonii by GCMS*. International Journal of Chemical and Pharmaceutical Sciences, 6(1), 63–69.

Parthipan, B., Suky, M. G. T., & Mohan, V. R. (2015). *GC-MS Analysis of phytocomponents in Pleiospermium alatum (Wal.l ex Wight & Arn.) Swingle, (Rutaceae)*. Journal of Pharmacognosy and Phytochemistry, 4(1), 216–222

Pascual, G.; Sotomayor, S.; Rodríguez, M.; Pérez-Köhler, B.; Kühnhardt, A.; Fernández-Gutiérrez, M.; Román, J.S.; Bellón, J.M. *Cytotoxicity of cyanoacrylate-based tissue adhesives and short-term preclinical in vivo biocompatibility in abdominal hernia repair.* PLoS ONE 2016, 11, e0157920.

Pei, X.; Wang, J.; Cong, Y.; Fu, J. (2021). *Recent Progress in Polymer Hydrogel Bioadhesives*. J. Polym. Sci., 59, 1312–1337

Q. Wang, H. Y. Huang, and Y. Z. Wang, (2020). *FTIR and UV spectra for the prediction of triterpene acids in Macrohyporia cocos*," Microchem. J., vol. 158, no. June, p. 105167, doi: 10.1016/j.microc.2020.105167.

Ramesh, M.; Kumar, L.R. (2020). *Bioadhesives. In Green Adhesives: Preparation, Properties and Applications*; John Wiley & Sons: Inc Hoboken, NJ, USA; pp. 145–163

Rashid, R. (2008). *Optimization and modeling of lactic acid production from pineapple waste.* dessertation, Phd UniversitiTeknologi Malaysia

Rathi, S.; Saka, R.; Domb, A.J.; Khan, W. (2019). *Protein-Based Bioadhesives and Bioglues*. Polym. Adv. Technol, 30, 217–234.

Salatino A, Salatino MLF, Negri G. (2020). *Traditional uses chemistry and pharmacology of Croton species (Euphorbiaceae).* Journal of Brazilian Chemical Society; 18:11-33.

Salem, M. Z. M., Aly, H., Gohar, Y., El-Sayed, A. W. (2013). *Biological activity of extracts from Morus alba L., Albizzia lebbeck (L.) Benth. and Casuarina glauca Sieber against the growth of some pathogenic bacteria*. International Journal of Agricultural and Food Research, 2(1): 9-22.

Samaram S, Mirhosseini H, Ping C, Mohd H, Bordbar S. (2015). *Optimisation of ultrasound-assisted extraction of oil from papaya seed by response surface methodology:* Oil recovery, radical scavenging antioxidant activity, and oxidation stability. FOOD Chem 172:7–17.

Sánchez-Fernández, M.J.; Hammoudeh, H.; Lanao, R.P.F.; van Erk, M.; van Hest, J.C.M.; Leeuwenburgh, S.C.G. (2019). *Bone-Adhesive Materials: Clinical Requirements, Mechanisms of Action, and Future Perspective*. Adv. Mater. Interfaces 2019, 6, 1802021.

Sardella, E.; Gristina, R.; Fanelli, F.; Veronico, V.; Da Ponte, G.; Kroth, J.; Fracassi, F.; Favia, P. (2020). *How to Confer a Permanent Bio-Repelling and Bio-Adhesive Character to Biomedical Materials through Cold Plasmas*. Appl. Sci, 10, 9101.

Saxena, D.K., Sharma, S.K. & Sambi, S.S. (2011). *Comparative Extraction of Cottonseed Oil by n-Hexane and Ethanol.* J. Eng. Appl. Sci. 6(1), 84–89. http://www.arpnjournals.com/jeas/

Scalzone, A.; Bonifacio, M.A.; Cometa, S.; Cucinotta, F.; De Giglio, E.; Ferreira, A.M.; Gentile, P. (2020). *PH-Triggered Adhesiveness and Cohesiveness of Chondroitin Sulfate-Catechol Biopolymer for Biomedical Applications*. Front. Bioeng. Biotechnol., 8, 1–14.

Schmitz, F.P.; Symietz, D. Klebstoffe im Fahrzeugbau. Die unsichtbaren Helfer. Chem. Unserer Zeit (2008), 42, 92–101.

S. Figalla, J. Petrůj, and T. Švestková, (2018). *Transesterification of lactic acid oligomers with ethanol, a way to anhydrous ethyl lactate: A kinetic study*," *Molecules*, vol. 23, no. 8, doi: 10.3390/molecules23082044.

Shahryarimorad, K.; Alipour, A.; Honar, Y.S. (2020). Abtahi, B. *In Silico Prediction and in Vitro Validation of the Effect of PH on Adhesive Behaviour of the Fused CsgA - MFP3 Protein*. AMB Express, 12, 1–13.

S. Jarmelo et al.,(2012) *Experimental (IR/Raman and 1H/13C NMR) and theoretical (DFT) studies of the preferential conformations adopted by l -lactic acid oligomers and Poly(l - lactic acid) homopolymer*,J. Phys. Chem. B, vol. 116, no. 1, pp. 9–21, doi: 10.1021/jp205033c.

Simson, J.; Crist, J.; Strehin, I.; Lu, Q.; Elisseeff, J.H. (2012). *An orthopedic tissue adhesive for targeted delivery of intraoperative biologics.* J. Orthop. Res, 31, 392–400.

Smith, D.C. Lutes. (1987). *Glues, Cements and Adhesives in Medicine and Dentistry*. Bio-Medical Eng, 8, 108–115. 100.

Sodeifan G, Ardestani NS, Sajadian SA .(2019). *Extraction of seed oil from Diospyros lotus optimized using response surface methodology*. J. For. Res.30(2): 709-719.

Sweah, Z.J. and A.J. Mohammed. (2021). *Study of mechanical properties behaviour of biodegradable blends based on wood adhesive, lactic acid, polyvinyl alcohol, and aloe Vera. Materials Today*: Proceedings, 42: p. 2134-2140.

Tabatabaei, F.; Rasoulianboroujeni, M.; Yadegari, A.; Tajik, S.; Moharamzadeh, K.; Tayebi, *L*. (2021). *Osteo-Mucosal Engineered Construct: In Situ Adhesion of Hard-Soft Tissues.* Mater. Sci. Eng. C, 128, 112255.

Tala MF, Tan NH, Ndonsta BL, Tane P .(2013). *Triterpinoids and phenolic commpounds from Croton macrostchyus.* Biochem Syst Ecolo 51:138–141.

Tan CX, Gun Hean C, Hamzah H, Ghazali HM .(2018). *Optimization of ultrasound-assisted aqueous extraction to produce virgin avocado oil with low free fatty acids.* J Food Process Eng. 41(2):1–9.

Taniguchi M, Kubo I. (1993). *Ethnothnobotanical drug discovery based on medicine men's trials in the African savanna:* Screening of East African Plants for antimicrobial activity II. Journal of Natural Products; 56:1539-1546.

Tao, C.; Jin, M.; Yao, H.; Wang, D.A. (2021). *Dopamine Based Adhesive Nano-Coatings on Extracellular Matrix (ECM) Based Grafts for Enhanced Host-Graft Interfacing Affinity*. Nanoscale, 13, 18148–18159.

Tariku Y, Hymete A, Hilu A, Rohloff J. (2010). Constituents, *antileishmanial activity and toxicity profile of volatile oil from berries of Croton macrostachyus*. Journal of Natural Product; 5:975-980.

Tatooles, C.J.; Braunwald, N.S. (1966). *The use of crosslinked gelatin as a tissue adhesive to control hemorrhage from liver and kidney*. Surgery, 60, 857–861.

Tefera M.(2006). .*In vitro Evaluation of Anti-Microbial activities of Albiza gummifera and Croton macrostachyus against clinical isolates of Neisseria Gonorrhoeae*. In: Graduate thesis for M.sc Addis Ababa University.

Tripathi, N. and V. Katiyar. (2018) *L.actic acid oligomer (OLLA) grafted gum arabic based green adhesive for structural applications*. International journal of biological macromolecules, . 120: p. 711-720.

Vainio, J.; Kilpikari, J.; Trml, P.; Rokkanen, P. (1979). *Experimental fixation of bone cement and composite resins to bone.* Arch. Orthop. Trauma Surg, 94, 191–195.

Wanasingha, N.; Dutta, N.K.; Choudhury, *N.R*. (2021). *Emerging bioadhesives: From traditional bioactive and bioinert to a new biomimetic protein-based approach.* Adv. Colloid Interface Sci, 296, 102521.

Wang, D.-A.; Varghese, S.; Sharma, B.; Strehin, I.; Fermanian, S.; Gorham, J.; Fairbrother, D.H.; Cascio, B.; Elisseeff, J.H. (2007). *Multifunctional chondroitin sulphate for cartilage tissue-biomaterial integration.* Nat. Mater, 6, 385–392.

Workitu F.,Arumuganainar S.,Abenezer T.,Binyam T.,Habib S., (2018). "*Bactericidal action of Croton macrostachyus leaf extract against common human pathogenic bacteria*''. Jornal of Medical Plants Study.

Wu, A.-M.; Bisignano, C.; James, S.L.; Abady, G.G.; Abedi, A.; Abu-Gharbieh, E.; Alhassan, R.K.; Alipour, V.; Arabloo, J.; Asaad, M.; et al. (2019). *Global, regional, and national burden of bone fractures in 204 countries and territories,*: A systematic analysis from the Global Burden of Disease Study. Lancet Health Longev, 2, e580–e592.

Xiang, L. (2020). *Molecular Interaction and Adhesion Mechanisms of Mussel-Inspired Adhesive Coatings*; University of Alberta: Alberta, Canada.

Yang, G.; Rothrauff, B.B. (2013). Tuan, R.S. *Tendon and ligament regeneration and repair: Clinical relevance and developmental paradigm*. Birth Defects Res. Part C Embryo Today Rev., 99, 203–222

Yolmeh M, Habibi Najaf MB, Farhoosh R (2014) *Optimisation of ultrasound-assisted extraction of natural pigment from annatto seeds by response surface methodology (RSM*). Food Chem 155:319–324

Yu, Y.; Brió Pérez, M.; Cao, C.; de Beer, S. (2021). Switching (Bio-) *Adhesion and Friction in Liquid by Stimulus Responsive Polymer Coatings.* Eur. Polym. J, 147, 110298.

Zelalem Yibralign. (2007). *Phytochemical investigation on the stem bark of croton macrostachyus (Bisana)*. MSc. thesis, Addis Ababa University, Ethiopia pp 2 &3

Zhang, Y.; Debenedictis, E.P.; Keten, S. (2019).*Cohesive and Adhesive Properties of Crosslinked Semi-flexible Biopolymer Networks*. Soft Matter, 15, 3807–3816.

Zhu, G.; Zhang, T.; Chen, M.; Yao, K.; Huang, X.; Zhang, B.; Li, Y.; Liu, J.; Wang, Y.; Zhao, Z. (2021). *Bone physiological microenvironment and healing mechanism: Basis for future bone-tissue engineering scaffolds*. Bioact. Mater, 6, 4110–4140.

Zou, C.Y.; Lei, X.X.; Hu, J.J.; Jiang, Y.L.; Li, Q.J.; Song, Y.T.; Zhang, Q.Y.; Li-Ling, J.; Xie, H.Q. (2022). *Multi-Crosslinking Hydrogels with Robust Bio-Adhesion and pro-Coagulant Activity for First-Aid Hemostasis and Infected Wound Healing.* Bioact. Mater, 16, 388–402.

Zussma, M.; Giladi, S.; Zilberman, M. (2022). *In Vitro Characterization of Injectable Chlorhexidine-Eluting Gelatin Hydrogels for Local Treatment of Periodontal Infections*. Polym. Adv. Technol. 2022, 1–12

APPENDIXE

A: Mass spectrum of leaf extract of *C.macrostachyus*

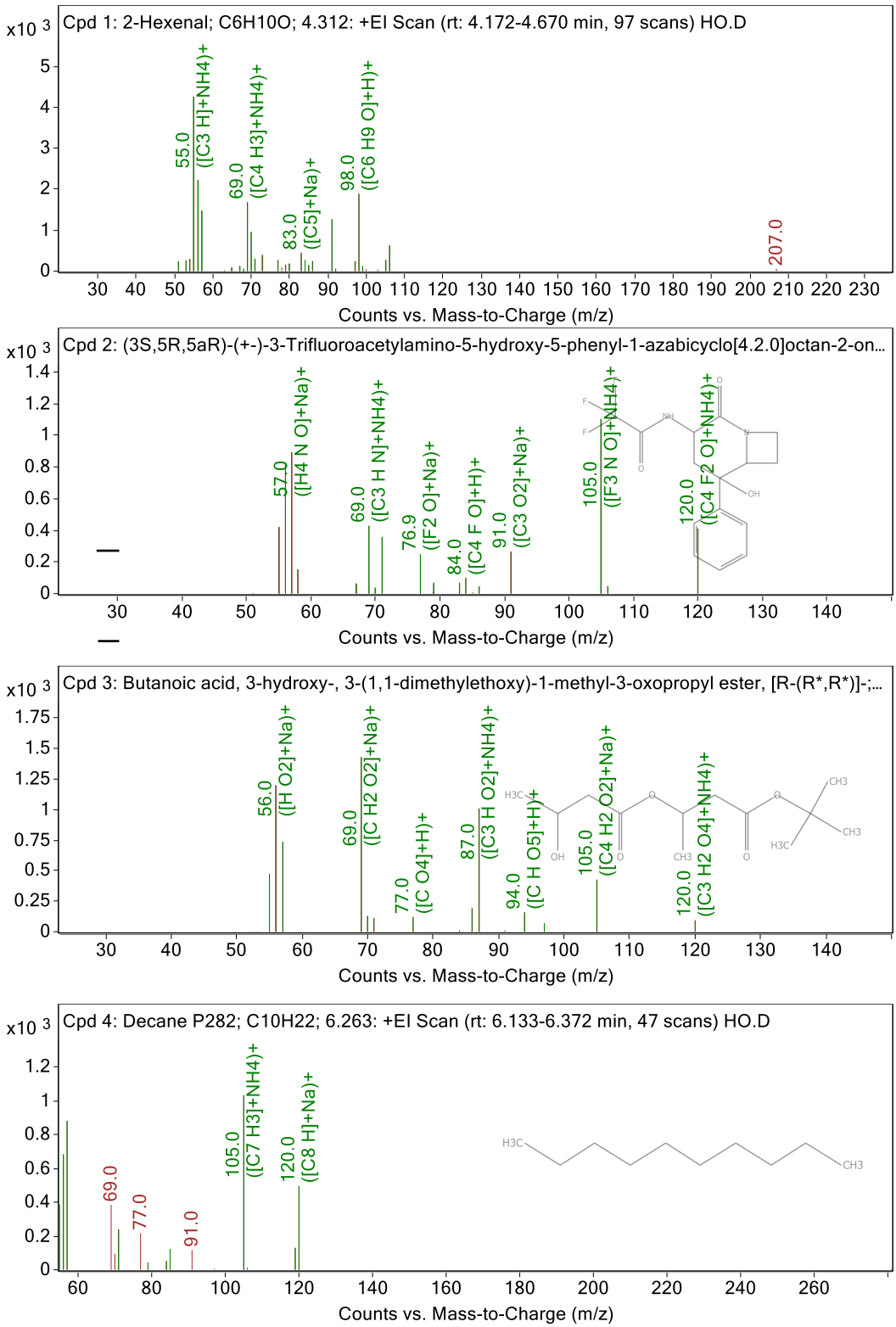

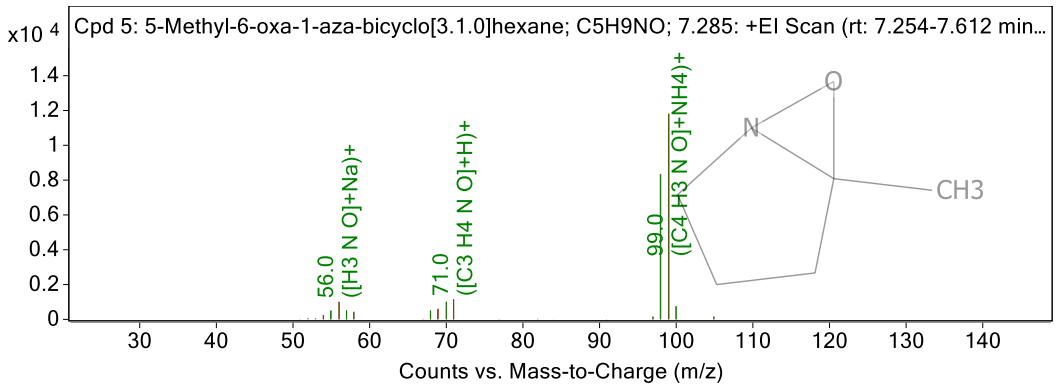
Cpd 5: 5-Methyl-6-oxa-1-aza-bicyclo[3.1.0]hexane; C5H9NO; 7.285: +EI Scan (rt: 7.254-7.612 min…
x10 4
56.0 ([H3 N O]+Na)+
71.0 ([C3 H4 N O]+H)+
99.0 ([C4 H3 N O]+NH4)+
O
N
CH3
Counts vs. Mass-to-Charge (m/z)

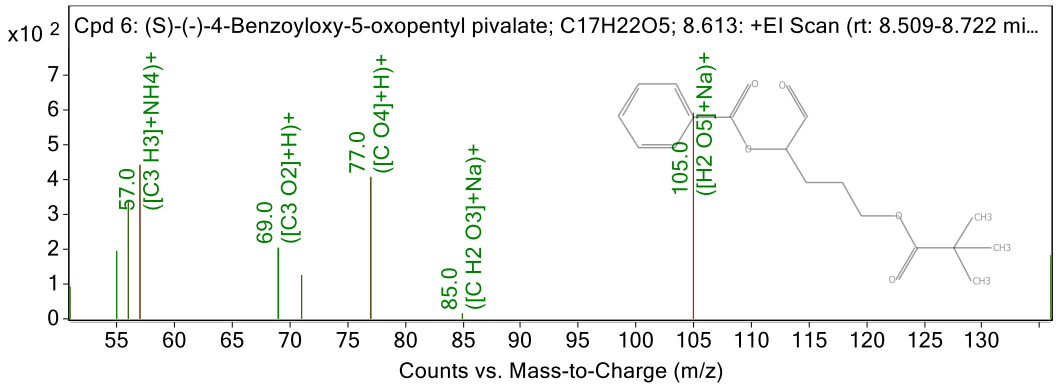
Cpd 6: (S)-(-)-4-Benzoyloxy-5-oxopentyl pivalate; C17H22O5; 8.613: +EI Scan (rt: 8.509-8.722 mi…
x10 2
57.0 ([C3 H3]+NH4)+
69.0 ([C3 O2]+H)+
77.0 ([C O4]+H)+
85.0 ([C H2 O3]+Na)+
105.0 ([H2 O5]+Na)+
Counts vs. Mass-to-Charge (m/z)

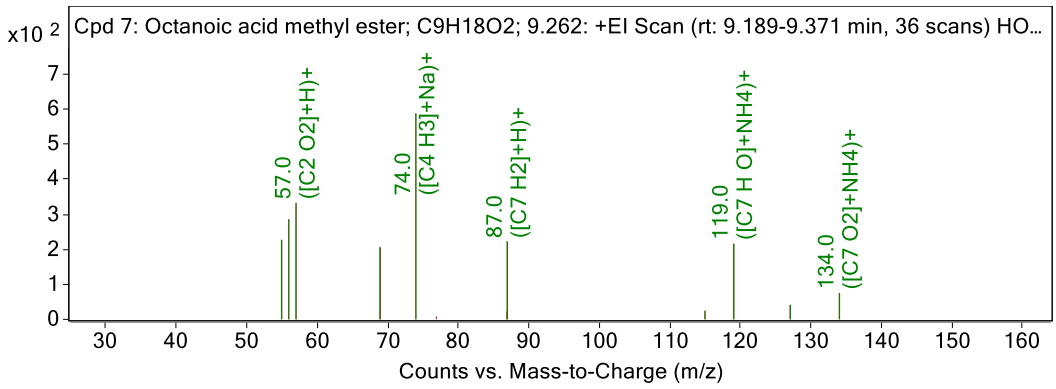
Cpd 7: Octanoic acid methyl ester; C9H18O2; 9.262: +EI Scan (rt: 9.189-9.371 min, 36 scans) HO…
x10 2
57.0 ([C2 O2]+H)+
74.0 ([C4 H3]+Na)+
87.0 ([C7 H2]+H)+
119.0 ([C7 H O]+NH4)+
134.0 ([C7 O2]+NH4)+
Counts vs. Mass-to-Charge (m/z)

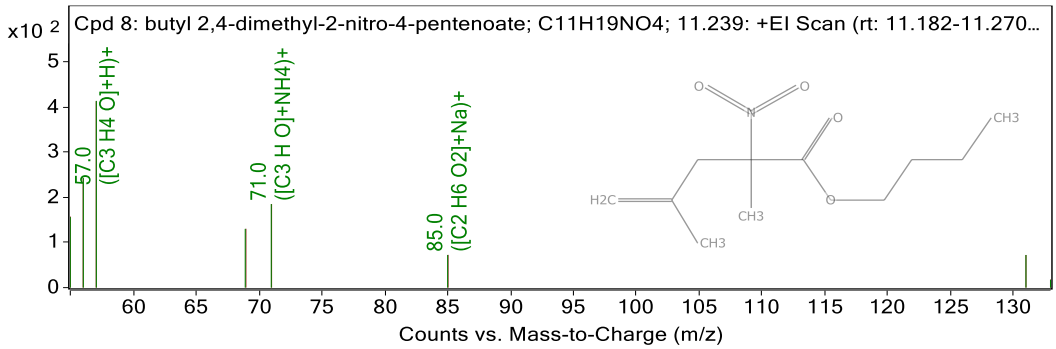
Cpd 8: butyl 2,4-dimethyl-2-nitro-4-pentenoate; C11H19NO4; 11.239: +EI Scan (rt: 11.182-11.270…
x10 2
57.0 ([C3 H4 O]+H)+
71.0 ([C3 H O]+NH4)+
85.0 ([C2 H6 O2]+Na)+
H2C
CH3
Counts vs. Mass-to-Charge (m/z)

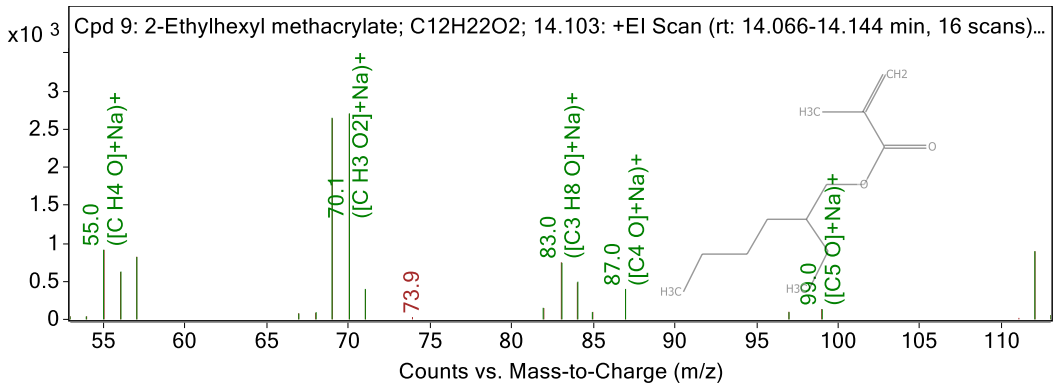
Cpd 9: 2-Ethylhexyl methacrylate; C12H22O2; 14.103: +EI Scan (rt: 14.066-14.144 min, 16 scans)...
x10 3
55.0 ([C H4 O]+Na)+
70.1 ([C H3 O2]+Na)+
73.9
83.0 ([C3 H8 O]+Na)+
87.0 ([C4 O]+Na)+
99.0 ([C5 O]+Na)+
Counts vs. Mass-to-Charge (m/z)

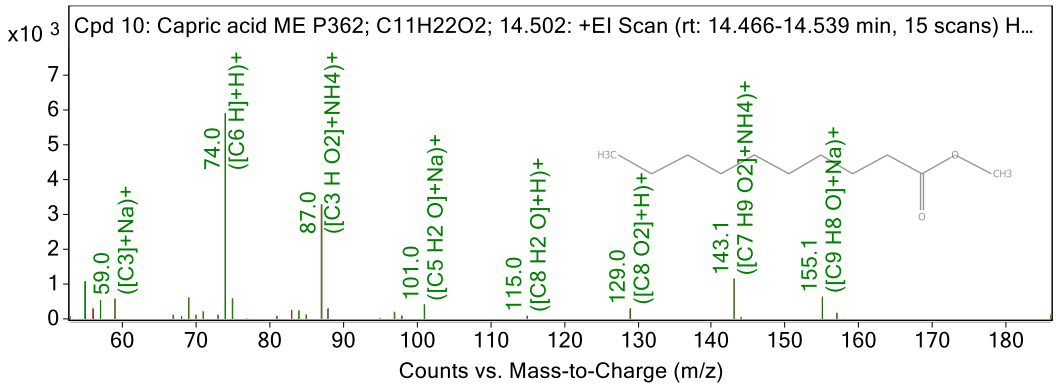
Cpd 10: Capric acid ME P362; C11H22O2; 14.502: +EI Scan (rt: 14.466-14.539 min, 15 scans) H...
x10 3
59.0 ([C3]+Na)+
74.0 ([C6 H]+H)+
87.0 ([C3 H O2]+NH4)+
101.0 ([C5 H2 O]+Na)+
115.0 ([C8 H2 O]+H)+
129.0 ([C8 O2]+H)+
143.1 ([C7 H9 O2]+NH4)+
155.1 ([C9 H8 O]+Na)+
Counts vs. Mass-to-Charge (m/z)

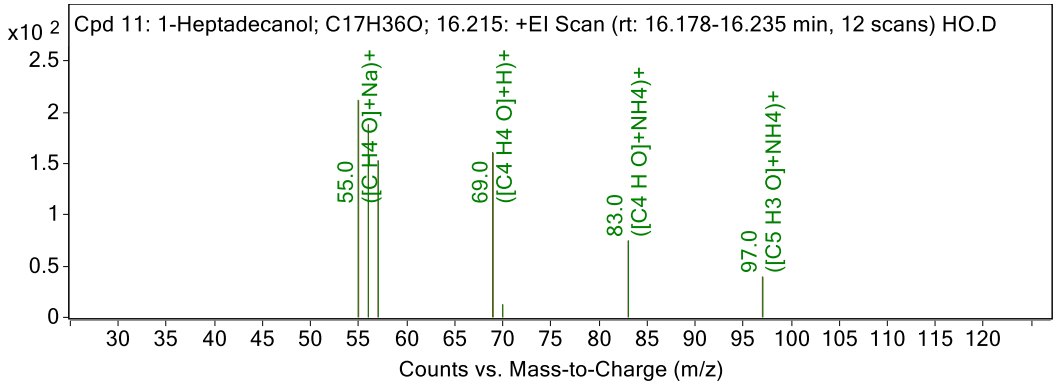
Cpd 11: 1-Heptadecanol; C17H36O; 16.215: +EI Scan (rt: 16.178-16.235 min, 12 scans) HO.D
x10 2
55.0 ([C H4 O]+Na)+
69.0 ([C4 H4 O]+H)+
83.0 ([C4 H O]+NH4)+
97.0 ([C5 H3 O]+NH4)+
Counts vs. Mass-to-Charge (m/z)

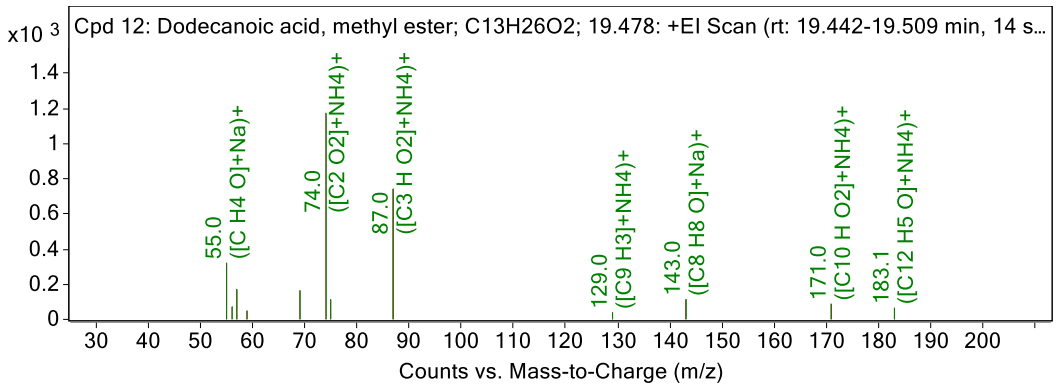
Cpd 12: Dodecanoic acid, methyl ester; C13H26O2; 19.478: +EI Scan (rt: 19.442-19.509 min, 14 s...
x10 3
55.0 ([C H4 O]+Na)+
74.0 ([C2 O2]+NH4)+
87.0 ([C3 H O2]+NH4)+
129.0 ([C9 H3]+NH4)+
143.0 ([C8 H8 O]+Na)+
171.0 ([C10 H O2]+NH4)+
183.1 ([C12 H5 O]+NH4)+
Counts vs. Mass-to-Charge (m/z)

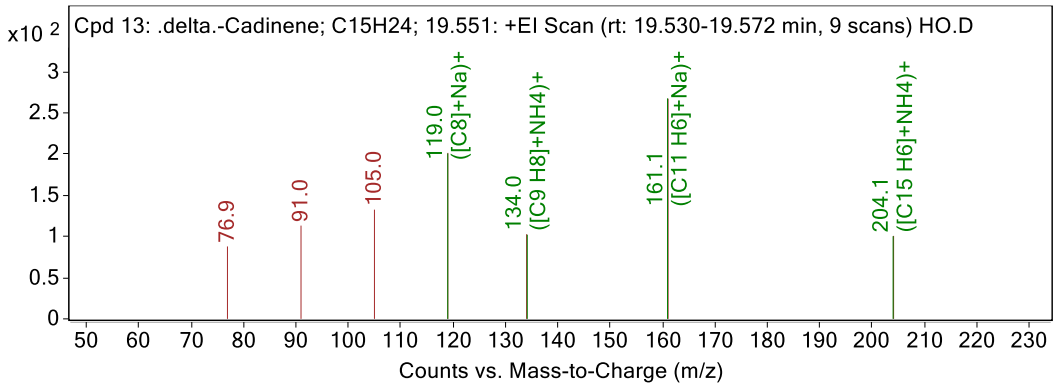
Cpd 13: .delta.-Cadinene; C15H24; 19.551: +EI Scan (rt: 19.530-19.572 min, 9 scans) HO.D
x10 2
76.9
91.0
105.0
119.0 ([C8]+Na)+
134.0 ([C9 H8]+NH4)+
161.1 ([C11 H6]+Na)+
204.1 ([C15 H6]+NH4)+
Counts vs. Mass-to-Charge (m/z)

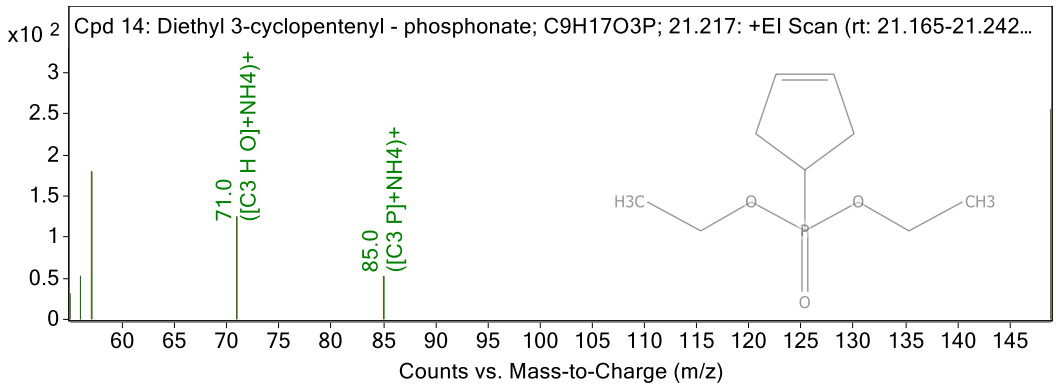
Cpd 14: Diethyl 3-cyclopentenyl - phosphonate; C9H17O3P; 21.217: +EI Scan (rt: 21.165-21.242...
x10 2
71.0 ([C3 H O]+NH4)+
85.0 ([C3 P]+NH4)+
H3C
O
P
O
O
CH3
Counts vs. Mass-to-Charge (m/z)

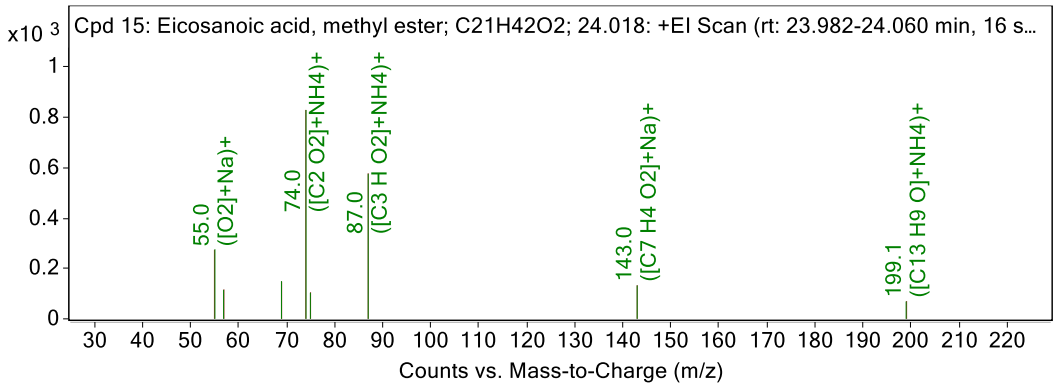
Cpd 15: Eicosanoic acid, methyl ester; C21H42O2; 24.018: +EI Scan (rt: 23.982-24.060 min, 16 s...
x10 3
55.0 ([O2]+Na)+
74.0 ([C2 O2]+NH4)+
87.0 ([C3 H O2]+NH4)+
143.0 ([C7 H4 O2]+Na)+
199.1 ([C13 H9 O]+NH4)+
Counts vs. Mass-to-Charge (m/z)

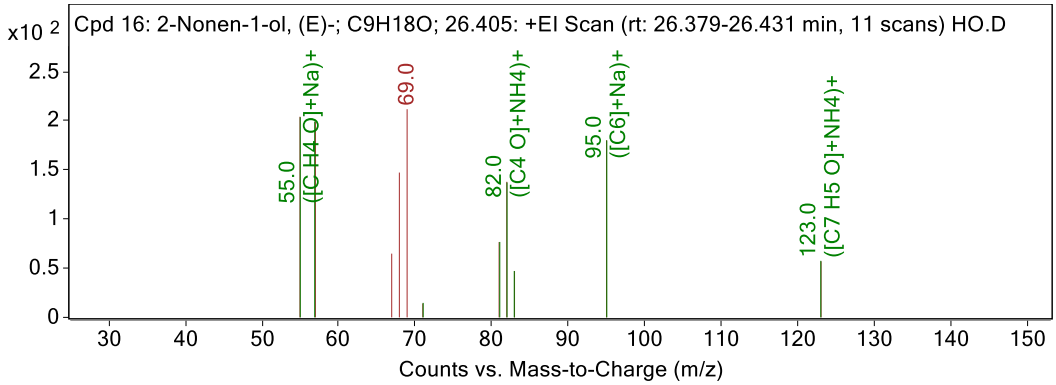
Cpd 16: 2-Nonen-1-ol, (E)-; C9H18O; 26.405: +EI Scan (rt: 26.379-26.431 min, 11 scans) HO.D
x10 2
55.0 ([C H4 O]+Na)+
69.0
82.0 ([C4 O]+NH4)+
95.0 ([C6]+Na)+
123.0 ([C7 H5 O]+NH4)+
Counts vs. Mass-to-Charge (m/z)

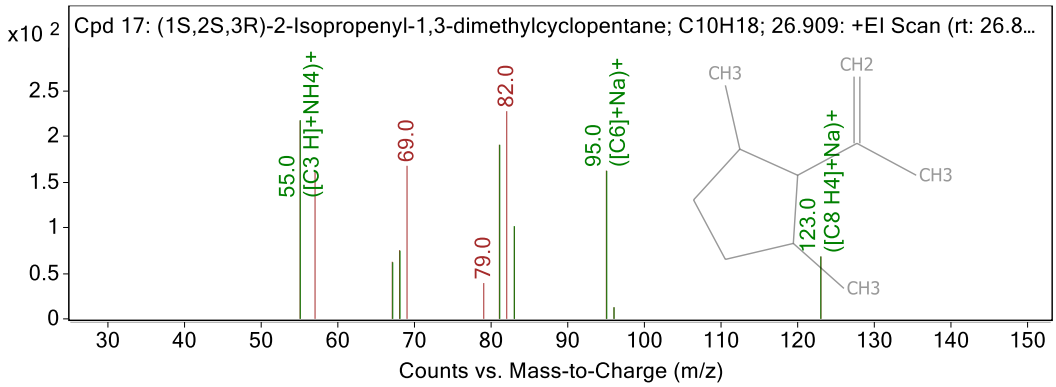
Cpd 17: (1S,2S,3R)-2-Isopropenyl-1,3-dimethylcyclopentane; C10H18; 26.909: +EI Scan (rt: 26.8...
x10 2
55.0 ([C3 H]+NH4)+
69.0
82.0
79.0
95.0 ([C6]+Na)+
123.0 ([C8 H4]+Na)+
CH3
CH2
CH3
CH3
Counts vs. Mass-to-Charge (m/z)

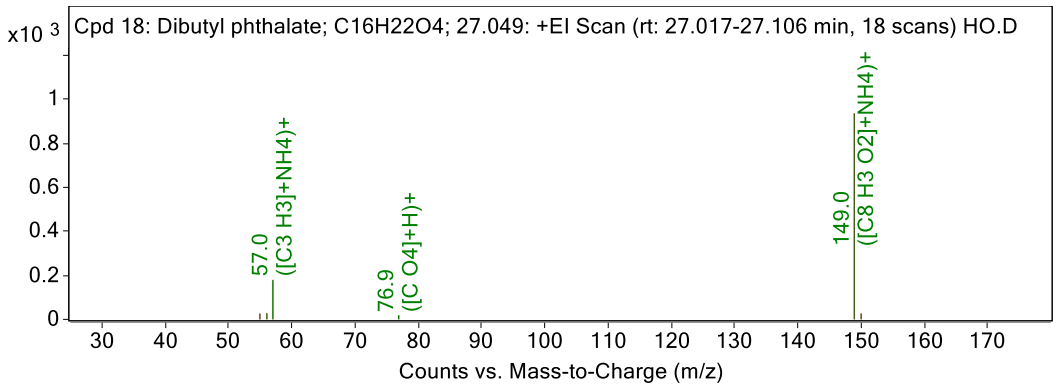
Cpd 18: Dibutyl phthalate; C16H22O4; 27.049: +EI Scan (rt: 27.017-27.106 min, 18 scans) HO.D
x10 3
57.0 ([C3 H3]+NH4)+
76.9 ([C O4]+H)+
149.0 ([C8 H3 O2]+NH4)+
Counts vs. Mass-to-Charge (m/z)

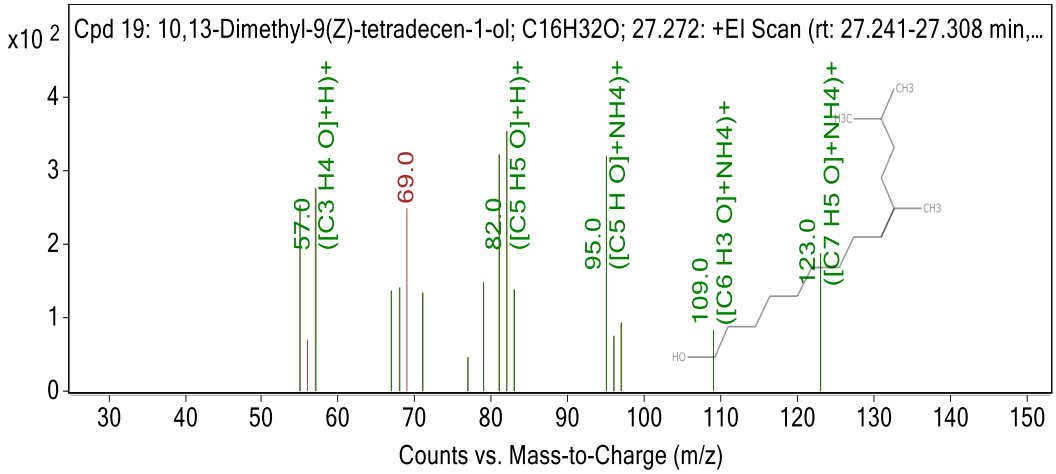
Cpd 19: 10,13-Dimethyl-9(Z)-tetradecen-1-ol; C16H32O; 27.272: +EI Scan (rt: 27.241-27.308 min,...
x10 2
57.0 ([C3 H4 O]+H)+
69.0
82.0 ([C5 H5 O]+H)+
95.0 ([C5 H O]+NH4)+
109.0 ([C6 H3 O]+NH4)+
123.0 ([C7 H5 O]+NH4)+
Counts vs. Mass-to-Charge (m/z)

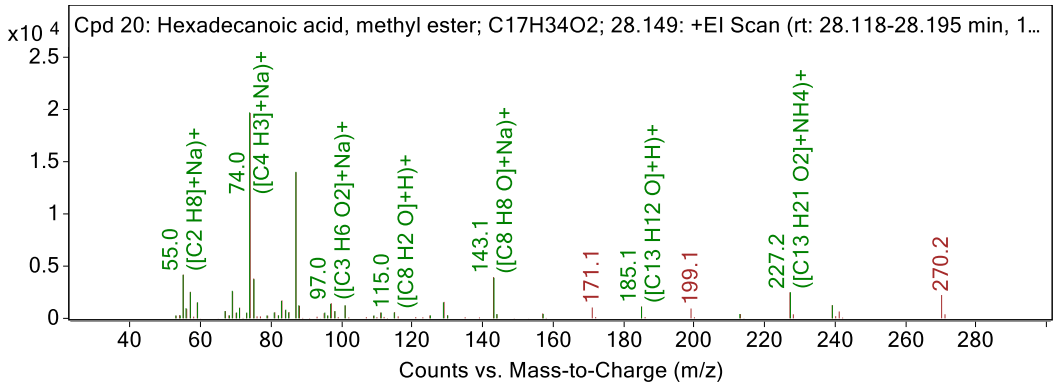
Cpd 20: Hexadecanoic acid, methyl ester; C17H34O2; 28.149: +EI Scan (rt: 28.118-28.195 min, 1...
x10 4
55.0 ([C2 H8]+Na)+
74.0 ([C4 H3]+Na)+
97.0 ([C3 H6 O2]+Na)+
115.0 ([C8 H2 O]+H)+
143.1 ([C8 H8 O]+Na)+
171.1
185.1 ([C13 H12 O]+H)+
199.1
227.2 ([C13 H21 O2]+NH4)+
270.2
Counts vs. Mass-to-Charge (m/z)

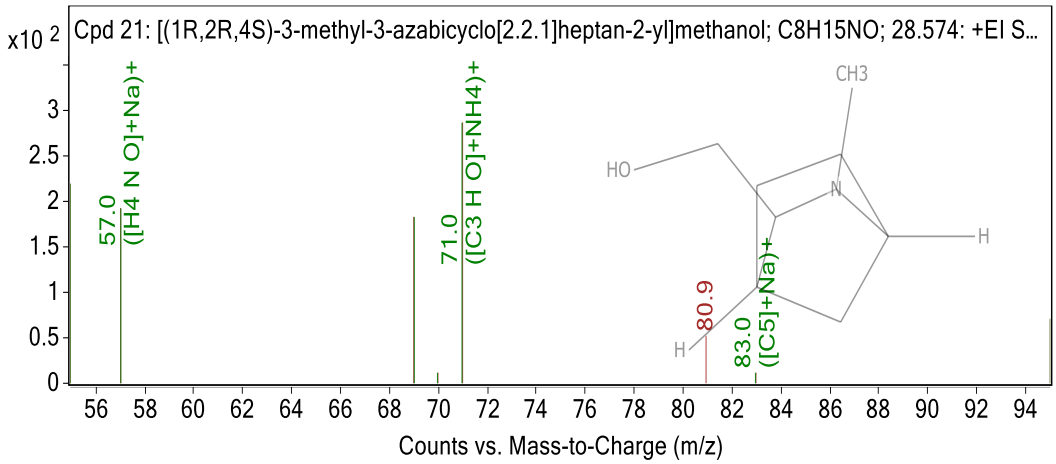
Cpd 21: [(1R,2R,4S)-3-methyl-3-azabicyclo[2.2.1]heptan-2-yl]methanol; C8H15NO; 28.574: +EI S...
x10 2
57.0 ([H4 N O]+Na)+
71.0 ([C3 H O]+NH4)+
80.9
83.0 ([C5]+Na)+
CH3
HO
N
H
H
Counts vs. Mass-to-Charge (m/z)

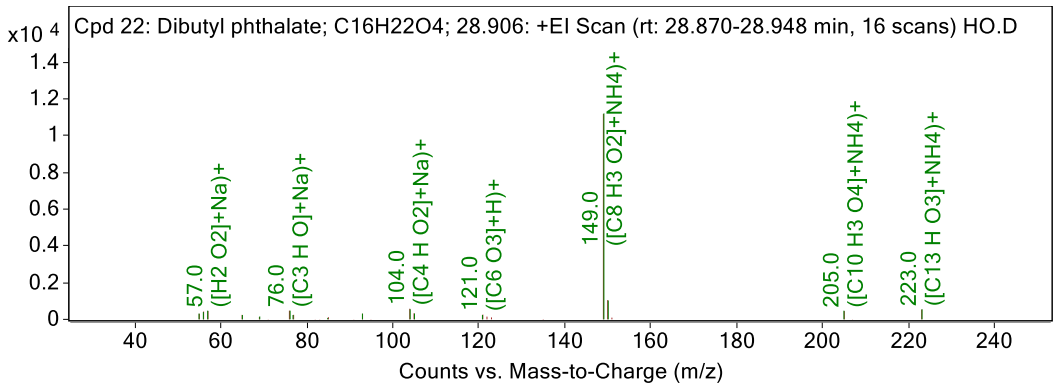
Cpd 22: Dibutyl phthalate; C16H22O4; 28.906: +EI Scan (rt: 28.870-28.948 min, 16 scans) HO.D
x10 4
57.0 ([H2 O2]+Na)+
76.0 ([C3 H O]+Na)+
104.0 ([C4 H O2]+Na)+
121.0 ([C6 O3]+H)+
149.0 ([C8 H3 O2]+NH4)+
205.0 ([C10 H3 O4]+NH4)+
223.0 ([C13 H O3]+NH4)+
Counts vs. Mass-to-Charge (m/z)

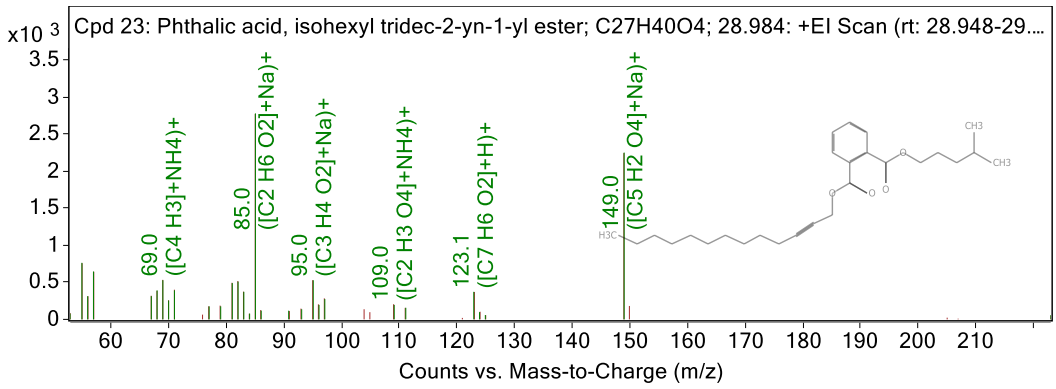
Cpd 23: Phthalic acid, isohexyl tridec-2-yn-1-yl ester; C27H40O4; 28.984: +EI Scan (rt: 28.948-29....
x10 3
69.0 ([C4 H3]+NH4)+
85.0 ([C2 H6 O2]+Na)+
95.0 ([C3 H4 O2]+Na)+
109.0 ([C2 H3 O4]+NH4)+
123.1 ([C7 H6 O2]+H)+
149.0 ([C5 H2 O4]+Na)+
Counts vs. Mass-to-Charge (m/z)

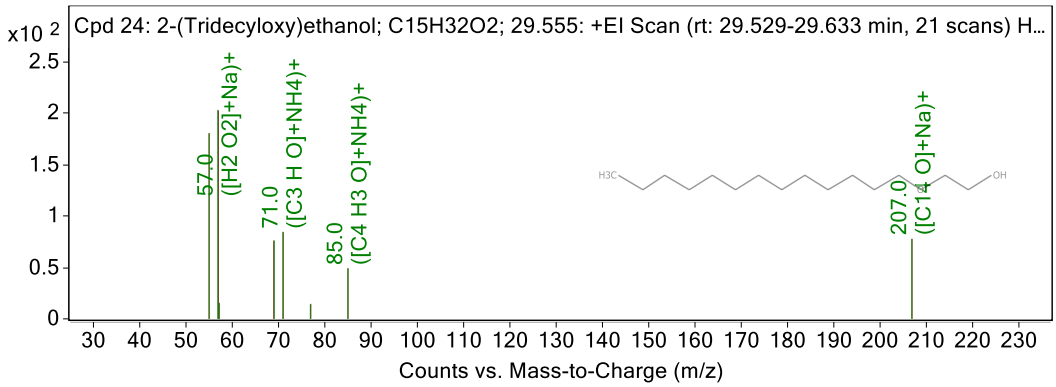
Cpd 24: 2-(Tridecyloxy)ethanol; C15H32O2; 29.555: +EI Scan (rt: 29.529-29.633 min, 21 scans) H...
x10 2
57.0 ([H2 O2]+Na)+
71.0 ([C3 H O]+NH4)+
85.0 ([C4 H3 O]+NH4)+
207.0 ([C14 O]+Na)+
Counts vs. Mass-to-Charge (m/z)

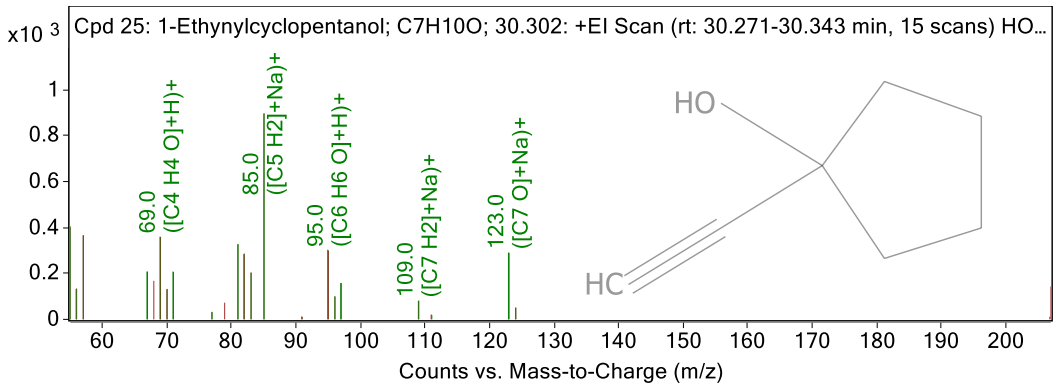
Cpd 25: 1-Ethynylcyclopentanol; C7H10O; 30.302: +EI Scan (rt: 30.271-30.343 min, 15 scans) HO...
x10 3
69.0 ([C4 H4 O]+H)+
85.0 ([C5 H2]+Na)+
95.0 ([C6 H6 O]+H)+
109.0 ([C7 H2]+Na)+
123.0 ([C7 O]+Na)+
HO
HC
Counts vs. Mass-to-Charge (m/z)

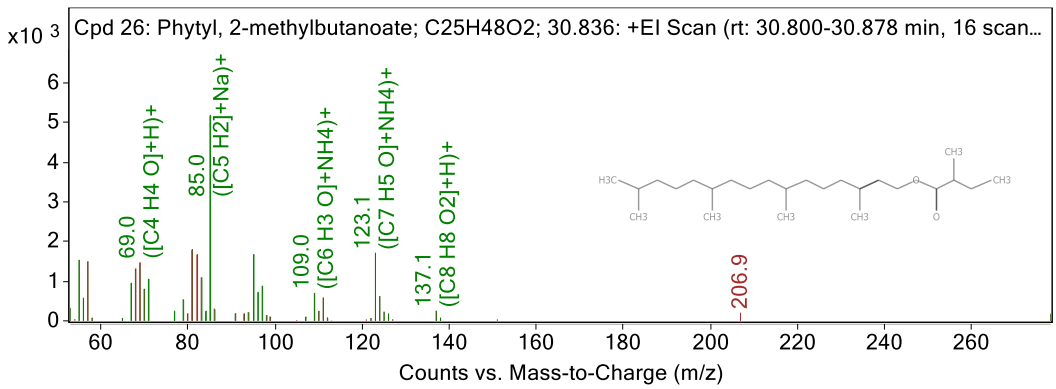
Cpd 26: Phytyl, 2-methylbutanoate; C25H48O2; 30.836: +EI Scan (rt: 30.800-30.878 min, 16 scan...
x10 3
69.0 ([C4 H4 O]+H)+
85.0 ([C5 H2]+Na)+
109.0 ([C6 H3 O]+NH4)+
123.1 ([C7 H5 O]+NH4)+
137.1 ([C8 H8 O2]+H)+
206.9
Counts vs. Mass-to-Charge (m/z)

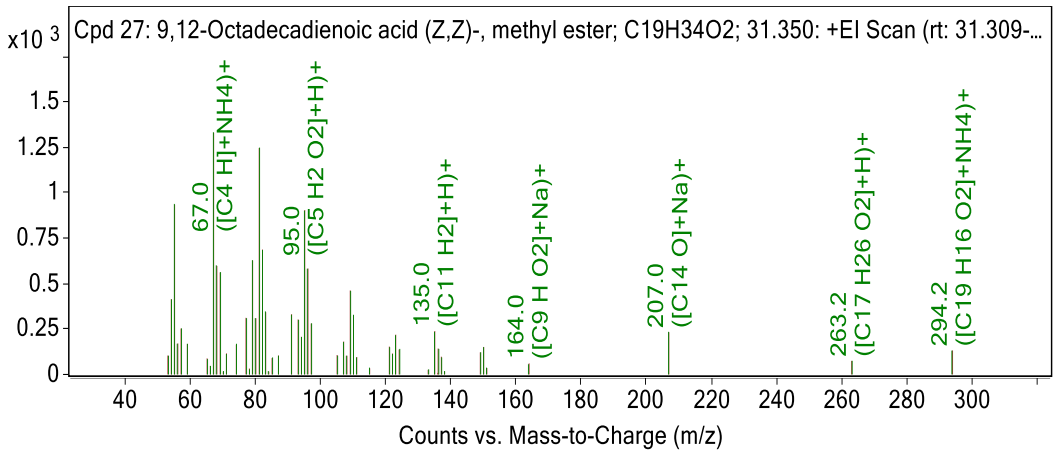
Cpd 27: 9,12-Octadecadienoic acid (Z,Z)-, methyl ester; C19H34O2; 31.350: +EI Scan (rt: 31.309-...
x10 3
67.0 ([C4 H]+NH4)+
95.0 ([C5 H2 O2]+H)+
135.0 ([C11 H2]+H)+
164.0 ([C9 H O2]+Na)+
207.0 ([C14 O]+Na)+
263.2 ([C17 H26 O2]+H)+
294.2 ([C19 H16 O2]+NH4)+
Counts vs. Mass-to-Charge (m/z)

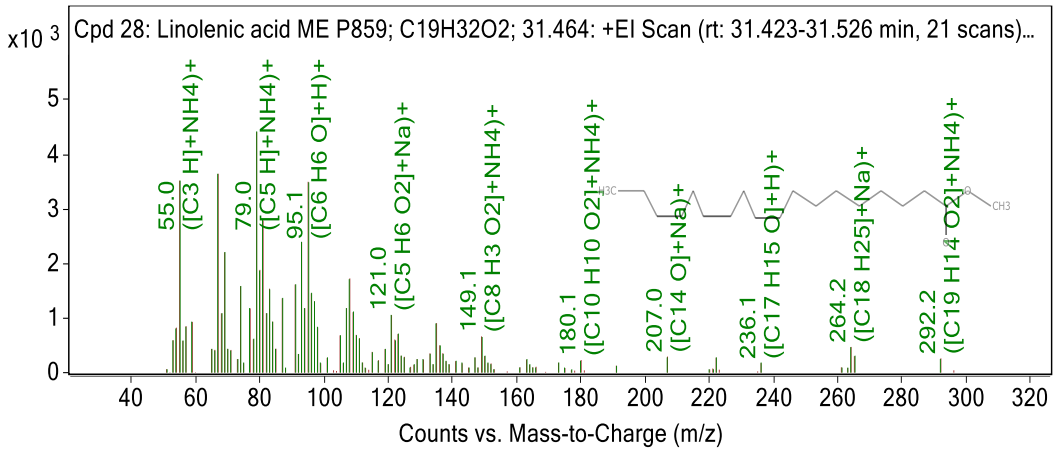
Cpd 28: Linolenic acid ME P859; C19H32O2; 31.464: +EI Scan (rt: 31.423-31.526 min, 21 scans)...
x10 3
55.0 ([C3 H]+NH4)+
79.0 ([C5 H]+NH4)+
95.1 ([C6 H6 O]+H)+
121.0 ([C5 H6 O2]+Na)+
149.1 ([C8 H3 O2]+NH4)+
180.1 ([C10 H10 O2]+NH4)+
207.0 ([C14 O]+Na)+
236.1 ([C17 H15 O]+H)+
264.2 ([C18 H25]+Na)+
292.2 ([C19 H14 O2]+NH4)+
Counts vs. Mass-to-Charge (m/z)

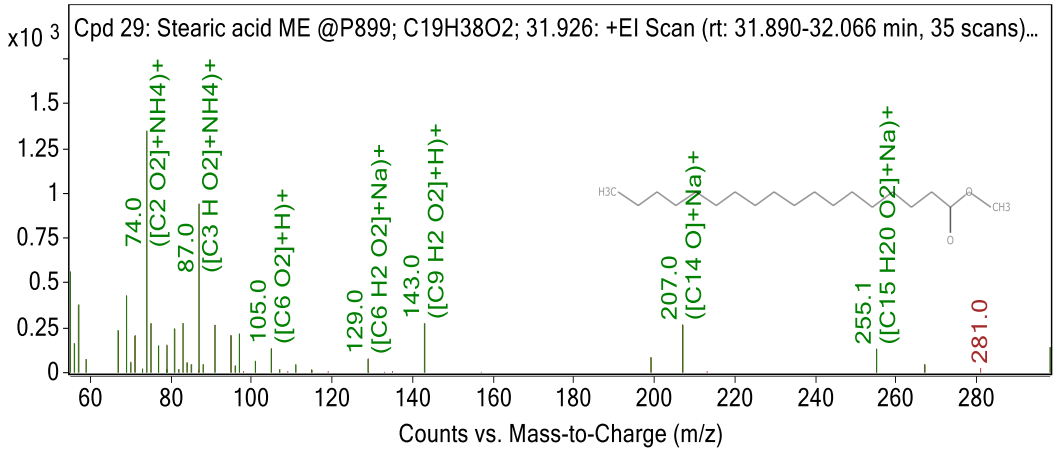
Cpd 29: Stearic acid ME @P899; C19H38O2; 31.926: +EI Scan (rt: 31.890-32.066 min, 35 scans)...
x10 3
74.0 ([C2 O2]+NH4)+
87.0 ([C3 H O2]+NH4)+
105.0 ([C6 O2]+H)+
129.0 ([C6 H2 O2]+Na)+
143.0 ([C9 H2 O2]+H)+
207.0 ([C14 O]+Na)+
255.1 ([C15 H20 O2]+Na)+
281.0
Counts vs. Mass-to-Charge (m/z)

B: Laboratory work pictures

Leaf of C.macrostachyus

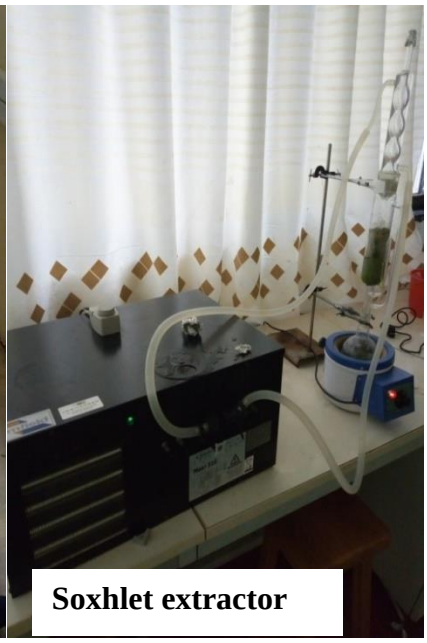

Soxhlet extractor

Animal bone

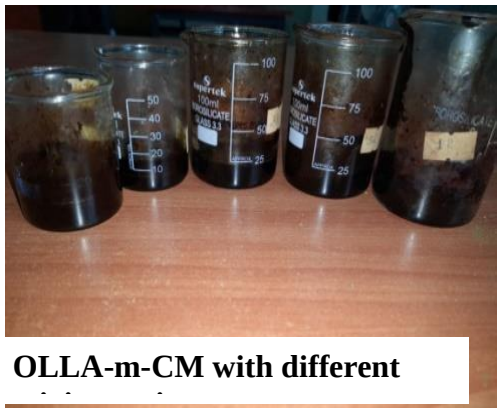

OLLA-m-CM with different

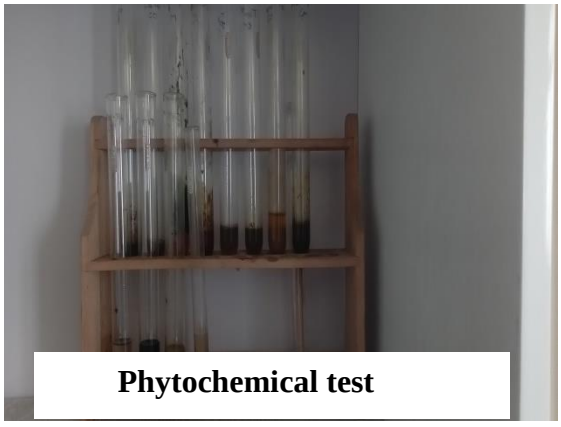

Phytochemical test